Ph.D. Dissertation

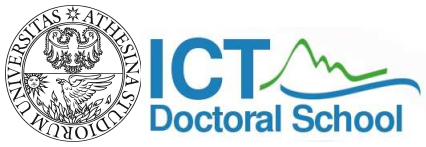

International Doctoral School in Information

and Communication Technology

DISI - University of Trento

Optimal Strategies for Antenna Array Design in Advanced Radar and Communications Systems through Convex Optimization

Le Trong Phuoc Bui

Advisor:
Paolo Rocca, Associate Professor
University of Trento
Co-Advisor:
Lorenzo Poli, Assistant Professor
University of Trento

October 2021

To my family, my colleagues and my friends inside and outside the ELEDIA Research Center. Thank you all.

Abstract

In this dissertation, convex programming (CP) as applied to antenna array synthesis is proposed as a methodology for the optimal synthesis of phased array antennas, and timed/pulsed array antenna as well. In particular, array antenna synthesis in frequency and time domain is formulated as an optimization problem for different types of architectures, systems, and applications in the CP paradigm. In addition, the CP-based optimization has shown great performance with efficient computation for a variety of canonical array synthesis problems due to its convexity property. Furthermore, the jointly satisfying geometrical and operation constraints are also presented because nowadays applications require unconventional array antennas able to guarantee high performance requirements. Therefore, the introduction of optimal synthesis methodologies for the unconventional array is shown for different applications. In this framework, the thesis is aimed to study and develop innovative CP-based methodologies for the optimal synthesis of the unconventional array antennas (e.g., sub-arrayed, wideband, reconfigure, timed arrays) for next-generation radar and wireless communication systems. A number of examples, including some requirements/constraints and realistic scenarios will be taken into account in order to numerically validate the proposed methodologies when considering both ideal and realistic antenna models.

Keywords
Convex programming (CP), sequential convex programming (SCP), optimal synthesis, array synthesis, phased array antenna, ultra-wideband (UWB) antenna, beam scanning, power synthesis, monopulse antenna, reconfigurable array antenna, wireless communications, pulse array synthesis, timed-array synthesis.

Published Journals Papers

[R1] L. T. P. Bui, N. Anselmi, T. Isernia, P. Rocca & A. F. Morabito, "On bandwidth maximization of fixed-geometry arrays through convex programming," *Journal of Electromagnetic Waves and Applications*, 34:5,581-600,DOI:10.1080/09205071.2020.1724832

[R2] M. Bertolli, M. Donelli, A. Massa, G. Oliveri, A. Polo, F. Robol, L. Poli, A. Gelmini, G. Gottardi, M. A. Hannan, L. T. P. Bui, P. Rocca, C. Sacchi, F. Viani, T. Moriyama, T. Takenaka, and M. Salucci, " Computational methods for wireless structural health monitoring of cultural heritages" *Journal of Phys*ics: Conf. Ser. 1131, 012005, 2018.

Published Conference Papers

[C1] L. T. P. Bui, L. Poli, and P. Rocca, "Optimal synthesis of wideband beam-forming weights for monopulse tracking radar: the linear array case," *Proc. 2018 IEEE AP-S International Symposium on Antennas and Propagation & USNC/URSI National Radio Science Meeting*, Atlanta, Georgia, 7-12 July 2019.

[C2] L. T. P. Bui, M. A. Hannan, N. Anselmi, L. Poli, and P. Rocca, "Optimal synthesis of wideband planar phased arrays with maximum bandwidth," *12th European Conference on Antennas and Propagation (EUCAP 2018)*, London, United Kingdom, April 9-13, 2018.

[C3] L. T. P. Bui, L. Poli, P. Rocca, and A. Massa, "Maximum-Bandwidth Synthesis of Monopulse Array Antennas with Fixed Geometry Through Convex Optimization," *Proc. 2018 IEEE AP-S International Symposium on Antennas and Propagation & USNC/URSI National Radio Science Meeting*, Boston, Massachusetts, 8-13 July 2018.

[C4] L. T. P. Bui, P. Rocca, and R. L. Haupt, "Aperiodic planar array synthesis using pseudo-random sequences," *Proc. 2018 International Applied Computational Electromagnetics Society Symposium (ACES)*, Beijing, China, 29 July - 1 August 2018.

[C5] N. Anselmi, M. A. Hannan, L. T. P. Bui, L. Dall'Asta, G. Gottardi, P. Rocca, and A. Massa, "Sparse wideband linear arrays synthesis via compressive sensing methods," *Proc. 2018 International Applied Computational Electromagnetics Society Symposium (ACES)*, Beijing, China, 29 July - 1 August 2018.

[C6] L. T. P. Bui, N. Anselmi, G. Gottardi, L. Poli, P. Rocca, "Wideband phased arrays synthesis with maximum bandwidth through iterative convex optimization," *Proc. 2017 IEEE AP-S International Symposium on Antennas and Propagation & USNC/URSI National Radio Science Meeting*, San Diego, CA, July 9-14, 2017.

Contents

List of Tables

List of Figures

List of Abbreviation

UWB	**U**ltra-**W**ide**B**and
CP	**C**onvex **P**rogramming
SCP	**S**equential **C**onvex **P**rogramming
5G	**F**ifth **G**eneration
PSO	**P**article **S**warm **O**ptimization
GA	**G**enetic **A**lgorithm
EM	**E**lectro**M**agnetic
FWB	**F**ractional **B**and**W**idth
UB	**U**pper**B**ound
G	**G**ain
D	**D**irectivity
HPBW	**H**alf **P**ower **B**eam**W**idth
EEP	**E**mbedded **E**lement **P**attern
AEP	**A**ctive **E**lement **P**attern
DRR	**D**ynamic **R**ange **R**atio
TD	**T**ime **D**omain

List of Symbols

λ	Wavelength
f_{min}	Minimum frequency
f_{max}	Maximum frequency
f_c	Center frequency
f	Frequency
N	Total number of elements
$\overrightarrow{r}$	Position in 3−dimension space
Ω	Sidelobes regions
θ	Theta angle
ϕ	Phi angle
$\mathbf{w}$	Complex excitations
b	Steering vector
Ξ	Notch filter region
c	Speed of light
η_s	Threshold for sharing elements
a^{Σ}	Amplitudes excitations of sum pattern
a^{Δ}	Amplitudes excitations of difference pattern
Γ	Ripple in the shaped-beam region
$\prod$	Product of many terms
$\sum$	Sum of multiple terms

Chapter 1

Introduction

In this Chapter, the main motivations of choosing this topic are briefly described. Moreover, the main objectives and contributions of this thesis are also listed.

1.1 Motivations

The rapid usage of wireless services, next generation communications (i.e., $5G$), and radar systems are increasing the need for bandwidth. In this regard, the array antenna synthesis in frequency or time domain is a key solution to meet the demand on high capacity for the evolution of the advanced communication systems. In addition, by synthesizing the antenna array, the resolution of antenna systems are enhanced dramatically when steering a beam to desired target.

So far, the synthesis of the array antenna systems in the framework of convex programming (CP) has received huge interest because it provides accurate and efficient computation compared to other framework such as: genetic algorithm (GA) or particle swarm optimization (PSO). Furthermore, low sidelobe level (SLL) and suppression region can help to prevent interference or outliers from entering the communications. In addition, wideband array antenna meet the demand for high throughput in the era of wireless communications and radar systems.

1.2 Objectives

The main objectives of this thesis are listed as follows:

1. study and development of CP-based innovative strategies for antenna array synthesis purpose;
2. adapt and apply the developed approaches to frequency domain:
   - applications: radars, and $5G$;
   - characteristics of the sources: wide band;
   - systems: linear array, planar array;
3. adapt and apply the developed approaches to time domain:
   - applications: radars, and $5G$;
   - characteristics of the sources: narrow band, and wide band
   - systems: linear array.

1.3 Contributions

The main contributions of this thesis are listed as follows:

1. theoretical - formulations of CP-based synthesis problem for UWB antenna array systems;
2. methodological - development of different $CP-$based strategies for different scenarioes;
3. resource - implementation of the developed strategies;
4. analytical - extensive numerical analysis of the behaviour of the proposed approaches.

1.4 Outline

The outline of this thesis is listed as follows:

- *Chapter 2* - the state-of-the-art $CP-$based antenna array synthesis problem is reviewed in details;
- *Chapter 3* - the general CP synthesis problem is formulated mathematically for an array antenna system, and analyzed extensively.
- *Chapter 4* - the general CP synthesis problem is formulated mathematically for an mono-pulse tracking system, and analyzed extensively.;
- *Chapter 5* - the general CP synthesis problem is formulated mathematically for shaped-beam array antenna and analyzed extensively;
- *Chapter 6* - the general CP synthesis problem is formulated mathematically for pulsed array antenna and analyzed extensively;
- *Chapter 7* - some concluding remarks are summarized and some scopes of future research are listed.

Chapter 2

Literature Review

In this Chapter, the state-of-the-art literature of $CP-$based antenna array synthesis is reviewed focusing on the methodological advancement in the context of different innovative systems and applications.

2.1 The state-of-the-art Survey and Analysis

For the last decades, antenna array synthesis has been a very popular area that attracts many researchers. There are many thorough studies in various fields and successfully applied to many disciplines of realistic scenarios including radar, localization, sonar, navigation, and smart antennas. Many methods for array antenna synthesis were proposed in the state-of-the-art literature. A large number of dedicated books [1][2][3] addressing array synthesis problem are published by many well known researchers. In addition, the unconventional phased array synthesis have been published recently with different design methodologies including sub-arrayed or clustered, sparse, thinned, and time-modulated arrays [4][5][6] [7][8][9].

Although the area is extensively studied, it has gained the great interest nowadays from many researchers which is obvious from a number of PhD [10][11] from well-known institutions and a high number of publications. The advancements of the different classical and modern array synthesis methods, and recent highly growing development of the wireless technologies are paving the way for huge potentialities for many innovative applications in next generation cellular communications, vehicular technology, radar system and so on [12][13][14][15].

Array antenna, is comprised of many radiators, gives an efficient solution to detect and process the electromagnetic (EM) signals incoming from various arrival of angle. Unlike a single radiating element that has poor performance on radiation patterns, an array of radiators outperform and provide an larger bandwidth, directivity, very low SLL, smaller beamwidth, higher resolution, and capability of beam-steering by only changing the corresponding control units (e.g., amplitude and phase excitations) [1][2][3][16].

The goal of the antenna array synthesis is to provide a set of the excitations (e.g., weights/amplitudes and phases) that fulfill some requirements on the radiation patterns, the EM waves in the far-field, near-field, and the geometry of the array. The optimal synthesis of the array antenna is play an important role in many wireless and communication applications. Indeed, optimal design could help to adjust the EM waves to the realistic scenarios, which efficiently transmits the radio power along the desired direction and suppresses the EM energy at the same time towards the unwanted interference [17][22][19][20].

In radar and surveillance systems, the optimal synthesis provides several the far-field radiation patterns (e.g., focus beams, difference beam) to enable system to detect the flying targets (e.g., monopulse radar). Furthermore, the optimal design results in very low SLL, narrow beamwidth, and high directivity to improve the resolution in order to correctly recognize, track, and distinguish multiple closed objects [21]. In wireless power transmission system, there is strict requirement for very high overall efficiency from a transmitter to a receiver in order

to focus almost transmitted EM energy to the desired area where the receiver located and eliminating transmitting power in the sensitive area (e.g., residential area) to reduce unwanted damage [22][23].

Furthermore, in the next generation of wireless communication (e.g., $5G$), the increasing number of wireless services is promoting the development of an efficient design technique to deal with the strict and complicated constraints on the demanding requirements. For example, [24] the number of portable electronic devices is surging leading to the huge data transmitting over the air. The old system seems to be not enough for that huge amount of data. Therefore, the new generation communication operating at "so called" the millimeter-wave band spanning from 30 [GHz] to 300 [GHz] is required to meet that demand. Phased array antenna transmits and receives the high gain in the desired direction and the design of phased array antenna is challenging, especially when a broadband of operation is needed to meet the high throughput. Indeed, beam squinting reduces and limits bandwidth in phased array antenna [1], for example the changing of the radiation pattern direction when operational frequency changes.

In order to synthesize antenna array operating at wideband, in general, there are two ways. The first method is phased array antenna operating over multiple frequencies in the band of interest. The second method is to synthesize input pulses for array system in time domain. In the first approach, the phased array depends on the phased shifter that is narrow band. Therefore, in order to force the phased array to operate at wideband, the bandwidth of interest is sampling into multiple frequencies that are constraints the synthesis methodology must fulfill. In the latter, pulse array depends on the time delay that is independent from frequency, so the time array antenna is able to work at wideband [25].

Phased array (or timed array) can be used for advanced communications and radar systems with the capability of operating at a wide rang of frequency. Operating bandwidths of phased array antennas are basically limited at the high frequency when the maximum inner-spacing between closest elements is beyond a certain wavelength. A unwanted phenomena (e.g., grating lobes) appears when the main beam is steered far away from the broadside direction if the inter-element spacing is not valid. At the lower frequency, the array can operate as low as possible, as long as the radiation patterns fulfill some conditions given by applications [1].

The antenna array synthesis has been studied extensively for over several decades. The analytical methods were deployed to synthesize different patterns including sum patterns, difference patterns, and arbitrary patterns (e.g., shape beam pattern, cosecant pattern, flattop pattern). More specifically, the authors in [26][27] proposed analytical method to generate focus pattern with uniform sidelobes. However, those uniform sidelobes will reduce the super gain of the array in case of large number of elements are used. Therefore, Taylor in [28] provided a new way to avoid this drawback by tailoring the sidelobes. In [29], the difference pattern where a deep null is placed in the boresight direction, which

is useful in detection and track moving objects. Furthermore, the arbitrary shape patterns can be synthesized using many orthogonal $p-sinc$ functions [30][31][32]. Another method can be used to synthesize sum, difference, or shape patterns using polynomial method in [33].

Although, the aforementioned classical or analytical methods are simple, fast, and easy to implement, they still have many drawbacks in the modern demanding requirements for antenna array. To name a few, they are designed in narrow bandwidth at single frequency, the analytical methods do not provide optimal design because there are many possibilities for achieving the appropriate solution, the analytic shaped pattern synthesis requires uniformly $\lambda/2$ inter-element locations, and simple constraints on the SLL.

The numerical methods have also studied extensively in array synthesis (e.g., deterministic method [34][35], stochastic strategy [36][37][38][39]). In the stochastic method, the optimal design is often not guaranteed if the initialization is not wisely chosen. In addition, stochastic optimization is meta-heuristic optimization, so the complexity of the optimization problem increases exponentially with the problem size (e.g., the number of array elements). Therefore, the overall performance of the far-field radiation pattern from the antenna array is affected or even not satisfied the requirements from the antenna design. Furthermore, those array antenna designed by deterministic and stochastic strategies often operating in the narrow bandwidth.

Convex optimization have recently become popular in antenna array design due to its flexibility and efficiency. Specifically, the optimization has shown the great performance, although the unconventional architectures are used. In addition, the time computation for each optimization is linear time, because the local optimal is also the global optimal solution. As a consequences of these benefits in using convex optimization, several fields of engineering have deployed $CP-$based methodology to solve their problem, such as controls systems [40], mechanical engineering [41], signal and image processing [42][43], electronics design [44][45], and optimal real scenario design [46].

A large number of EM applications and array antenna have been deployed $CP-$based strategies to obtain the optimal design. For instance, to fulfill the adaptive beam-forming requirements, the control units (e.g., weights and phases) must be optimized by using $CP-$based synthesis procedure. Indeed, array system with the optimal excitations are likely to produce the radiated power enhanced at the desirable directions and suppressed along the unwanted angles [47][48][49][50][51]. However, to provide an antenna array that satisfy the high demand of the next generation of wireless communication era (e.g., $5G$), the adaptive beam-former needs to operate at wide bandwidth and avoids using many control units at different frequencies. For example in [52][53][54], the authors used an innovative strategy based on iterative$-CP$ to maximize the bandwidth of the operating antenna array.

In the application of radar such as monopulse radar where moving object

are detected and tracked by using the short-time observation of the echoes from target based on the processing of the sum and difference received signals. The fabrication cost of control units for the monopulse increases dramatically if sum and difference patterns are treated independently. Therefore, in order to reduce the cost, the joint $CP-$based synthesis procedure is taken into account [69][56][57].

In some applications (e.g., satellite), the transmitters and receivers have to match the polarization if the receiver side wants to receive the signals from transmitter end. Therefore, to guarantee the EM waves sent successfully sent to the receiver, the $CP-$based strategy can be used to promote the adaptive beam-forming [58]. In radar or remote sensing, the antennas are required to produce the far-field radiated power following some pre-defined shape (e.g., flat-top, cosecant, or isoflux) depending on the geographical area or orbit of the targets/radars. In those circumstance, the sequential $CP-$based optimization can be used to generate the required shaped-beam with high performance and efficiency [60][101].

However, the antenna array synthesis is not always convex. For example, phased-only array where amplitudes are fixed and known values, only phases are unknown. In addition, shaped-beam synthesis where the radiated power are bounded between the required upper and lower bounds. Furthermore, reconfigurable array in which many patterns are generated with common excitations. Therefore, those non-convex original problems can not be solved by using CP. An innovative method is used to convert those non-convex problems to new form of convex problem with some relaxation assumptions [61][62].

The problem being addressed in the dissertation is the optimal synthesis of wideband/ultra- wideband array antennas through an innovative Convex Optimization strategy. The synthesis is aimed at determining the excitations of the array elements such that the radiation pattern satisfies an user-defined power mask over the largest possible operation bandwidth. The addressed problem is important to the next-generation communications because wideband/ultra-wideband arrays are a key enabling technology for a wide number of nowadays applications related to radar and electromagnetic sensing and imaging, and will be more and more important for next-generation $5G$ and small-satellites communications.

The novelty of the dissertation over the existing synthesis methods:

1. A theoretical formulation exploiting "at best" the degrees of freedom of the synthesis;

2. The capability of ensuring the bandwidth maximization by exploiting nothing but Convex Programming routines guaranteeing both the uniqueness and the optimality of the retrieved solution;

3. The applicability of the introduced design tool to any kind of fixed-geometry

array whenever the fulfillment of a given power mask and the maximization of bandwidth must be jointly pursued.

This thesis work aims at addressing the following issues of antenna array synthesis in CP framework:

1. developing innovative strategies to design array operate at wide bandwidth;
2. developing innovative strategies to design monopulse operate at wide bandwidth;
3. developing innovative strategies to design shaped-beam operate at wide bandwidth;
4. developing innovative strategies to design pulse/timed array.

All the aforementioned issues are addressed successfully in this thesis. The outcomes have already been published [53][54] [64][65]in the state-of-the-art literature and some are in under review process.

2.2 Fundamental of Convex Optimization

The convex optimization problem, in general, can be defined in the form [102]

$$\underset{x}{minimize} \quad \chi(x) \tag{2.1}$$

$$subject\ to \quad \chi_i(x) \leq \nu_i \quad i = 1, ..., m \tag{2.2}$$

$$\chi_j(x) = \nu_j \quad j = 1, ..., n, \tag{2.3}$$

in which the objective function in Eq. 2.1, the inequality constraint functions in Eq. 2.2, and the equality constraint functions in Eq. 2.3 are convex.

A function χ_ς to be considered convex if and only if, for all x, $y \in R^n$ and there exist two numbers $\iota, \kappa \in R$ such that

$$\chi_\varsigma(\iota x + \kappa y) \leq \iota\chi_\varsigma(x) + \kappa z_\varsigma(y),$$

is satisfied with $\iota + \kappa = 1$, $\iota \geq 0$, $\kappa \geq 0$, R^n denotes the any real number in n dimensional space. There are many common functions can easily proved to be convex as: affine function $\rho^T x + b$ form where ρ, x are n dimensional vectors and b is scalar, quadratic function $x^T R x$ form in which R is a symmetric positive semi-definite matrix, and norms of vectors $||x||$ (which include the Euclidean norm, the absolute value, and the maximum value of a set of elements).

A set Υ is convex if the line connecting between any two points in Υ belongs to Υ. Mathematically, for any $x_1, x_2 \in \Upsilon$, and for any ι, κ, $\iota + \kappa = 1$, $\iota \geq 0$, $\kappa \geq 0$, this following property

$$\iota x_1 + \kappa x_2 \in \Upsilon,$$

should fulfill.

Linear programming problem is a special case of convex optimization when the objective functions and constraint functions are having the affine form. In general, a convex optimization problem is the minimization of a convex function over a convex set and any local minimum of a convex function is also a global minimum.

In order to say an optimization problem is a convex optimization problem, first all the functions in the optimization problem must be convex, and all constraints in the optimization must be convex over convex set. Indeed, in [102], the intersection of all the convex sets still a convex set, therefore the whole problem in Eq. 2.1, Eq. 2.2, and Eq. 2.3 is equivalent to minimization of convex function over a convex set, which is convex programming problem.

The goal of this thesis is to identify and reformulate the array synthesis such that the convex programming can be deployed to solve the array synthesis in frequency or time domain. The beauty of convex programming applied to the array synthesis is the optimal solution that can be found in efficient computation time.

Chapter 3

Wideband Array Synthesis

The method presented in this chapter related to a strategy for the synthesis of an array antenna that is able to operate at multiple frequencies by using the only optimal set of excitation. By exploiting the EM property, for a fixed array geometry, there is a operating maximum frequency for that array. If the antenna operates at a frequency higher than certain maximum frequency, then grating lobes is likely to appear and degrade the antenna performance. Towards this end, an iterative CP strategy is proposed to find out the maximum operating bandwidth. Finally, a set of numerical examples, including full-wave synthesis of linear realistic array antennas, were carried out and their results presented in order to assess the array antenna's capability of achieving ultra-wideband performances.

3.1 Introduction

The bandwidth (BW) and the SLL are the most important parameters for array performance [2]. The bandwidth is considered as a range of frequencies over which the antenna operate correctly. Fractional bandwidth (FBW) is often used to describe for BW [66][67][48] and FBW limits in the range from 0 and 2 and, for a system which operates between the minimum frequency f_{min} and the maximum frequency f_{max}, it is given by:

$$FBW = \frac{f_{max} - f_{min}}{f_c} = 2\frac{f_{max} - f_{min}}{f_{max} + f_{min}}, \tag{3.1}$$

wherein, $f_c = \frac{f_{max}+f_{min}}{2}$ denotes the center frequency.

An antenna is considered WB, only if $0.2 < FBW < 0.5$ and UWB on condition $FBW \geq 0.5$ [48]. Several benefits of WB devices compared to narrowband systems, such as high precision in distance, shorter broadcast time, low EM radiation , and low energy spending [66]. There are many UWB array applications, such as medical imaging, personal area networks, tracking and real-time localization systems, through-the-wall imaging, and time-of-arrival-based localization approaches [67]. Strategies for effective antenna array synthesis can be found in[48][68][69][70][71][72].

The SLL in [2] can be defined as the relative maximum value of sidelobes to the maximum value of the radiation pattern. The SLL can be expressed as follows:

$$SLL = \underset{\theta \in \Omega}{max} \left| \frac{AF(\theta_0)}{AF(\theta)} \right|, ^2 \tag{3.2}$$

wherein, θ is the angular direction, θ_0 is the target direction, $AF(.)$ represents for the radiated field, and Ω is the angular region outside of the main beam region or the sidelobes regions [69].

Many applications requires very low SLL to increase the performance, such as transmission of wireless power, radar and satellite applications, hyperthermia treatments, and synthesis of high-beam-efficiency antennas [69][73][74][50][76]. Many methods have been used effectively to synthesize single beam [74]-[79] and reconfigurable [80]-[84] pattern arrays as well.

However, almost all SLL minimization optimization problems have a crucial restriction that is using either a single-frequency or a narrow-band assumption [48]. Clearly, this restriction strongly limits the applicability range of the obtained results while making the synthesis algorithm simpler. As a consequences, it is required to propose a new synthesis strategy that enables for the optimization of both SLL and FBW indicators at the same time. It is similar to the idea that minimizing the SLL for a given fixed FBW using PSO algorithm to determine the array-element locations and excitations [48].

By exploiting the available strategies available for the single-frequency/narrow bandwidth optimal array synthesis and considering the approaches presented in

[48], a new and effective approach is proposed here for designing array antennas. The new approach can be stated as: the FBW is maximized subject to the minimum fixed SLL performance. Specifically, a new method is proposed to determine the maximum possible FBW while an array of given geometry architecture and size is able to obtain a fixed SLL performance.

For any fixed-geometry arrays, the proposed approaches enable the fast and efficient synthesis of sum beams. If the field can be expressed in terms of the array factor, shaped patterns synthesis based on the mask-constrained power can be achieved by deploying the proposed strategy. In all the cases, the overall synthesis problem is cast as an iterative$-CP$ optimization, with solutions optimality and efficient computational time.

3.2 Mathematical Formulation

Let us assume an array comprised of N antenna elements positioned at location $\vec{r}_n = (x_n, y_n, z_n)$ with $n = 1, 2, .., N$. Every array element of antenna system radiates a far-field radiation pattern $E_n(f, \theta, \phi)$, $n = 1, 2, ..., N$ at specific frequency f, along the direction (θ, ϕ) and is weighted with weights w_n, $n = 1, 2, ..., N$, respectively. Therefore, the total far-field radiation pattern at the outputs of the array is simply the linear combination of fields generated by all the single antenna and expressed in far-field as follows:

$$AF(f, \theta, \phi; \mathbf{w}) = \sum_{n=1}^{N} w_n E_n(f, \theta, \phi) e^{j\frac{2\pi f}{c}\left[\vec{r}_n . \hat{r}(\theta, \phi)\right]} \tag{3.3}$$

wherein, $\hat{r}(\theta, \phi) = \left[sin\theta cos\phi,\ sin\theta sin\phi,\ cos\theta\right]$ is the unit vector in the spherical coordination, and c is the speed of light.

The Eq. (3.3) can be re-written in matrix form as follow:

$$AF(f, \theta, \phi; \mathbf{w}) = b(\theta, \phi)^H \mathbf{w} \tag{3.4}$$

in which, $b(\theta, \phi) = \left[E_1(f, \theta, \phi) e^{j\frac{2\pi f}{c}\left[\vec{r}_1 . \hat{r}(\theta, \phi)\right]}, \cdots, E_N(f, \theta, \phi) e^{j\frac{2\pi f}{c}\left[\vec{r}_N . \hat{r}(\theta, \phi)\right]}\right]^H$ is the steering vector, and $\mathbf{w} = \left[w_1, w_2, ..., w_N\right]^T$ is the complex excitations, $.^H$ denotes the Hermitian transposition.

From the Eq. (3.4),the power radiated by the array is defined as:

$$|AF(f, \theta, \phi; \mathbf{w})|^2 = \mathbf{w}^T Q \mathbf{w},\ with\ Q = b^T b \tag{3.5}$$

wherein, $b \in C^{1\times N}$, $\mathbf{w} \in C^{N\times 1}$, and $.^T$ is the transpose operator.

The approach in [79] address the optimal synthesis of array antenna for a single frequency, in which for a fixed antenna geometry $\vec{r}_n$, a given null-to-null beamwidth Ω, then the best possible SLL is optimized using $CP-$based strategy. Finally, the optimal weights of the array can be found in following procedure:

$$\underset{\mathbf{w}}{Maximize} \quad \Re\left[AF(f,\theta_0,\phi_0;\mathbf{w})\right] \tag{3.6}$$

$$Subject\ to \quad \Im\left[AF(f,\theta_0,\phi_0;\mathbf{w})\right] = 0 \tag{3.7}$$

$$\Re\left[AF(f,\theta_0,\phi_0;\mathbf{w})\right] \geq 0 \tag{3.8}$$

$$\left|AF(f,\theta,\phi;\mathbf{w})\right| \leq UB(\theta,\phi) \quad \forall(\theta,\phi) \in \Omega, \tag{3.9}$$

wherein, $UB(\theta)$ is the maximum allowed user-defined power pattern in the sidelobes regions. The two constraints (3.7), (3.8) aim at maximizing the radiation power towards the boresight direction. $\Re$ and $\Im$ are denote for the the real and imaginary part of any complex terms. As a consequences, the maximization of the power is cast as the maximization of linear combination of unknowns, which help to increase the computational time and obtain the optimal results.

If the interest is not minimizing the SLL, but keep SLL below a certain threshold. The optimization problem can be formulated and solved by determining the intersection among all possible constraints, such as:

$$\begin{cases} AF(f,\theta_0,\phi_0;\mathbf{w}) = 1 \\ \left|AF(f,\theta,\phi;\mathbf{w})\right|^2 \leq UB(\theta,\phi) \quad \forall(\theta,\phi) \in \Omega \end{cases} \tag{3.10}$$

The eq. 3.10 gives us a guaranteed level for SLL, and makes room for insertion of objective function to maximize antenna parameters such as: Gain (G), Directivity (D) [77].

The goal of the thesis is to find the array element's complex excitation weights in order to maximize the FBW while keeping the SLL below the given threshold over the whole operating frequency range. Because the synthesized procedure is for linear array and planar array, then $\vec{r}_n$ is used in general. In case of linear array, $\vec{r}_n = (0, 0, z_n)$, $n = 1, 2, ..., N$, and for cases of planar array, $\vec{r}_n = (x_n, y_n, 0)$, $n = 1, 2, ..., N$, however $\vec{r}_n$ is fixed.

Supposing that the maximum frequency $f_{max}$is fixed, and frequency step δf is the difference between two nearest frequencies, then the sampling set of frequencies can be shown as f_1, f_2,..., f_Q where $f_1 = f_{max}$, $f_Q = f_{min}$, and $f_q = f_{max} - (q-1)\delta f$. Supposing that signals is independent from the fast oscillating behaviour over the frequency range $[f_1, f_Q]$ when transmitted. Let's us now assume that the the source of radiation is isotropic, so the element radiation pattern $E_n(f,\theta,\phi) = 1$, $n = 1, 2, ..., N$.

Under some simplified assumptions, the optimization problem of maximization of array's FBW with given threshold of SLL can be recast as follows:

$$\underset{\mathbf{w},Q}{Maximize} \quad Q \tag{3.11}$$

$$Subject\ to \quad \Im\left[AF(f_q,\theta_0,\phi_0;\mathbf{w})\right]=0 \qquad q=1,2,..,Q \tag{3.12}$$

$$\Re\left[AF(f_q,\theta_0,\phi_0;\mathbf{w})\right]=1 \qquad q=1,2,..,Q \tag{3.13}$$

$$\left|AF(f_q,\theta,\phi;\mathbf{w})\right|^2 \leq UB(\theta,\phi) \quad \underset{q=1,2,..,Q}{\forall(\theta,\phi)\in\Omega}, \tag{3.14}$$

As the matter of fact, determining the intersection among the constraints in eq. (3.12),(3.13),(3.14) over the possible largest range of frequency $[f_1, f_Q]$ is equivalent to the one in eq. (3.7),(3.8),(3.9). The eq. (3.11) aims to maximize (FBW) to finally obtain the possible largest operating BW of the array.

However, in some applications the directivity can be more preferred to added in the objective function[77][57]. The directivity can be defined as follows [85]:

$$D=\frac{4\pi\left|AF(f_{max},\theta_0,\phi_0;\mathbf{w})\right|^2}{\int_0^{\pi}\int_0^{2\pi}\left|AF(f_{max},\theta,\phi;\mathbf{w})\right|^2 sin\theta d\theta d\phi}, \tag{3.15}$$

here, if the boresight direction is know, f_{max} is determined, array geometry is fixed, then the nominator of D is known. Therefore to maximize D,the only thing to do is minimize the denominator. In [85], the denominator can be written as:

$$\int_0^{\pi}\int_0^{2\pi}\left|AF(f_{max},\theta,\phi;\mathbf{w})\right|^2 sin\theta d\theta d\phi = J^H B J, \tag{3.16}$$

wherein, $J=\mathbf{w}$, and B is a matrix with each entry is $b_{\alpha\beta}=\frac{sin(k\rho_{\alpha\beta})}{k\rho_{\alpha\beta}}$ if $\alpha\neq\beta$ and $b_{\alpha\beta}=1$ otherwise. The $\rho_{\alpha\beta}$ is the Euclidean distance between $\alpha-th$ element and $\beta-th$ element in the array. The α,β are the indices of number elements array along each dimension in $2-D$ array in general. As the matter of fact that, B is positive semi-definite, then the denominator of D is convex over convex set. Therefore, the CP strategy in eq. (3.11),(3.12),(3.13),(3.14) can be recast as follows:

$$\underset{\mathbf{w}}{Minimize} \quad \int_0^{\pi}\int_0^{2\pi}\left|AF(f_{max},\theta,\phi;\mathbf{w})\right|^2 sin\theta d\theta d\phi \tag{3.17}$$

$$Subject\ to \quad \Im\left[AF(f_q,\theta_0,\phi_0;\mathbf{w})\right]=0 \qquad q=1,2,..,Q \tag{3.18}$$

$$\Re\left[AF(f_q,\theta_0,\phi_0;\mathbf{w})\right]=1 \qquad q=1,2,..,Q \tag{3.19}$$

$$\left|AF(f_q,\theta,\phi;\mathbf{w})\right|^2 \leq UB(\theta,\phi) \qquad \underset{q=1,2,..,Q}{\forall(\theta,\phi)\in\Omega} \tag{3.20}$$

In eq. (3.17),(3.18),(3.19),(3.20), the optimal solution can be obtained by the virtue of limited bandwidth [86]. Constraints in eq. (3.18),(3.19),(3.20) can be replicated with different sampling frequency and therefore can be seen as a system of linear and quadratic equations/inequations in the unknowns. As

a results, finding the intersection among them is the CP problem leading to efficient and fast computation manner. Therefore, the solution of entire eq. (3.17),(3.18),(3.19),(3.20) can be solved in two-step procedure as follows:

1. Computation of the maximum frequency f_{max} of the FBW, because the frequency beyond the f_{max} is likely to create the grating lobes phenomena and degrade the antenna array performance. Setting $q = 1$ and run iteratively the eq. (3.17),(3.18),(3.19),(3.20) to find the f_{max}. Stop the $CP-$based when grating lobes appearing in the visible range. From there, f_{max} is determined.

2. In this step, the eq. (3.17),(3.18),(3.19),(3.20) are executed in a iterative loop. Each time the in the loop, the constraints for lower sampling frequency is added to procedure to validate and find the possible minimum frequency in the FBW. Specifically, a set of frequency f_1,f_2,..., f_Q are sampling from the $f_1 = f_{max}$with $f_q = f_{max} - (q-1)\delta f$, $q =$ 2,3, ...,Q, δf is the difference between two consecutive frequencies. The minimum frequency f_{min}will be defined as the the lower value of $f_q q = 2, 3, ..., Q$, which admits a solution of the convex programming problem in eq. (3.17),(3.18),(3.19),(3.20).

3.3 Numerical Results

This section is aimed at validating the effectiveness of the proposed methodology through a set of results in both linear array and planar array from several numerical simulations, including linear array in full-wave simulation. The remaining of this section is organized as follows. Firstly, some results of the isotropic linear array operating at wideband radiating in broadside direction, including the full-wave simulation are presented in sub-section (Sub-sect. 3.3.1) is presented and accessed. Finally, some more results of isotropic array radiated in non-broadside.

3.3.1 Isotropic Sources-Broadside radiation

In this test, the centrosymmetric linear array layout is composed of $N = 20$ elements with a constant inter-element spacing $d = 15$ [cm]. All seven test cases, with different SLL from -25 [dB] to -50 [dB] with step -5 [dB], are carried out by setting the boresight direction $\theta_0 = 90$ [deg], $\Omega = \{\theta | 0^o \leq \theta \leq 75^o \cup 105^o \leq \theta \leq 180^o\}$, $f_{max} = 2.5$ [GHz] is found after using iterative $CP-$based. Beyond this f_{max} the given array geometry will appear grating lobes that affect the performance of the array. The θ domain is sampling into 2000 samples and all simulations for seven test cases are run in such a way to achieve the UWB performances.

For each frequency, fourteen examples are carried out by applying, with and without the presence of objective function in eq. (3.11), the threshold of $SLL \leq$

$\{-20, -25, -30, -35, -40, -45, -50\}$ [dB], and more than 80 radiation patterns created.

The whole synthesis procedure of the array, using the personal computer having 2.5 GHz CPU and a 8 GB RAM, needed average time of around one minute. Each single CP optimization requires a few seconds to finish the job. This short and efficient in computation time allows the CP procedure to quick determine the δf such that maximize the FBW for a fixed value of Q. All of the experiments are carried out by following [54] in order to achieve the maximum FBW for $Q = 6$.

3.3.1.1 Without Notch Filter

In the first step, the proposed strategy is executed with no maximization directivity (D) applied to the CP procedure, it is equivalent to find the intersection only for constraints in eq. (3.12),(3.13),(3.14). In all experiments the results are all fulfilled the constraints. More specifically, in numerical evidence from Tab. 3.1 that shows the achieved radiation performances with respect to SLL, Directivity, and $HPBW$ when the constraints on sidelobes regions less than -30 [dB] applied. The Fig. 3.1 shows the achieved FBW is a function of the enforced SLL. From this figure, it is obviously that there is a price to pay when decreasing the SLL from -20 [dB] to -50 [dB], the FBW also reduces from 1.22 to , respectively. However, the array performances are still guaranteed to operating over an ultra-wide bandwidth.

	D [dB]		$HPBW$ [dB]		SLL [dB]	
	$No\ Max\ D$	$Max\ D$	$No\ Max\ D$	$Maxi\ D$	$No\ Max\ D$	$Max\ D$
$f_1 = f_{max}$	14.46	14.60	3.93	3.79	-30.2	-30.0
f_2	13.12	13.36	5.24	5.05	-30.2	-30.0
f_3	12.25	12.40	6.56	6.31	-30.2	-30.0
f_4	10.80	10.94	9.38	9.02	-30.2	-30.0
f_5	10.21	10.37	10.65	10.25	-30.2	-30.0
$f_6 = f_{min}$	9.70	9.86	11.94	11.49	-30.2	-30.0

Table 3.1: Performance for synthesis scenario of $SLL \leq -30$ [dB]

In some applications that require not only FBW but also Directivity performances [87], there is a need for joint optimization of FBW and D to meet the requirement. Therefore, all the previous experiments are repeated with the objective function D that is maximized over a full range of operating frequency. Towards this end, the objective function in eq. (3.17) is minimized together with a set of constraints in eq. (3.18), (3.19), (3.20) are enforced. The Tab. (3.1) is summarized about the achieved results in terms of D, $HPBW$,and SLL for the situation in which the SLL is imposed to less than -30 [dB]. Also, in the Fig.

(3.2) illustrates the amplitude excitations and the far-field radiation patterns obtained for f_{max} and f_{min}. Some notes that the phases is not shown here due to its values are zeros when applying the simplified assumption on the symmetric geometry along broadside direction, and those frequencies between f_{min} and f_{max} also do not depict here for the sake of simplicity.

As can be seen from Tab. (3.1) solving the problem with maximizing D clearly gives a Directivity increase, a slightly increase in SLL, and a slightly drop in $HPBW$ compared to without maximizing D. The trade-off curve between FBW and SLL remain unchanged for the case of maximizing D, then it is not shown here.

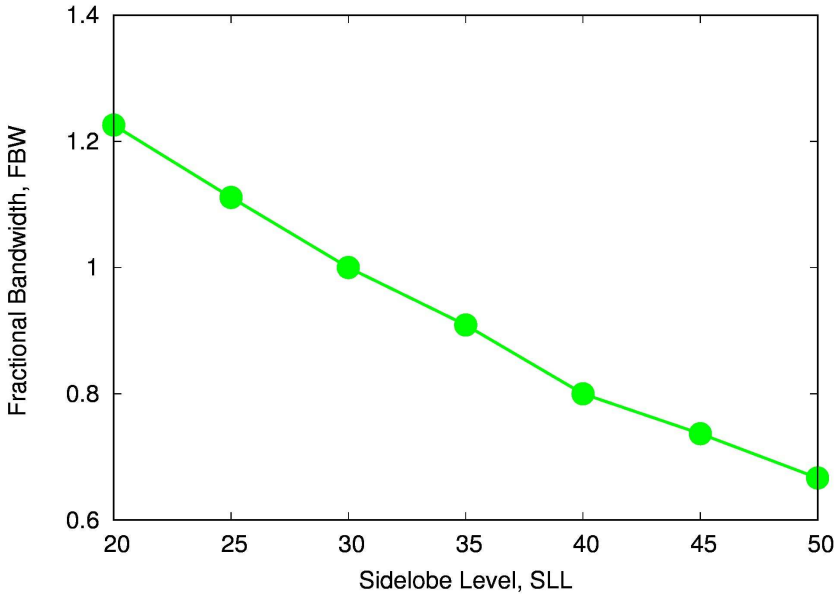

Figure 3.1: Graph showing that the achieved FBW is a function of the constrained SLL. The results are obtained by setting UB in the form of $\Omega = \{\theta | 0^o \leq \theta \leq 75^o \cup 105^o \leq \theta \leq 180^o\}$.For $f_{max} = 2.5$[GHz], reducing the SLL from -20 [dB] to -50 [dB] leading to the decreasing of FBW from 1.22 at $f_{min} = 0.61$ [GHz] to 0.68 at $f_{min} = 1.23$ [GHz]. The array performances are still guaranteed operating over ultra-wide bandwidth.

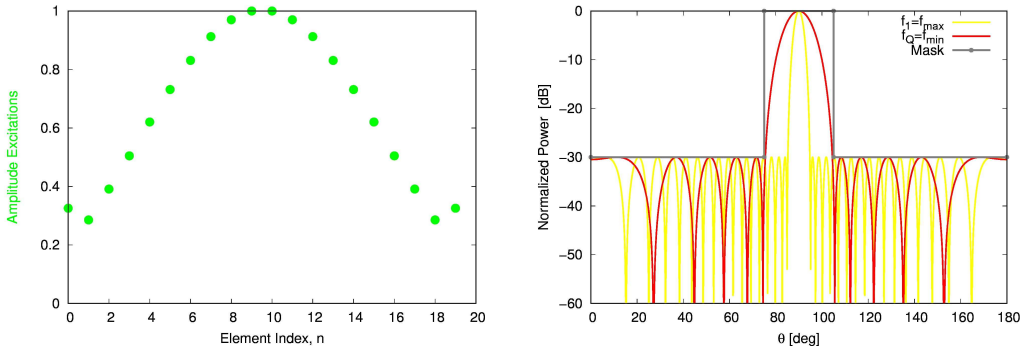

(a) (b)

Figure 3.2: (a) Real and positive excitations and (b) UWB power pattern obtained by enforcing $SLL \leq -30$ [dB] for $\Omega = \{\theta | 0^o \leq \theta \leq 75^o \cup 105^o \leq \theta \leq 180^o\}$ during the maximizing the Directivity (D).

To evaluate the fault tolerance on the radiation patterns in this test case due to the manufacture errors on the excitations, a Monte-Carlo simulation is carried out to analyze the patterns parameters related to the far-field radiation (e.g., SLL, D, and $HPBW$). The simulation is carried out repeatedly 1000 times, in which each time is done by randomly adding noise to the amplitude excitations with a bound ($\pm 5\%$) on each element, and calculating the radiation pattern parameters. Finally, the statistical analysis is reported in Tab. 3.2 for SLL, Tab. 3.3 for D, and Tab. 3.4 for $HPBW$.

In the Tab. 3.2, the mean value of SLL is -28.3 [dB] for six frequencies with standard deviation of 0.6 [dB]. This is equivalent to maximum 7.8% difference from the optimized pattern. In the Tab. 3.3, the mean value of D is very closed to the optimized pattern with very small standard deviation of 0.02 [dB] for six frequency. This is equivalent to maximum 1% difference from the optimized pattern. In the Tab. 3.4, the mean value of $HPBW$ is very closed to the optimized pattern with very small standard deviation of 0.02 [dB]. This is equivalent to maximum 1% difference from the optimized pattern.

	min	max	$mean$	std
$f_1 = f_{max}$	-29.48	-26.32	-28.21	0.56
f_2	-29.46	-26.32	-28.21	0.56
f_3	-29.47	-26.33	-28.22	0.56
f_4	-29.83	-26.33	-28.26	0.63
f_5	-29.87	-26.33	-28.37	0.64
$f_Q = f_{min}$	-30.03	-26.33	-28.37	0.64

Table 3.2: SLL [dB] - Statistical analysis of fault tolerance for Isotropic source broadside radiation

	min	*max*	*mean*	*std*
$f_1 = f_{max}$	14.54	14.64	14.59	0.02
f_2	13.31	13.41	13.36	0.02
f_3	12.34	12.45	12.40	0.02
f_4	10.89	10.99	10.95	0.02
f_5	10.31	10.42	10.37	0.02
$f_Q = f_{min}$	9.80	9.91	9.86	0.02

Table 3.3: D [dB] - Statistical analysis of fault tolerance for Isotropic source broadside radiation

	min	*max*	*mean*	*std*
$f_1 = f_{max}$	3.75	3.83	3.79	0.01
f_2	4.99	5.11	5.05	0.02
f_3	6.25	6.39	6.31	0.02
f_4	8.93	9.13	9.02	0.03
f_5	10.14	10.37	10.24	0.04
$f_Q = f_{min}$	11.37	11.63	11.49	0.04

Table 3.4: $HPBW$ [deg] - Statistical analysis of fault tolerance for Isotropic source broadside radiation

3.3.1.2 With Notch Filter

In the second test, a notch filter is added to the power pattern in the sidelobes regions to assess the effectiveness of the proposed method when dealing with more challenging demand from realistic scenario.

In this case, isotropic elements are deployed, and a notch filter with depth of 10 [dB] and region $\Xi = \{\theta | 30^o \leq \theta \leq 50^o \cup 130^o \leq \theta \leq 150^o\}$ are added to the sidelobe regions in the without notch test case $\Omega = \{\theta | 0^o \leq \theta \leq 75^o \cup 105^o \leq \theta \leq 180^o\}$. This mask constraint are often preferred in those practical applications such as, monopulse radar and communications [69].

To recap the process are done in previous test case Section 3.3.1.1, there are seven SLL from -20 [dB] to -50 [dB] with step size of -5 [dB], and optimization problem is carried out on without adding objective function eq. (3.11) and with adding objective function eq. (3.17). Therefore in total, fourteen experiments will be carried out. In this test, the same process will be applied to find the optimal solution over a possible largest BW.

Due to the non-uniform of the mask when adding the notch filter, this time, to see the effectiveness of the optimization problem all radiation patterns of operating f_{min},f_{max}, and those intermediate frequencies between will be shown.

However, There are more than 80 radiation patterns, then the only hardest constraints when SLL less than -50 [dB] are shown.

The obtained FBW for those discussed requirements are shown in the Fig. (3.3) is a function of the constrained SLL values. It can be evident that reducing the SLL from -20 [dB] causing FBW to drop from 1.18 to 0.63. As a consequences, adding a notch filter to the sidelobes regions induce a small drop in array performance compared to those results reported in Section 3.3.1.1. For example, the maximum FBW decrease from 1.22 to 1.18 and minimum FBW drop from 0.68 to 0.63. Although the performance drops slightly, the UWB array is still guaranteed ($FBW \geq 0.5$) even in case of $SLL = -50$ [dB] with notch.

The Fig. 3.4(b) shows the radiation pattern perfectly satisfied the enforced $SLL = -50$ with notch depth of 10 [dB], while Fig. 3.4(a) provides the optimized amplitudes for the array operating over a wide bandwidth. More specifically in numerical evidence, the Tab. 3.5 shows the achieved results in terms of SLL, $HPBW$, and Directivity.

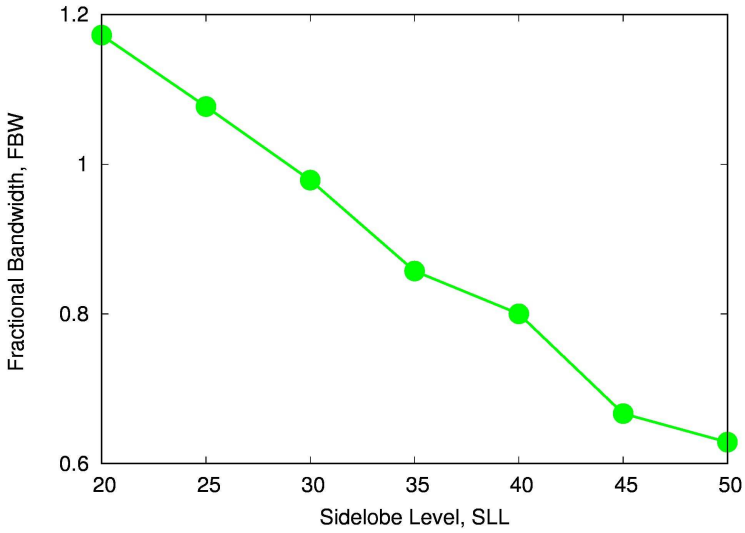

Figure 3.3: The achieved FBW in Section 3.3.1.2 is a function of the enforced SLL plus notches filter constraints. The results are obtained by setting UB in the form of $\Omega = \{\theta | 0^o \leq \theta \leq 75^o \cup 105^o \leq \theta \leq 180^o\}$ added to notch depth of 10 [dB] at $\Xi = \{\theta | 30^o \leq \theta \leq 50^o \cup 130^o \leq \theta \leq 150^o\}$. For $f_{max} = 2.5$[GHz], decreasing the SLL from -20 [dB] to -50 [dB] results in the decreasing of FBW from 1.18 at $f_{min} = 0.64$ [GHz] to 0.63 at $f_{min} = 1.30$ [GHz]. The array performances are still guaranteed operating over ultra-wide bandwidth.

	D [dB]		$HPBW$ [dB]		SLL [dB]	
	$No\ Max\ D$	$Max\ D$	$No\ Max\ D$	$Maxi\ D$	$No\ Max\ D$	$Max\ D$
$f_1 = f_{max}$	13.42	13.54	4.85	4.78	−50.1	−50.0
f_2	12.17	12.28	6.47	6.37	−50.1	−50.0
f_3	11.66	11.77	7.36	7.20	−50.1	−50.0
f_4	11.19	11.32	8.10	7.97	−50.1	−50.0
f_5	10.78	10.90	9.00	8.86	−50.1	−50.0
$f_6 = f_{min}$	10.59	10.70	9.34	9.22	−50.1	−50.0

Table 3.5: Performance for synthesis scenario of $SLL \leq -50$ [dB]

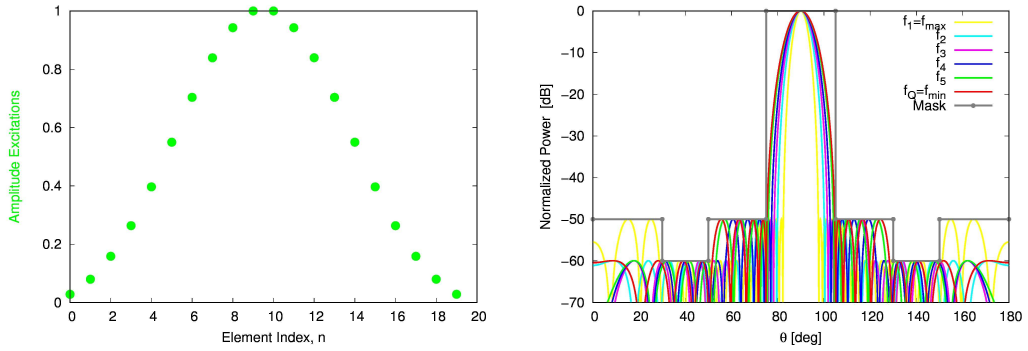

(a) (b)

Figure 3.4: (a) Real and positive excitations and (b) UWB power pattern obtained by enforcing $SLL \leq -50$ [dB] for $\Omega = \{\theta | 0^o \leq \theta \leq 75^o \cup 105^o \leq \theta \leq 180^o\}$and notch filter of depth 10 [dB] at $\Xi = \{\theta | 30^o \leq \theta \leq 50^o \cup 130^o \leq \theta \leq 150^o\}$ during the maximizing the Directivity (D).

3.3.2 Full-Wave Test Case

In this test, a full-wave synthesis using UWB microstrip patch antennas arrays is conducted. More in detail, the antenna structure and the specifications used in this test is the same with that of previous section (Section 3.3.1.1), such as $SLL \leq -30$ [dB], $Q = 6$, $f_{min} = 0.8$ [GHz], $f_{max} = 2.5$ [GHz], and the array described in Fig. 3.5 and Tab. 3.6. The isotropic radiating system now is converted to the patch radiating systems in CST^{TM} simulations. In order to make it more closer to the practical implementation, the substrate below each element and between elements (or neighboring elements) are extended to a single substrate layer Fig. 3.5(b).

In this case, the designed realistic radiators are utilized to verify the robustness of the proposed synthesis methodology. In addition, the radiating element array are fed by the excitations shown in Fig. 3.2(a). Towards this end, an microstrip patch array is deployed (see Fig. 3.5), and characterized by a list

of parameters in Tab. 3.6. Then, the CST^{TM} full-wave simulation are used to compute the radiated power patterns for the cases with $Q = 6$, and the far-field radiation patterns are shown in Fig. 3.6. It is very noticeable that the far-field radiation pattern behaviour here is likely to similar to that of the isotropic broadside radiation pattern in Fig. 3.2(b). More in detail, the realistic patch antenna array guaranteed the UWB performance (e.g., $f_{min} = 0.8$ [GHz] and $FBW = 1.03 > 0.5$) while the SLL is enforced to be less than -30 [dB].

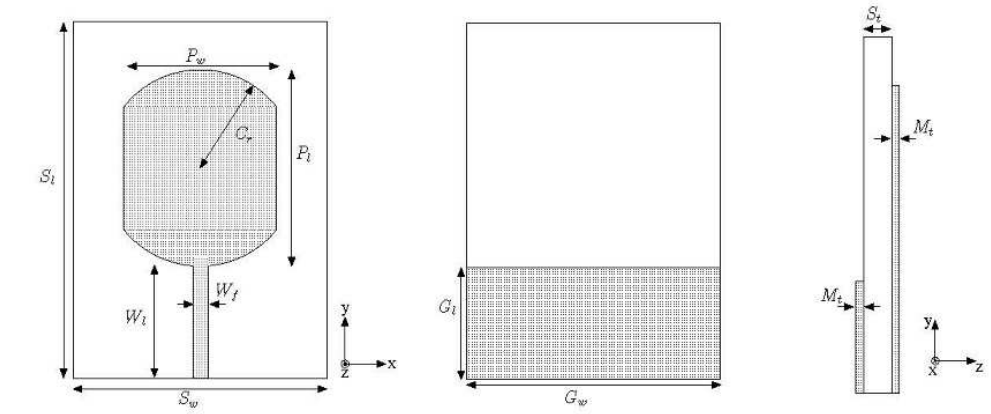

(a)

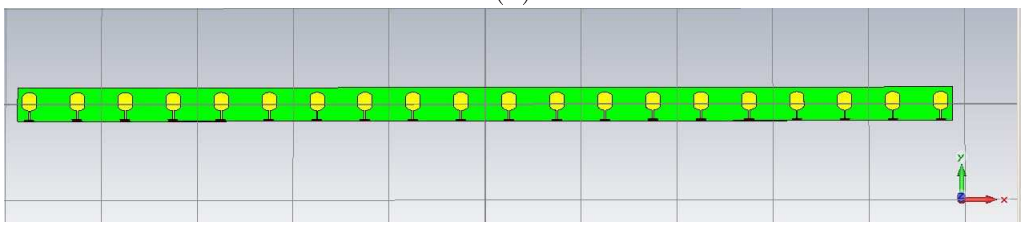

(b)

Figure 3.5: Microstrip array simulated using the CST^{TM} full-wave software: (a) front, bottom, and side views from single radiating element, and (b) overall array of the radiating elements view

Acronym	Meaning	Value
S_l	Substrate length	70 mm
S_w	Substrate width	50 mm
S_t	Substrate thickness	1.6 mm
P_l	Patch length	38.4 mm
P_w	Patch width	30 mm
C_r	Cutting radius	19.2 mm
W_l	Feeding line length	22 mm
W_f	Feeding line width	3 mm
G_l	Ground plane length	22mm
G_w	Ground plane width	50mm
M_t	Metal thickness	0.035mm
ε_r	Relative permitivity	4.3 F/m
μ_r	Relative permeability	1 H/m
$tan\delta$	Dielectric loss tangent	0.025
d	inter-element spacing	15×10^{-2}m

Table 3.6: Geometrical and Electrical Parameters of the Microstrip Antenna Depicted in Fig. 3.5

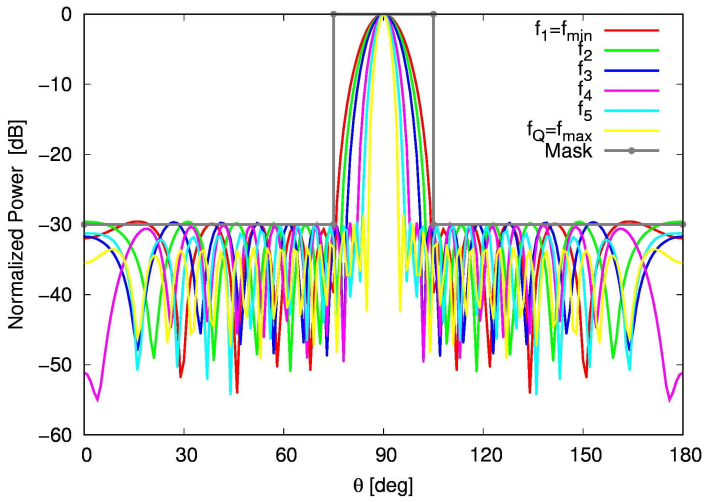

Figure 3.6: The UWB radiation pattern, calculated by CST^{TM} full-wave simulations, generated by the array antenna in Fig. 3.5(b) when fed by the amplitudes shown in Fig. 3.2(a). The antenna fulfilled the $SLL \leq -30$ [dB] and the UWB performances as well (e..g., $f_{min} = 0.8$ [Ghz], $f_{max} = 2.5$ [GHz], and $FBW = 1.03 > 0.5$)

3.3.3 Isotropic Sources - Non Broadside Radiation

The last set of numerical experiments is carried out to verify the reliability and the effectiveness of the proposed synthesis technique in achieving the UWB performances in the case of non-broadside radiation. Therefore, the example is set up with target radiation direction $\theta_0 = 60^o$[deg], maximum frequency fixed $f_{max} = 10$ [GHz], $\delta f = 365$ [MHz], and required the proposed iterative $CP-$based methodology in eq. (3.17,3.18,3.19,3.20) to determine the optimized excitations guaranteeing $SLL \leq -25$ [dB] for $\Omega = \{\theta | 0^o \leq \theta \leq 40^0 \cup 80^o \leq \theta \leq 180^o\}$, and $Q = 6$, wideband performances with $FBW = 0.201$.

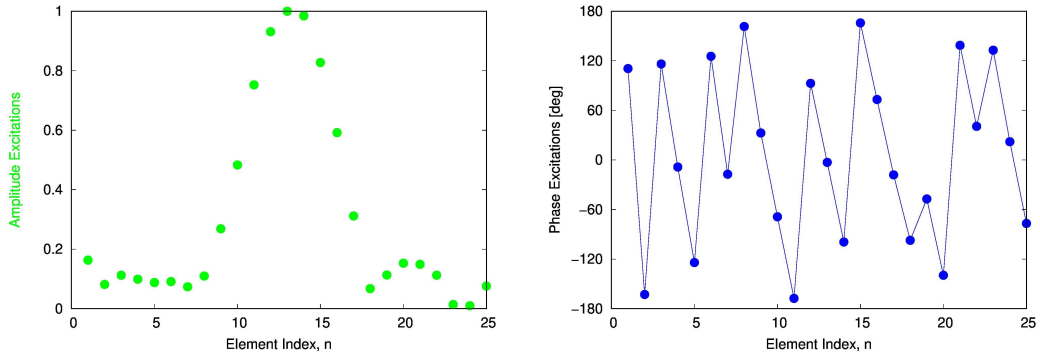

(a) (b)

Figure 3.7: Complex excitations generating a non-broadside radiation for constraints and requirements listed in section 3.3.3: (a) amplitudes, (b) phases distribution.

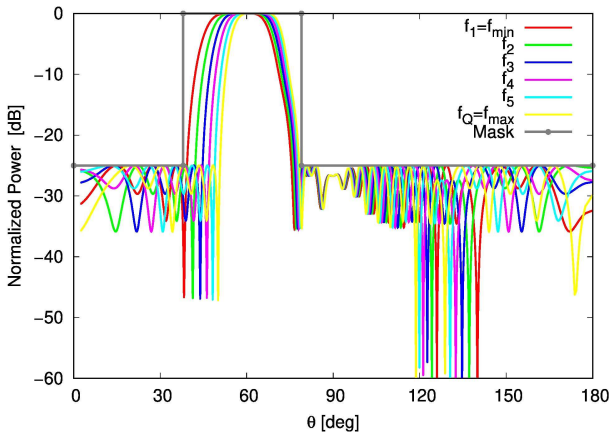

Figure 3.8: Wideband power pattern according to the amplitude and phase excitations in Fig. 3.7. The obtained directivity values are between 7.9 [dB] for $f = f_{min}$ and 8.8 [dB] for $f = f_{max}$.

An array comprised of $N = 25$ isotropic elements with unchanged inter-element spacing $d = 0.5c/f_{min}$ (follows the rules in the Appendix [54]) is selected as the radiating antenna system.

The obtained complex excitations for amplitudes and phases are shown in the Fig. 3.7 (a) and 3.7 (b) , respectively, generate the radiation pattern from Fig. 3.8 that are perfectly fit the unsymmetrical mask.

It is clearly that the propose approach results in fulfillment of all enforced requirements. In addition, because a unique set of common excitations are created for all radiation patterns at different frequencies, there are a slightly, but unavoidable, misalignment of the beams at the target direction. However, the cost and complexity of the beam forming network for the wideband array antenna is reduced dramatically with the frequency-independent set of excitations generating from the iterative $CP-$based strategy, and the flexibility of the system configuration among the different frequencies are introduced as well.

3.4 Conclusion

In this chapter, the innovative approach to cast the synthesis of fixed-geometry array antennas as a sequence of convex optimization, ensuring the maximum possible bandwidth for a fixed SLL mask constraint, has been introduced. A set of examples (e.g., isotropic sources broadside array, isotropic sources non-broadside array, and full-wave simulation) have been carried out in order to assess the capability of designing a optimal wideband array with low SLL values and high directivity array. The achieved results of the array synthesis are not only optimal, but also in efficiently computational time executions. In addition, to evaluate the manufacture errors on the excitations, the Monte Carlo simulation is deployed to do statistical analysis on the radiation patterns results which are quite similar to the optimized performance.

Chapter 4

Wideband Monopulse Synthesis

In this chapter, an efficient and innovative strategy for the synthesis of optimal monopulse array operating simultaneously at multiple frequencies in the band of interest is presented. In addition, the fixed-geometry array is able to produce an optimal sum pattern and a compromised optimal difference pattern with arbitrary upper-bound constraints enforcing on the patterns and a number of common/sharing amplitudes between two patterns. Moreover, the proposed strategy is formulated to maximize the directivity of the sum pattern and the slope of the difference beam along the bore-sight direction to possibly increase the performance of the monopulse. The convex programming is progressively utilized in the proposed procedure in order to determine the optimal weights, including sharing amplitude weights and possibly largest operating bandwidth fulfilling user-defined mask constraints on far-field radiation of the sum and difference patterns.

4.1 Introduction

The synthesis of focus and difference patterns from an array antenna aperture is one of the important approaches in tracking radar systems, such as monopulse technique (see in [1][56][69][88][89]). The best sensitivity of the tracking radar (e.g., the smallest angular errors) can be obtained if some constraints and requirements are enforced on the radiation patterns, such as the maximum directivity for the pencil pattern, and the possibly highest difference slope.

If sum and difference patterns are synthesized independently, the cost for fabrication the array and complexity of the beam forming network are likely to increase dramatically. Therefore in many scenarios, a few approaches together with joint synthesis of sum and difference patterns were deployed in literature to overcome the above-mentioned limitations. Firstly, in [90], the author exploited the grouping strategy to gather the array elements into many clusters to simplify the circuit complexity. To this end, one of the beam patterns is synthesized, and then the other beam pattern is realized by properly selecting the excitations from each subarray in the partition array. Furthermore, in [91], sum and difference beams are jointly synthesized by using differential evolution optimization with subarray strategy while enforcing some constraints on the far-field radiation patterns. Secondly, compromised synthesis of sum and difference patterns was conducted (see [56][69][92]) to produce an optimal sum and sub-optimal difference while partially sharing the amplitude excitations at the tails of the array. More in detail, the optimal focus beam is achieved by maximizing the directivity (D) along the boresight direction while the sub-optimal difference beam is obtained by iteratively tuning the rate of difference slope along the target direction to the possible largest value.

Despite of effectiveness in simplifying the beam-forming network of the monopulse radar, all the aforementioned works designed the monopulse antenna array operating at single frequency. This implies that the monopulse tracking system is likely to degrade the performance and operate improperly when dealing with many different frequencies.

Extending the spirit in the work [56] for the simplification of array architecture, this chapter aims at overcoming the limitations in narrow bandwidth operation by proposing an innovative strategy based on convex optimization CP for synthesizing monopulse arrays operating over multiple frequencies. The proposed approach overcomes the issue by finding an optimal array excitations fulfilling the user-defined upper-bound masks on the sum and difference patterns simultaneously at different frequencies. The possible largest bandwidth is obtained by progressively applying the $CP-$based array optimization in an iterative loop.

4.2 Mathematical Formulation

Considering an array of all isotropic antenna elements ($N = 2P$, $p = 1, 2, ..., P$) is located along $z-axis$ with equal spacing between adjacent pairs d. The array is also centro-symmetric that means if there is an element positioned at $(0, 0, z_p)$, there is always another element located at $(0, 0, z_{-p})$, $m = 1, 2, ..., P$ being the index of element in the considering array.

Under the assumption, the array factor of the sum pattern 4.1 and difference pattern 4.2 at considering frequency f can be defined as follows:

$$F^{\Sigma}(\theta, f) = \sum_{p=-P, p\neq 0}^{P} a_p^{\sum} e^{\frac{2\pi}{c} f z_p cos(\theta)} \tag{4.1}$$

$$F^{\Delta}(\theta, f) = \sum_{p=-P, p\neq 0}^{P} a_p^{\Delta} e^{\frac{2\pi}{c} f z_p cos(\theta)}, \tag{4.2}$$

wherein, f is the operating frequency of the considering array, c is speed of light in vacuum, θ is the angular direction between the $z-axis$ and any point in space, z_p $(p = -P, ..., -1, 1, ..., P)$ is the location of $p-th$ element in the array, $a^{\Sigma} = \{a_p^{\sum}, p = -P, ..., -1, 1, ..., P\}$ represents the vectors of weights in order to generate sum pattern, and $a^{\Delta} = \{a_p^{\Delta}, p = -P, ..., -1, 1, ..., P\}$ denotes for the excitations for producing the difference pattern.

In [97], the main idea is that the center distribution of the amplitude excitations of sum and difference radiation patterns is likely to be huge different. Therefore, the amplitude excitations of array elements at the tail of the array are shared between sum and difference patterns in order to decrease the complexity of the beam-forming network and fabrication cost Fig. 4.1. The number of shared elements between two patterns is defined by nearby peripheral elements with indices $|p|$ no less than a threshold η_s $(0 < \eta_s \leq P)$.

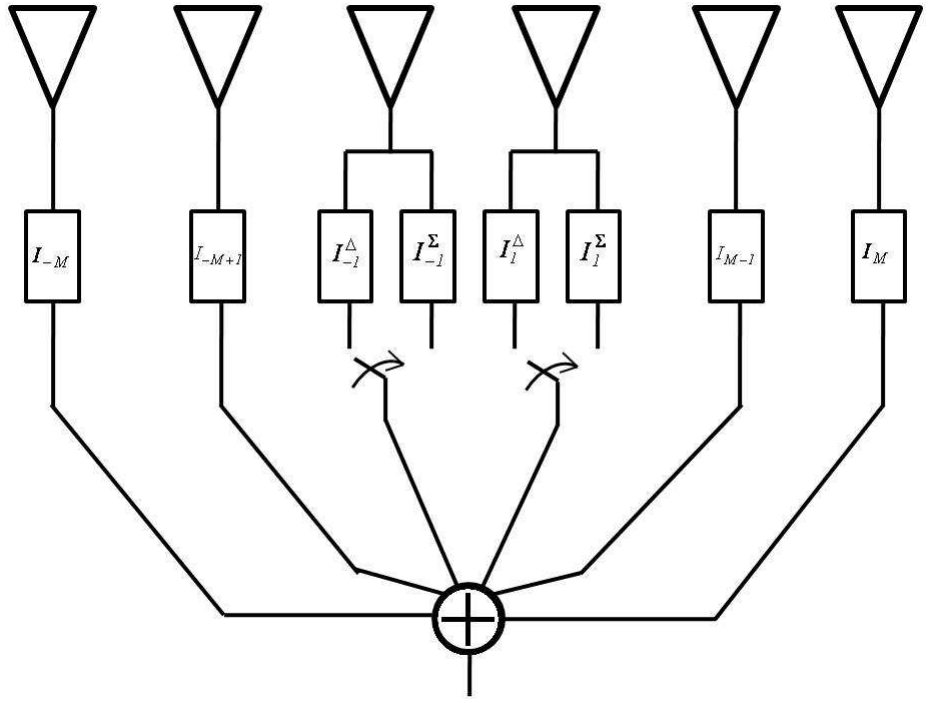

Figure 4.1: Geometry array showing the center elements shifted to generate sum and difference patterns

The goal of the joint synthesis of the focus and difference patterns is to define the a set of excitations $a^{\Sigma}$and a^{Δ}under several constraints on far-field radiation patterns. For example, the shared amplitudes of the peripheral elements in order to make the beam-forming network simpler to fabricate. Furthermore, the directivity of the focus pattern 4.10 is maximized while imposing the sidelobe level (SLL) to be less than the arbitrary level of the upper mask. In addition, the slope of difference pattern $\left(\frac{\partial F^{\Delta}(\theta_0,f)}{\partial \theta_0}\right)$, along the boresight direction θ_0, is compromised optimal while region outside of the main lobe is subject to the user-defined upper bound. To guarantee the generation of difference pattern, the sign of the left half of the excitations is changed to opposite with respect to the right half such that: $a^{\Delta} = \{a^{\Delta}_{p} = -a^{\Delta}_{-p},\, p = 1, 2, ..., P\}$. Last but not least, the monopulse systems is designed in a way such that it is able to operate over multiple frequencies in the band of interest $BW = [f_{min} : f_{max}]$.

Extended the achieved results in the [56], the Convex programming CP-based procedure can be recast to multiple frequencies as follows:

$$
\begin{aligned}
&\textit{Maximize} && \Upsilon(\theta_0, f_1) && && (4.3)\\
&\textit{Subject to} && \tfrac{\delta F^{\Delta}(\theta_0, f_q)}{\delta \theta_0} \geq A && \theta = \theta_0\,, q = 1, 2, ..., Q && (4.4)\\
& && I_p^{\Sigma}(f_q) = I_p^{\Delta}(f_q) && |p| \geq \eta_s\,, \eta_s > 0\,, q = 1, 2, ..., Q && (4.5)\\
& && |F^{\Sigma}(\theta_i, f_q)|^2 \leq UB^{\Sigma}(\theta_i) && i = 1, 2, ..., K\,, q = 1, 2, ..., Q && (4.6)\\
& && |F^{\Sigma}(\theta_j, f_q)|^2 \leq UB^{\Delta}(\theta_j) && j = 1, 2, ..., K\,, q = 1, 2, ..., Q && (4.7)\\
& && a_{-p}^{\Sigma}(f_q) = a_p^{\Sigma}(f_q) && p = 1, 2, ..., P\,, q = 1, 2, ..., Q && (4.8)\\
& && a_p^{\Delta}(f_q) = -a_{-p}^{\Delta}(f_q) && p = 1, 2, ...P\,, q = 1, 2, ..., Q, && (4.9)
\end{aligned}
$$

wherein, the objective function in 4.3 is defined as:

$$\Upsilon(\theta, f_0) = \frac{4\pi \left|G^{\Sigma}(\theta_0, f_1)\right|^2}{2\pi \int_{\theta=0}^{\pi} \left|G^{\Sigma}(\theta, f_1)\right|^2 sin(\theta) d\theta}, \tag{4.10}$$

and $f_1$is the maximum frequency in the band of interest, $I_p = a_p$, K is the total sampling samples in the angular domain, Q is the total number of frequencies, A is the variant value to control the slope of the difference pattern, and $UB^{\Sigma}(\theta)$ and $UB^{\Delta}(\theta)$ represent for the upper-bound constraints imposing on the sum and difference pattern, respectively.

In order to define BW or fractional bandwidth (FBN) [48], two extreme frequencies must be defined through the process defined in [54]. The right extreme frequency (f_{max}) is achieved by progressively carrying out the convex programming based (CP-based) procedure with single frequency f until the grating lobe appear [1]. After computation of f_{max}, to determine where is the minimum frequency (f_{min}), the CP-based procedure is iteratively applied within a loop with starting at $f_q = f_{max}$ with $q = 1$ and keep adding lower frequency $f_q = f_q - \delta f$ with $q = q + 1$ in the next iteration into CP-based procedure, wherein δf is user-defined frequency step. The iterative procedure ends when the constraints in the loop is not valid. Let assume that $q = Q + 1$ is the index in which the procedure halts, then the minimum frequency can be defined as $f_{min} = f_Q$.

According to [56], the Eq. 4.4, 4.5, 4.6, 4.7, 4.8, 4.9 are convex over the convex set. In addition, the objective function in Eq. 4.3 is also the convex in. Therefore, the whole CP-based procedure is maximization of a convex objective function over a convex set and this procedure can be solved by using any convex programming.

4.3 Numerical Results

The maximization of the CP-based procedure from eq. (4.3) to (4.9) are carried out by using the available CVX software [93] to solve optimally for the excitations for the monopulse antenna. This section carried out two isotropic example and report one test example using full-wave CST^{TM} simulation to confirm the proposed synthesis. A number of test cases has been performed for isotropic for an array of $N = 10$ elements and extended to larger array of $N = 20$ elements.

4.3.1 Isotropic Sources

In the first example, a joint synthesis of two patterns involves with a isotropic linear array of $N = 10$ elements used in [56], (the inter-element spacing between any two adjacent elements are fixed to $d = 0.025$ [m]) with total of six shared amplitude excitations accounting for 60% of total number of elements in sum and difference patterns ($\eta_s = 3$). The upper-bound mask imposing on the sum pattern has null-to-null width of 30.4 [deg] (or main beamwidth equal to 30.4 [deg]) and the enforcing SLL value of -24 [dB] outside of the mainlobe region or ($SLL = -24$ [dB]). In the similar way, the setting parameters for the difference pattern are provided as null-to-null width value of 52 [deg] and $SLL = -18.8$ [dB]. In [56], the linear array produces sum and difference pattern operating at single frequency according to $\lambda_0 = c \times f_0$. Therefore, to improve the flexibility of the array in terms of bandwidth, this experiment uses the iterative CP-based procedure proposed in eq. (4.3) to eq. (4.7). As a results, the Fig. 4.2 shows the amplitude and phase excitations of the considering sum and difference arrays when using the proposed $CP-$based strategy. These set of excitations are used to generate the sum patterns of six frequencies in the Fig. 4.3(a) and difference patterns of six frequencies in Fig. 4.3(b). As it can be seen, the sidelobe regions of sum and difference patterns for over six frequencies are fulfilled the enforcing SLL. More specifically, SLL^{Σ} is below -30 [dB], and the SLL^{Δ} is under 20 [dB].

More in numerical detail, maximum frequency $f_1 = f_{max} = 8.9$ [GHz] is found to avoid the appearance of gratings lobes in the visible domain, the minimum $f_{min} = f_Q = 6$ [GHz] is determined in the iterative loop, and sampling (intermediate) frequencies $f_p = f_{max} - (q-1)\delta f$, $q = 2, ..., Q$ with $Q = 6$ are also optimally found. In addition, two sets of excitations for sum and difference pattern also presented in Tab. 4.1 (for the sake of simplicity, only a half of excitations are reported due to its symmetric behaviour). As shown in the Tab. 4.2, the sum pattern has the highest directivity value of 11.14 [dB] at $f_1 = f_{max}$and minimum directivity 9.22 [dB] at $f_Q = f_{min}$, while the difference pattern has the highest bore-sight slope of 1.04 [1/rad] at the $f_1 = f_{max}$ and the lowest bore-sight slope of 0.85 [1/rad] at the $f_Q = f_{min}$.

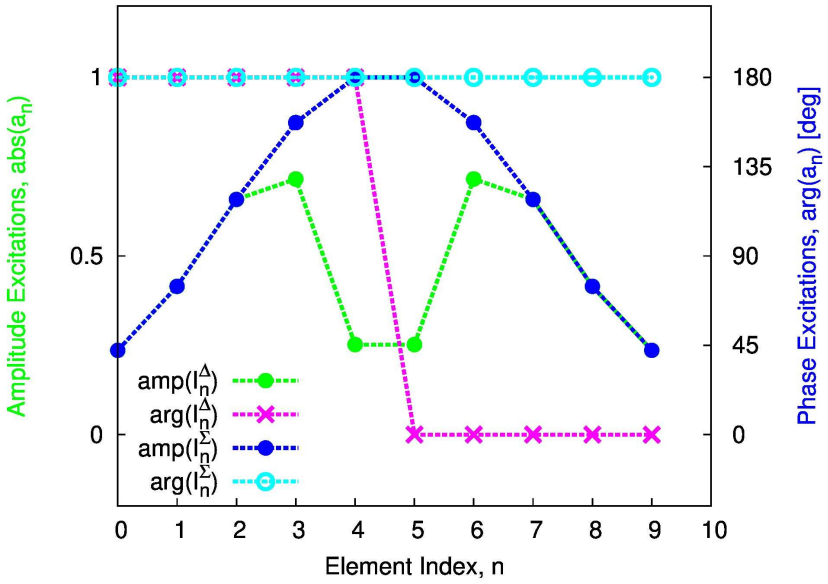

Figure 4.2: Weight coefficients resulted from synthesis for an array of total number of $N = 10$ elements with equal inter-element spacing ($d_s = 0.025$ [m]). The dot-blue and dot-green points represent for the amplitude of each element in the array, which are partially shared by elements in the peripheral elements. The circle-cyan and the cross-pink represent for the phases of each element in the array.

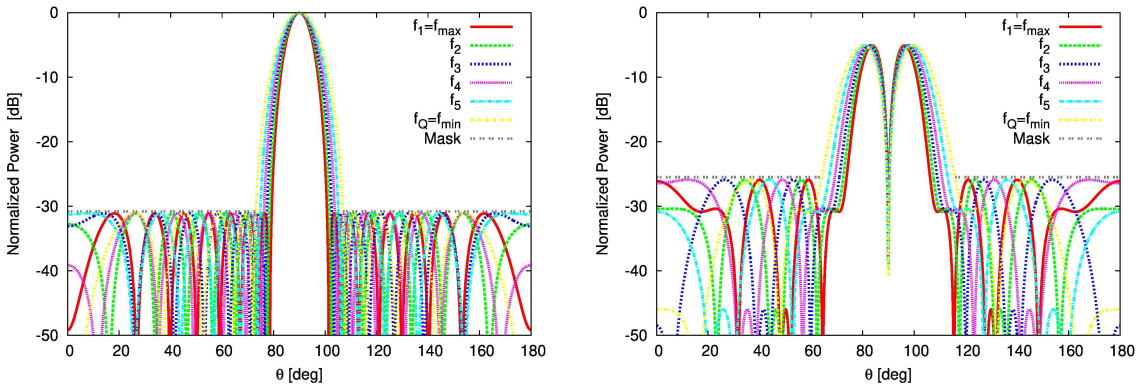

(a) (b)

Figure 4.3: Sum pattern (a) and difference pattern (b) generated by the distribution currents in Fig. 4.2 fed into an linear array comprised of $N = 10$ elements with equally spaced elements. As in Fig. 4.3, the dashed curve represents for the maximum allowed sidelobe level (SLL)

m	a^{Σ}	a^{Δ}
1	1.000	0.252
2	0.874	0.716
3	0.658	0.658
4	0.415	0.415
5	0.236	0.236

Table 4.1: Excitation coefficients for $\eta_s = 3$ corresponding to the radiation performances shown in Fig. 3

f	SLL^{Σ} [dB]	SLL^{Δ}[dB]	D^{Σ}_{max} [dB]	$K_{bs}[1/rad]$
$f_1 = f_{max}$	-31.06	-20.82	11.14	1.04
f_2	-31.06	-20.82	10.82	1.01
f_3	-31.06	-20.82	10.47	0.98
f_4	-31.06	-20.82	10.10	0.94
f_5	-31.06	-20.82	9.68	0.90
$f_Q = f_{min}$	-31.06	-20.82	9.22	0.85

Table 4.2: Patterns parameters when $N = 10$, $d_s = 0.025$ [m],$\eta_s = 3$, and $Q = 6$

To validate the performance of the linear array when applied the proposed method dealing with the change of degree of freedom (DoF) (e.g., the total number of the common amplitude excitations at the peripheral of the array varied to 40% ($\eta_s = 2$) and 80% ($\eta_s = 4$)), the constraints on the patterns and geometry structure in the first test is kept unchanged in this example (e.g. $N = 10$, $d_s = 0.025$ [m]). The proposed method in eq. (4.3) to eq. (4.9), provides the new variable is bandwidth BW (or FBW), then increases the choice between the overall number of elements, the number of common excitations, the SLL, and the bandwidth B. As shown in Tab. 4.3, the values of SLL^{Σ} is around -30 [dB], SLL^{Δ} is in range of -20 [dB] when η_s is varied from $2, 3, 4$. On the other hand, the FBW is reduced from 0.401 to 0.295 when η_s increases from 2 to 4.

η_s	SLL^{Σ} [dB]	SLL^{Δ}[dB]	FBW	BW
$\eta_s = 2$	-30.03	-20.80	0.401	$[6.0, 8.9]$ [GHz]
$\eta_s = 3$	-31.06	-20.82	0.345	$[6.0, 8.5]$ [GHz]
$\eta_s = 4$	-30.18	-20.40	0.295	$[6.6, 8.0]$ [GHz]

Table 4.3: Patterns parameters when $N = 10$, $d_s = 0.025$ [m], and $\eta_s = 2, 3, 4$

For the sake of simplicity, the test case of isotropic with $N = 20$ elements are not shown here. However, there is an interesting note about the FBW when

the number of elements are increasing. The Fig. 4.4 shows that, when the total number of the array increase, the FBW also improves.

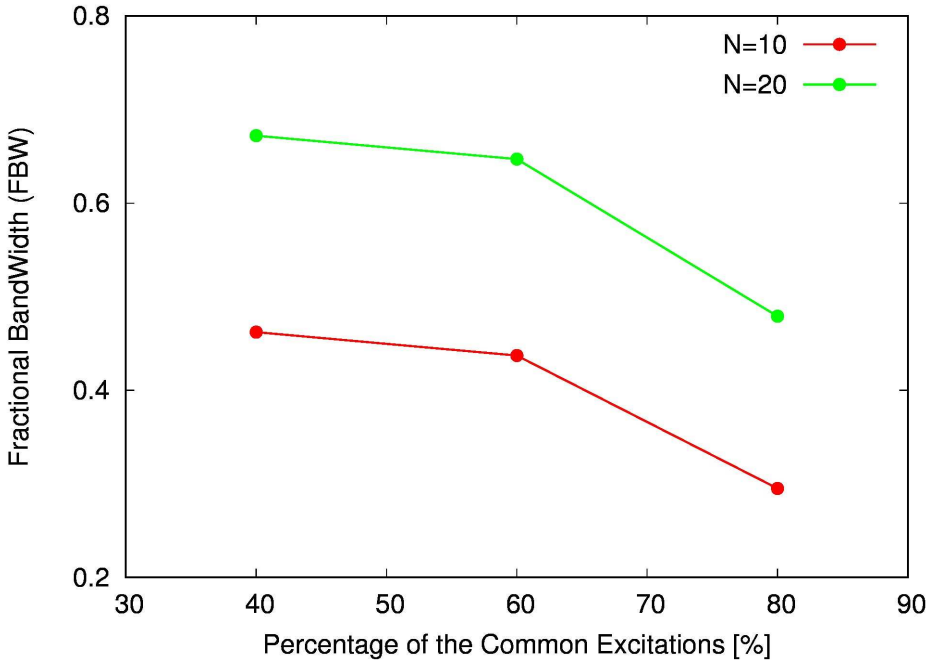

Figure 4.4: The graph shows the relation between the fractional bandwidth (FBW) and the overall number of common excitations of sum and difference pattern in two test cases $N = 10$ and $N = 20$. The solid-red line shows the fractional bandwidth versus the percentage of the common excitation in the array of $N = 10$ elements, while the solid-green line depicts the percentage of bandwidth versus the ratio of common excitations.

In the final test of isotropic sources, to evaluate the effectiveness of the proposed method, the array geometry is used the same as in [56] with $N = 20$, $\eta_s = 6$, $d = 0.025$ [m]. Moreover, two notch filters are added to the user-defined upper bound at position centered at $\theta = 53$ [deg] and $\theta = 127$ [deg] with the notch depth value of 14 [deg] and notch width value of 20 [dB]. The synthesis is conducted and the results are presented in the Fig. 4.5 and Fig. 4.6. The Fig. 4.6 illustrates that the difference between the lowest and highest level among the side lobes in the suppression region is lower than 20 [dB], which confirms the effectiveness and robustness of the proposed method.

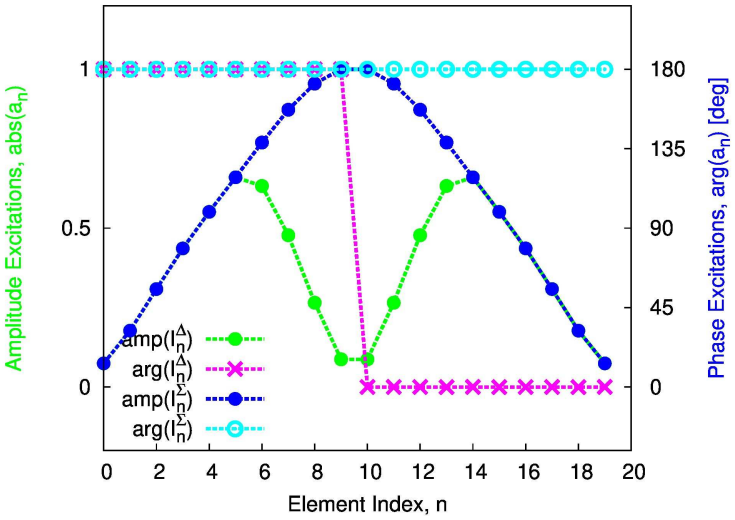

Figure 4.5: Weight coefficients resulted from synthesis for an array of total number of $N = 20$ elements with equal inter-element spacing ($d_s = 0.025$ [m])

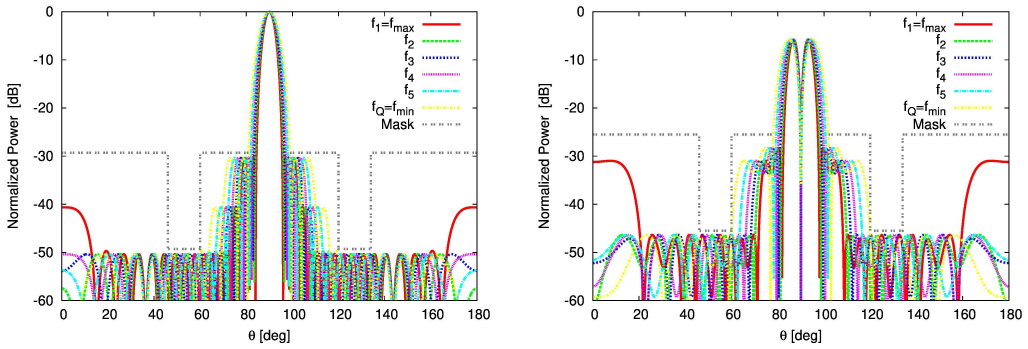

(a) (b)

Figure 4.6: Sum pattern (a) and difference pattern (b) generated by the distribution currents in Fig. 4.5 fed into an linear array comprised of $N = 20$ elements with equally spaced elements. As in Fig. 4.6, the dashed curve represents for the maximum allowed sidelobe level (SLL) with two depression regions centered at $\theta = 53$ [deg] and $\theta = 127$ [deg]

4.3.2 Full-Wave CST^{TM} simulation

In this part, in order to verify the results from the UWB synthesis using $CP-$based procedure proposed in Section 4.2, a full-wave CST^{TM} simulation is carried out on the realistic patch array antenna operating at wideband instead of using isotropic array antenna that is not really exist in the real scenario. Indeed, for the isotropic element, the radiated power is equal in all directions, however the patch element used in Fig. 4.7 the radiation is more complicated and focus on preferred directions.

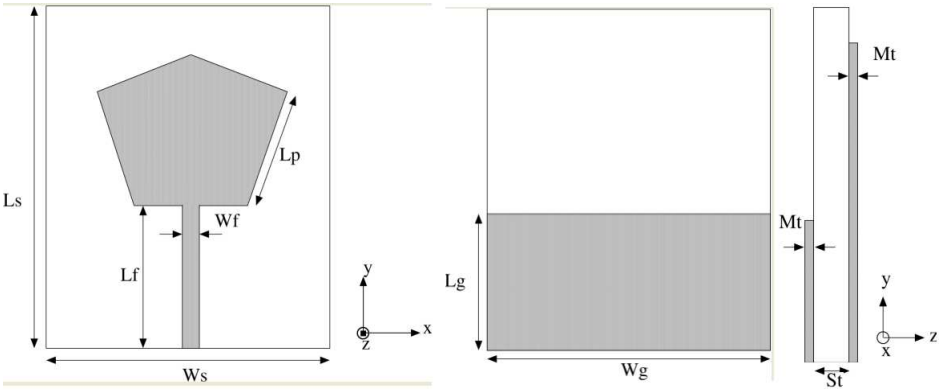

(a)

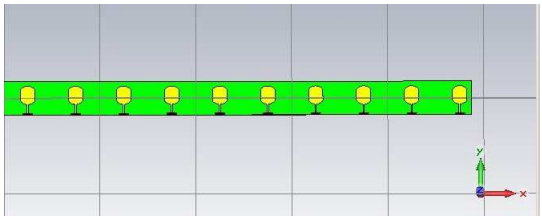

(b)

Figure 4.7: Microstrip array simulated using the CST^{TM} full-wave software: (a) front, bottom, and side views from single radiating element, and (b) overall array of the radiating elements view

More specific, starting from the antenna structure and specifications mentioned in the section 4.3.1. For example, for $\sum-$pattern the null-to-null beamwidth 30.4 [deg], the enforced SLL is less than -24 [dB], for the $\Delta-$pattern the null-to-null beamwidth 52 [deg], and the imposed SLL is lower than -18.8 [dB], $Q = 6$, $f_{max} = 8.9$ [GHz], $f_{min} = 6$ [GHz], and the array described in Fig. 4.7, Tab. 4.4. One more notice that the substrate below the metal part for each antenna is extended to connected to each other to make it more practical implementation.

Acronym	Meaning	Value
L_s	Substrate length	30 mm
W_s	Substrate width	25 mm
L_f	Feedline length	10.5 mm
W_f	Feedline width	3.08 mm
L_p	Pentagon side length	10.5 mm
L_g	Ground length	9.5 mm
W_g	Ground width	25 mm
M_t	Metal thickness	1.5 mm
S_t	Substrate thickness	0.8mm
ε_r	Relative permitivity	4.4 F/m
μ_r	Relative permeability	1 H/m
$tan\delta$	Dielectric loss tangent	0.025
d	inter-element spacing	25×10^{-2}m

Table 4.4: Geometrical and Electrical Parameters of the Microstrip Antenna Depicted in Fig. 4.7(a)

Finally, the patch array in Fig. 4.7(b) is fed by the excitations obtained in Fig. 4.2. As a consequence, the result shown in Fig. 4.8 satisfying for SLL and null-to-null width for sum and difference patterns.

4.4 Conclusions

An innovative method for synthesis of the sum and difference pattern used in monopulse radar systems operating at multiple frequencies with sharing a number of elements at the tail of the array has been presented and analyzed. The convex optimization is used in CP-based procedure to provide the optimal excitations including common parts for both patterns. The strategy enables the monopulse systems to operate over a wide bandwidth and manage user-defined bounds on sum and difference pattern. A set of numerical results are shown to prove the effectiveness of the proposed method.

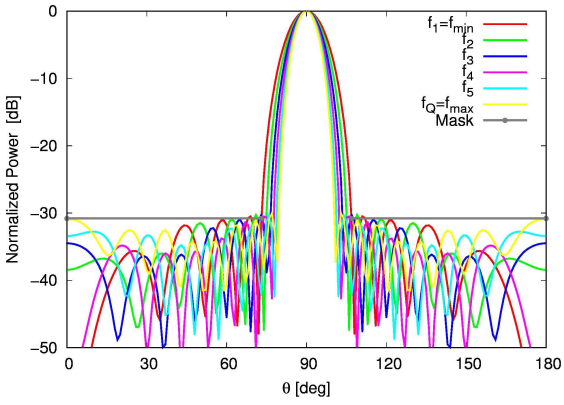

(a)

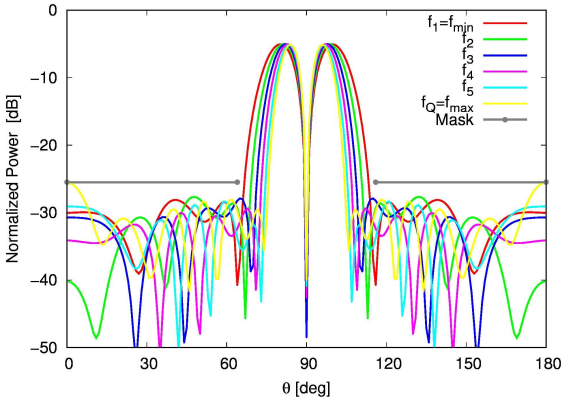

(b)

Figure 4.8: The UWB radiation pattern, calculated by CST^{TM} full-wave simulations, generated by the array antenna in Fig. 4.7(b) when fed by the amplitudes shown in Fig. 4.2(a). The antenna fulfilled the $SLL^{\Sigma} \leq -24$ [dB], $SLL^{\Delta} \leq -18.8$, and the WB performances as well (e..g., $f_{min} = 6$ [Ghz], $f_{max} = 8.9$ [GHz], and $FBW = 0.4$)

Chapter 5

Wideband Shape Beam Synthesis

In this chapter, given the array layout, the objective is optimization of excitations (amplitudes and phases) in order to fit a set of requirements and constraints on the radiated field in order to generate a desired shaped beam including flat-top beam, cosecant beam and Iso-flux. The synthesis is performed over the square array factor or radiation power using technique in [86] and the synthesized array is able to generate shaped-beam operating over multi-frequencies using the two-step method in [54]. Finally, some examples on Flattop shaped-beam pattern and Cosecant shaped-radiation pattern has been presented to show the effectiveness and reliability of the proposed method.

5.1 Introduction

The synthesis of shaped-patterns is very popular problem [3] and its application is applied to many fields such as radar systems, remote sensing, communications systems. The shaped-beam synthesis are often related to the power pattern synthesis where the phases are arbitrary. In addition, the synthesis also requires constraints to simultaneously impose the upper and lower bounds of the main-lobe. Therefore, the shaped-beam problem is often non-convex and may have many solutions.

To deal with non-linearity and non-convex problem in shaped-beam synthesis, a flexible way was proposed, using so called "global" optimum method such as GA in [94], to successfully synthesize the shaped-pattern. However, this method is very inefficient in computation and slow due to its stochastic property. Unlike the stochastic methods, there are also many other deterministic approaches that have successfully synthesized the shaped-beam patterns such as Iterative projection method in[95], the least square methods in[96], the deterministic strategies[97].

The shaped-beam synthesis based on convex optimization problem has only a few works in research literature. For example, in [60], the author used the conjugate symmetric beam-forming weights method to cancel out the non-convex lower bound constraints on the radiation patterns. By doing this, an complex-valued array factor can be recast as a real-valued array factor that is just a linear combination of weights in affine form that can be applied the lower bound constraints and the synthesis problem now convex over convex set. In [98][99] the authors overcome the non-convex lower bound constraints by using the array weight auto-correlation sequence. However, this method is restricted to the uniformly linear array. Furthermore, in [101], the sequential convex optimization method was successfully applied to the shaped-beam pattern for arbitrary mask imposing on the shaped radiation patterns.

To overcome the non-convex set when applying the lower bound on the square array factor, in [85] the the efficient two-step method are proposed. In the first step the author converted the square array factor into another form of representation in which the power pattern is just a linear combination of new weights in new domain and $\{sin(.), cosine(.)\}$. Because the power pattern now just a linear functions in new domain, therefore the convex programming can be applied in the new domain. In the second step, the weights in new domain is converted back to the excitations (e.g., that is amplitudes and phases using polynomial method) that fed to the antenna for generating shaped-beam pattern.

However, all of these mentioned convex optimization methods are synthesizing the shaped-beam pattern in narrow bandwidth domain. In this chapter, extending the method in [100] to synthesize an shaped-beam pattern to be able to operate in many frequencies by using another two-step approach in [54].

5.2 Mathematical Formulation

The array factor of an uniform linear array is defined as, with reference to the Fig. 5.1:

$$F(f,\theta) = \sum_{n=0}^{N-1} I_n e^{j\frac{2\pi}{c} fndcos(\theta)} \tag{5.1}$$

where I_n, $n = 0, ..., N-1$, is the complex excitation of the n-th element of the array, c being the speed of light in the vacuum space, f is the operating frequency of the array, d is the inter-element spacing along z-axis, and θ is the angle measured from the array axis.

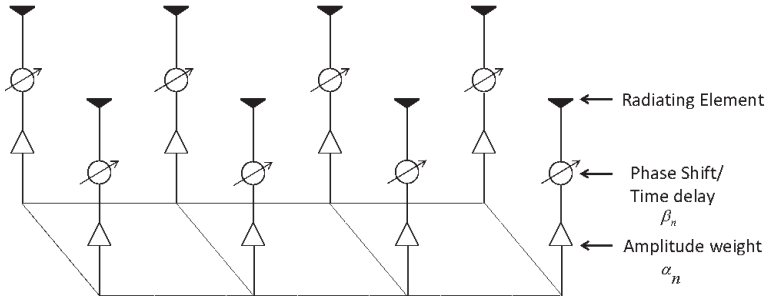

Figure 5.1: Sketch of the array antenna

The goal of synthesis of Shaped Beams is to define the set of element excitations $\{I_n\} = \{I_n;\, n = 0, ..., N-1\}$ such that

$$\left\{ LB\left(u(f_q)\right) \leq \left|F\left(u(f_q)\right)\right|^2 \leq UB\left(u(f_q)\right) \quad k = 1, 2, ..., K, \right. \tag{5.2}$$

where $u(f_q) = \frac{2\pi}{c} f_q dcos\left(\theta\right)$, and q is sampling frequency in the wideband. However, in the eq. (5.2), the lower bound inequalities are not convex over a convex set. Then, in this chapter, this condition is converted to another form in which the converted form become convex over convex set and the convex programming can be applied. Towards the end, the synthesis of shaped beam antennas is done by means of a two-step procedure:

1) Firstly, the feasibility of the UWB power synthesis problem is ensured by means of a Convex Programming (CP) procedure;

2) Secondly, the excitation coefficients are defined.

5.2.1 Solve Convex Programming CP

5.2.1.1 Simplification Power pattern

Using some mathematical manipulations to make equivalence, in which the original power pattern depending on I_n,$n = 0, 1, ..., N-1$ to the new representation power pattern depending on $D_p, p = 0, \pm 1, .., \pm N-1$, then,

$$|F(u(f))|^2 = \left| \sum_{n=0}^{N-1} I_n e^{jnu(f)} \right|^2 = \sum_{p=-N+1}^{N-1} D_p e^{jpu(f)}. \qquad (5.3)$$

The converted form of $|F(u(f))|^2$ in eq. 5.3 is now linear combination of real value D_p, then convex program is used to enforce for multiple frequencies on the shaped-beam power pattern for common set of the excitations (D_p $p = 0, \pm 1, .., \pm N-1$).

The eq. 5.3 can be obtained by applying some following manipulation operations. Power pattern of the linear array can be expressed as:

$$\begin{aligned} |F(u(f))|^2 &= \left| \sum_{n=0}^{N-1} I_n e^{jnu(f)} \right|^2 \\ &= \left(\sum_{n=0}^{N-1} I_n e^{jnu(f)} \right) \left(\sum_{m=0}^{N-1} I_m e^{jmu(f)} \right)^* \\ &= \left(\sum_{n=0}^{N-1} I_n e^{jnu(f)} \right) \left(\sum_{m=0}^{N-1} I_m^* e^{-jmu(f)} \right). \end{aligned} \qquad (5.4)$$

Expanding the summations in eq. (5.4) it follows that

$$\begin{aligned} |F(u(f))|^2 = \; & I_o \left[I_{N-1}^* e^{-j(N-1)u(f)} + ... + I_1^* e^{-ju(f)} + I_o^* \right] + \\ & + I_1 e^{ju(f)} \left[I_{N-1}^* e^{-j(N-1)u(f)} + ... + I_1^* e^{-ju(f)} + I_o^* \right] + \\ & + ... + \\ & + I_1 e^{j(N-1)u(f)} \left[I_{N-1}^* e^{-j(N-1)u(f)} + ... + I_1^* e^{-ju(f)} + I_o^* \right]. \end{aligned} \qquad (5.5)$$

Thus, it is simple to observe from eq. (5.5) that eq. (5.4) can be rewritten as the summation of $2N-1$ terms as

$$|F(u(f))|^2 = \sum_{p=-N+1}^{N-1} D_p e^{jpu(f)}, \qquad (5.6)$$

where the Hermitian condition $D_p = D_{-p}^*$, $p = 0, \pm 1, .., \pm N-1$ holds true, and $D_p = \mathcal{F}(\{I_n\})$, $\mathcal{F}$ being a generic function.

Finally, eq. (5.6) can be expressed in series of sine and cosine functions as

$$|F(u(f))|^2 = D_0 + \sum_{p=1}^{N-1} D_p^{'} cos(pu(f)) - \sum_{p=1}^{N-1} D_p^{''} sin(pu(f)) \tag{5.7}$$

where $D_p^{'} = 2Re\{D_p\}$ and $D_p^{''} = 2Im\{D_p\}$, $p = 1, ..., N-1$, $Re\{.\}$ and $Im\{.\}$representing the real and the imaginary part, respectively.

Clearly, in eq. (5.7), the power pattern (square of the array factor) $|F(u(f))|^2$ is just a linear combination of $\{sin(.), cos(.)\}$ and the real-valued unknowns $\{D_p^{'}, D_p^{''}\}$, therefore the lower bound constraints on the eq. (5.7) are clearly convex over a convex set.

5.2.1.2 Solving CP problem

A necessary (not sufficient) condition which must be satisfied for the existence of the excitation set I_n, $n = 0, ..., N-1$ is

$$LB(u(f)) \leq \sum_{p=-N+1}^{N-1} D_p e^{jpu(f)} \leq UB(u(f)) \quad \forall u(f), \tag{5.8}$$

where the functions $LB(u(f))$ and $UB(u(f))$ identify the user-defined mask on the power pattern.

Numerically, the condition (5.8) need to be verified on a set of M points at each frequency f_q, $q = 1, ..., Q$

$$\begin{cases} LB(u_1(f_1)) \leq \sum_{p=-N+1}^{N-1} D_p e^{jpu_1(f_1)} \leq UB(u_1(f_1)) \\ \vdots \\ LB(u_M(f_1)) \leq \sum_{p=-N+1}^{N-1} D_p e^{jpu_M(f_1)} \leq UB(u_M(f_1)) \\ LB(u_1(f_2)) \leq \sum_{p=-N+1}^{N-1} D_p e^{jpu_1(f_2)} \leq UB(u_1(f_2)) \\ \vdots \\ LB(u_M(f_2)) \leq \sum_{p=-N+1}^{N-1} D_p e^{jpu_M(f_2)} \leq UB(u_M(f_2)) \\ \vdots \\ LB(u_1(f_Q)) \leq \sum_{p=-N+1}^{N-1} D_p e^{jpu_1(f_Q)} \leq UB(u_1(f_Q)) \\ \vdots \\ LB(u_M(f_Q)) \leq \sum_{p=-N+1}^{N-1} D_p e^{jpu_M(f_Q)} \leq UB(u_M(f_Q)), \end{cases} \tag{5.9}$$

where a sufficient discretization of these functions required that $M \simeq 10NQ$.

The system (5.9) contains $2MQ$ linear inequalities, and the solution D_p, $p = -N+1, ..., N-1$, can be computed by means of a Linear programming problem (e. g., *linprog* solver in Matlab, or CVX).

The LP problem concludes with two possible alternatives. Firstly, system (5.9) does not admit any solution, the constraints on the mask (i.e., $LB(u(f))$,$UB(u(f))$)

should be relaxed, the number of element N should be increased, the inter-element distance d should be modified, or the number of frequencies K should be chosen properly. Secondly, the system admits solution $\{D_p\}$.

5.2.2 Conversion D_p to I_n

However, our interest is the excitations I_n that are being fed to the antenna system to generate radiation patterns, not the variable D_p that has meaningless in the antenna systems. Therefore, based on some mathematical manipulations, I_n can easily obtained if D_p exists.

In case the problem in the system Eq. (5.9) results solution $\{D_p\}$, we ask whether it is possible to obtain the set of element excitations $\{I_n\}$ with the given $\{D_p\}$. To solve this problem, let us proceed as follows:

Let us first manipulate Eq. (5.6) by extracting the term $e^{j(1-N)u} = e^{-j(N-1)u}$ outside the summation. More specifically,

$$\begin{aligned} |F(u(f))|^2 &= \sum_{p=-N+1}^{N-1} D_p e^{jpu(f)} \\ &= e^{-j(N-1)u(f)} \sum_{p=0}^{2N-2} \hat{D}_p e^{jpu(f)} \\ &= e^{-j(N-1)u(f)} \sum_{p=0}^{2N-2} \hat{D}_p z^P, \end{aligned} \tag{5.10}$$

where $z(f) = z = e^{ju(f)}$ ($|z(f)| = 1$). ($D_p$and $\hat{D}_p$in general are the same, only different from index coefficient).

By virtue of the fundamental theorem of arithmetic, Eq. (5.10) can be expressed as product of $2N-2$ terms given by

$$|F(u(f))|^2 = e^{-j(N-1)u} \hat{D}_{2N-2} \prod_{i=1}^{2N-2} (z - z_i) \ . \tag{5.11}$$

It is possible to demonstrate that since (a) $|F(u)|^2$ is a positive function and (b) $D_p = D_{-p}^*$, $p = \pm 0, .., \pm N-1$, if the polynomial $|F(u)|^2$ has a root of value equal to z_i, then also $\frac{1}{z_i^*}$ is root of $|F(u)|^2$ (Fig. 5.2).

Therefore, (5.11) can be written as

$$|F(u(f))|^2 = e^{-j(N-1)u} \hat{D}_{2N-2} \prod_{i=1}^{N-1} (z - z_i) \prod_{i=1}^{N-1} \left(z - \frac{1}{z_i^*} \right) . \tag{5.12}$$

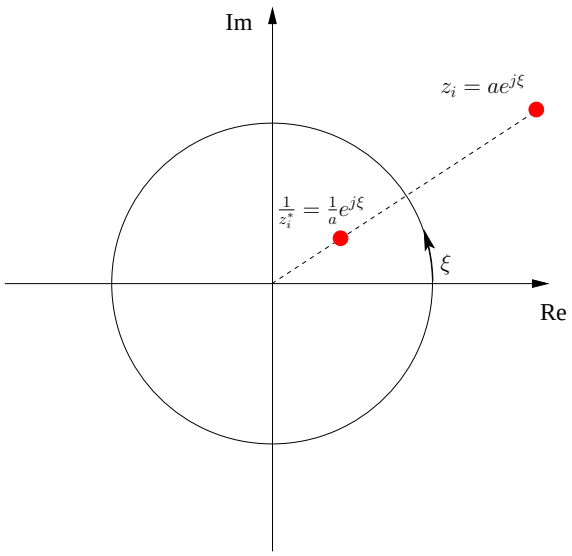

Figure 5.2: Complementary root

Let us consider the following mathematical steps starting from a general term $\left(z - \frac{1}{z_i^*}\right)$. More in detail:

$$\begin{aligned} z - \frac{1}{z_i^*} &= e^{ju} - \frac{1}{z_i^*} \\ &= \frac{1}{z_i^*}\left(z_i^* e^{ju} - 1\right) \\ &= \frac{e^{ju}}{z_i^*}\left(z_i^* - e^{-ju}\right) \\ &= (-1)\frac{e^{ju}}{z_i^*}\left(e^{-ju} - z_i^*\right) \\ &= (-1)\frac{e^{ju}}{z_i^*}\left(e^{ju} - z_i\right)^* . \end{aligned} \tag{5.13}$$

Thanks to (5.13), the second product of Eq. (5.12) can be written as

$$\prod_{i=1}^{N-1}\left(z - \frac{1}{z_i^*}\right) = e^{j(N-1)u}(-1)^{N-1}\prod_{i=1}^{N-1}\frac{1}{z_i^*}\prod_{i=1}^{N-1}\left(e^{ju} - z_i\right),^* \tag{5.14}$$

and substituting (5.14) into (5.12) it turns out that

$$|F(u)|^2 = \frac{(-1)^{N-1}}{\prod_{i=1}^{N-1} z_i^*}\hat{D}_{2N-2}\prod_{i=1}^{N-1}(z - z_i)\prod_{i=1}^{N-1}(z - z_i)^* . \tag{5.15}$$

Now, by considering $\frac{(-1)^{N-1}}{\prod_{i=1}^{N-1} z_i^*}\hat{D}_{2N-2} = K^2$, then eq. (5.15) can be written as

$$|F\left(u(f)\right)|^2 = \left[K\prod_{i=1}^{N-1}\left(z-z_i\right)\right]\left[K\prod_{i=1}^{N-1}\left(z-z_i\right)^*\right] \tag{5.16}$$

It is very interesting that the eq. (5.16) has the same pattern as the eq. (5.4), that is:

$$|F\left(u(f)\right)|^2 = \left(\sum_{n=0}^{N-1} a_n e^{jnu(f)}\right)\left(\sum_{m=0}^{N-1} a_m e^{jmu(f)}\right),^* \tag{5.17}$$

where $I_n = a_n$, $n = 0, ..., N-1$ (5.4). Therefore, to find I_n from D_p, the roots of $|F\left(u(f)\right)|^2$ need to be found, then coefficients of the polynomial $K\prod_{i=1}^{N-1}\left(z-z_i\right)$ result in I_n.

5.3 Numerical Results

In this section, two examples of shaped-pattern synthesis (e.g., Flattop and Cosecant) are presented to show the effectiveness and efficiency of the proposed method in section 5.2. To make it more clear, the flattop and cosecant mask used in eq. (5.8), and eq. (5.9) are introduced as follows:

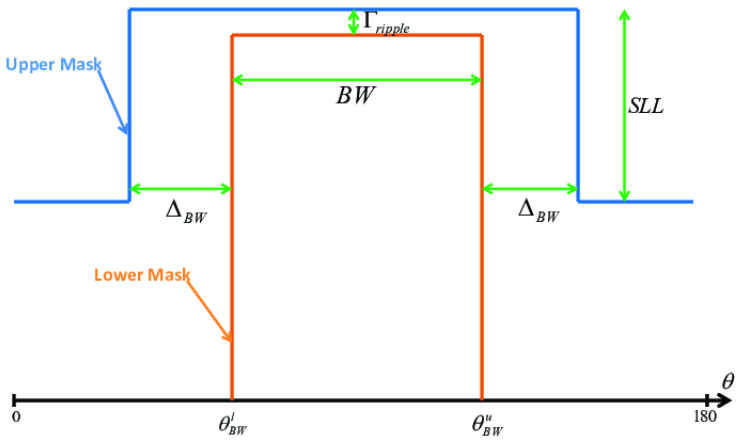

(a)

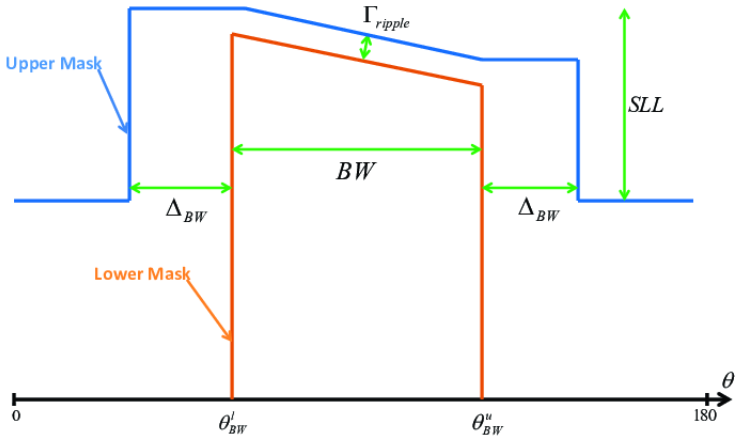

(b)

Figure 5.3: Flattop (a) and Cosecant (b) mask used in shaped-beam patterns in section 5.2

In the fig. 5.3(a) and 5.3(b) show the flattop mask and cosecant, respectively. There are some definitions about those masks. In the mainbeam region where the shaped-beam is defined, the Γ_{ripple} is ripple level and defined as the difference between the upper bound and the lower bound. This value is usually small to keep the pattern in this region smooth, but it depends on the $DoFs$ of the problem. The Δ_{Bw} shows the region in the sidelobe regions. The θ^l_{BW} and θ^u_{BW} are the two ends of the lower bound.

5.3.1 Flattop Pattern

The test for flattop patterns is configured as, the number of the linear array is $N = 18$ element, the ripple in the shaped-beam region $\Gamma_{ripple} = 0.5$ [dB], the sidelobes level $SLL = -25$ enforcing to all the sidelobes, the slope region $\Delta_{Bw} = 16\,[deg]$ in the sidelobes; the shaped-beam width of interest $BW = 28\,[deg]$ located from $\theta^{l}_{BW} = 76\,[deg]$ to $\theta^{u}_{BW} = 104\,[deg]$ in the visible domain.

CP Solution:

In the first step is to solve the convex programming (CP), the optimized solution $\left\{D'_p, D''_p\right\}, p = 0, 1, ..., N-1$ of the synthesis problem with given user-defined mask in eq. (5.9) and the two-step method in [54] with $Q = 5$ are used to obtain the shaped-beam pattern operating at multiple frequencies, as shown in the fig. 5.4.

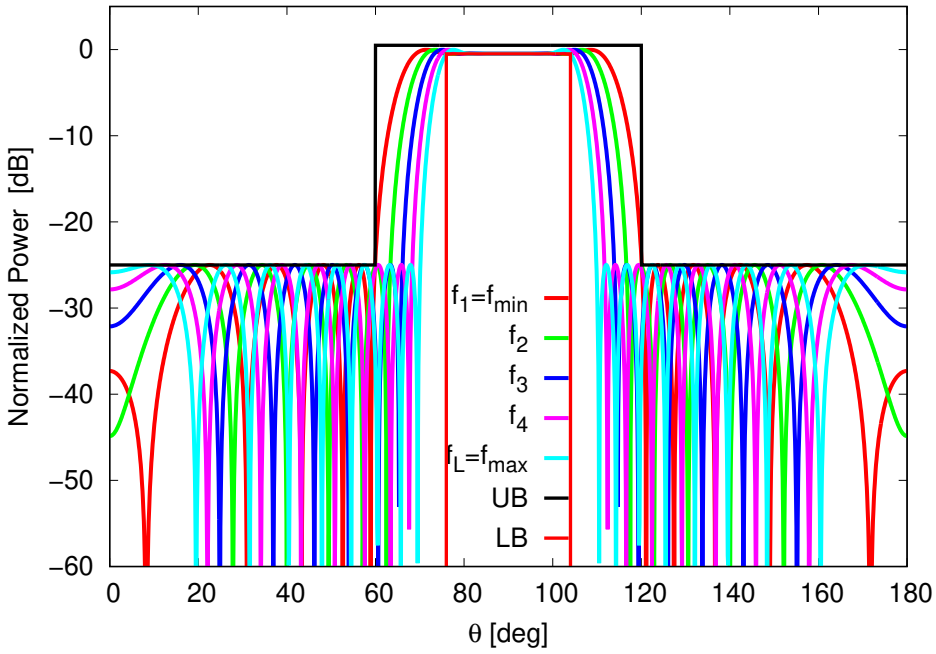

Figure 5.4: The power pattern at multi-frequency $f_i, i = 1, 2, 3, 4, 5$.

Roots:

In the next step, because $\{D_p\}, p = 0, \pm 1, ..., \pm N - 1$ are not of our interest. The only complex-valued I_n, $n = 1, 2, .., N$ comprised of amplitudes and phases excitations are our interest. Then, to convert from $\{D_p\}, p = 0, \pm 1, ..., \pm N - 1$ into $I_n n = 1, 2, .., N$. The Roots z_i, $i = 1, 2, ..., 2N - 2$ of polynomial $|F(u)|^2$ in eq. (5.10) is found as in fig. 5.5:

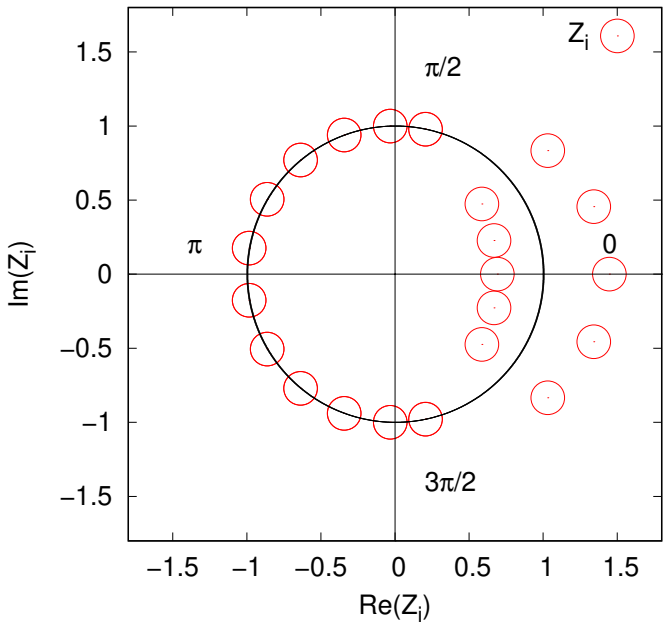

Figure 5.5: Roots z_i, $i = 1, 2, ..., 2N-2$

One interested point here, the array only need $N-1$ roots to recover the I_n. However in the fig. 5.5 there are more than $N-1$ roots due to the polynomial $|F(u)|^2$ in eq. (5.10) is the polynomial of $2N-2$ order.

Indeed, the number of roots inside (outside) the unitary circle is equal to $N_0 = 5$. Therefore, there are $K = 2^{N_0} = 32$ different set of excitations $\{I_n\}^k = \{I_n^k, n = 0, 1, ..., N-1\}$,$k = 1, 2, ..., K$, generating the power pattern operating over multiple frequencies defined by the solution of the CP problem.

Excitation Amplitudes: $\{|I_n|; n = 0, 1, .., N-1\}$

Conversion from optimized $\{D_p\}, p = 0, \pm 1, ..., \pm N-1$ to the excitations in the eq. (5.3), indeed results in a set of $K = 32$ of $\{I_n^k\}$,$n = 0, 1, .., N-1, k = 1, 2, ..., K$. That means that conversion from one optimized solution using CP in new domain to the original domain gives 32 complex-valued solutions as in fig. 5.7 and fig. 5.8. And very important note that, each solution generates shaped-beam pattern operating at multiple frequencies.

Patterns:

Obtained by means of the combinations of all roots outside of the unitary circle for $Q = 5$ frequencies. The fig. 5.6 shows the all possible $K = 32$ patterns for the 32 set of achieved $\{I_n\}^k = \{I_n^k, n = 0, 1, ..., N-1\}$,$k = 1, 2, ..., K$ for each frequency $q = 1, 2, 3, 4$, and $Q = 5$ in fig. 5.6(a),(b),(c),(d), and (e), respectively.

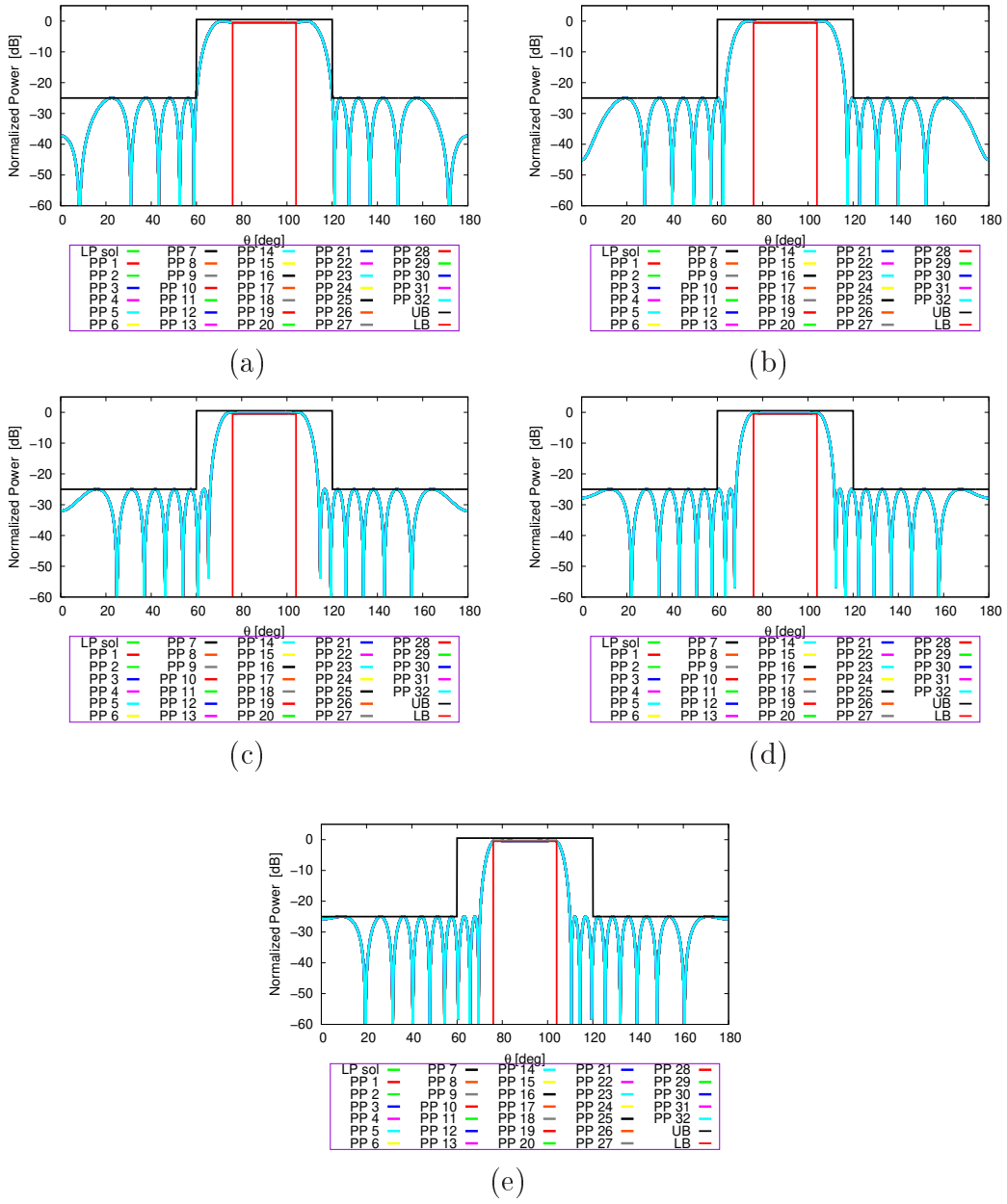

Figure 5.6: Pattern reconstruction from Power to Array at different frequencies - (a) $f_1 = f_{min}$, (b) f_2, (c) f_3, (d) f_4, and (d) $f_Q = f_{max}$. Each amplitude and phase among 32 possible amplitudes and phases (solutions) in 5.7 and 5.8, respectively, generate patterns for Q frequencies. And at each frequency, because 32 possible solutions (amplitude + phase) generate the same pattern, so they overlap and just appear here one color (cyan).

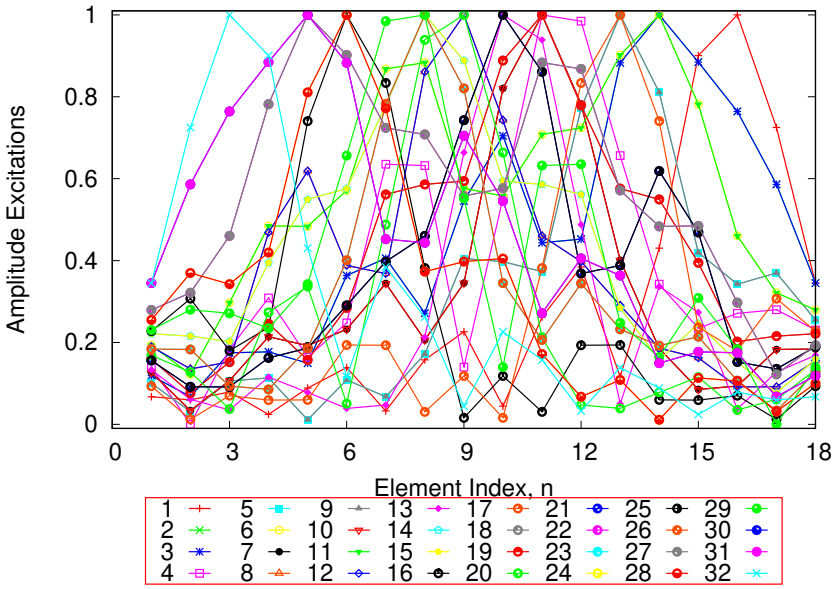

Figure 5.7: Excitation Amplitudes: $|I_n|$;$n = 1, 2, .., N$

Excitation Phases: $\{\phi_n^k, n = 0, 1, ..., N-1,\ k = 1, 2, ..., K\}$

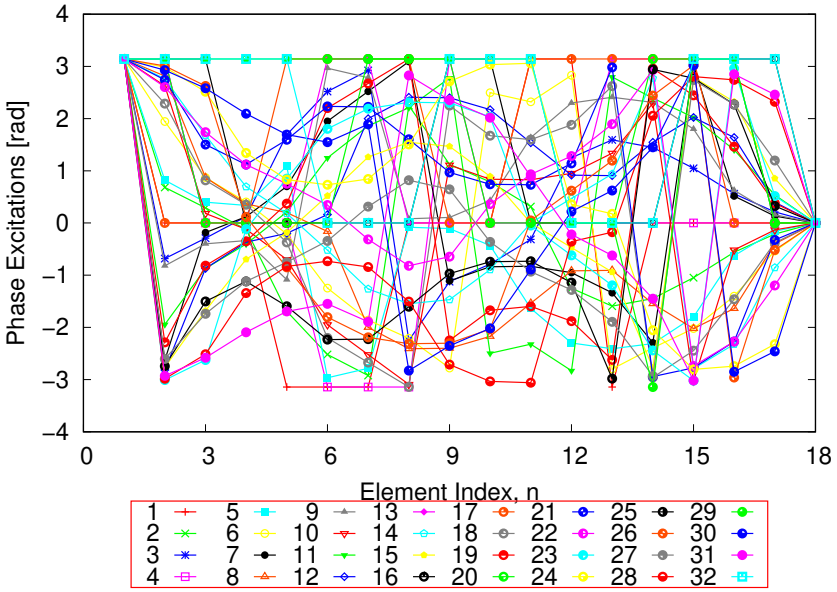

Figure 5.8: Excitation Phases: $\{\phi_n^q, n = 1, 2, ..., N\}$, $q = 1, 2, ..., Q$

Dynamic range ratio (DRR)

The DRR is important value for fabrication, this is the ratio of the maximum absolute and minimum absolute value of excitations. The smaller DRR is, the easier to fabricate the array. In the previous discuss, the achieved flattop synthesis have 32 solutions, and the DRR for each solution is computed and reported in Tab. 5.1. The solutions 6,11, 22,and 27 have good DRR, and can be used to fabricate.

q	DRR_Q	$min\{DDR_q\}$	q	DRR_q	$min\{DDR_q\}$	q	DRR_Q	$min\{DDR_q\}$	q	DRR_q	$min\{DDR_q\}$
1	41.06		9	90.61		17	81.64		25	10.94	
2	14.77		10	29.65		18	13.13		26	29.65	
3	14.77		11	8.18	**X**	19	13.13		27	8.18	**X**
4	2898		12	10.94		20	28.42		28	90.61	
5	90.61		13	28.42		21	10.94		29	2898	
6	8.18	**X**	14	13.13		22	8.18	**X**	30	14.77	
7	29.65		15	13.13		23	29.65		31	14.77	
8	10.94		16	81.64		24	90.62		32	41.06	

Table 5.1: Dynamic range of all solutions obtained

Fractional Bandwidth (FBW)

The array operates in the bandwidth $BW = [4.8 : 7.44]$ [GHz], which is equivalent to $FBW = 0.42$. The array operates in WB.

5.3.2 Cosec^2 Pattern

The example for Cosec^{2}flattop patterns is defined as, the number of the linear array is $N = 18$ element, the ripple in the shaped-beam cosec^2 region $\Gamma_{ripple} = 0.5$ [dB], the sidelobes level $SLL = -25$ enforcing to all the sidelobes, the slope region $\Delta_{Bw} = 16\,[deg]$ in the sidelobes; the shaped-beam width of interest $BW = 40\,[deg]$ located from $\theta^l_{BW} = 70\,[deg]$ to $\theta^u_{BW} = 110\,[deg]$ in the visible domain.

CP Solution:

In the first step is to solve the convex programming (CP), the optimized solution $\left\{D'_p, D''_p\right\}, p = 0, 1, ..., N-1$ of the synthesis problem with given user-defined mask in eq. (5.9) and the two-step method in [54] with $Q = 5$ are used to obtain the shaped-beam pattern operating at multiple frequencies, as shown in the fig. 5.9.

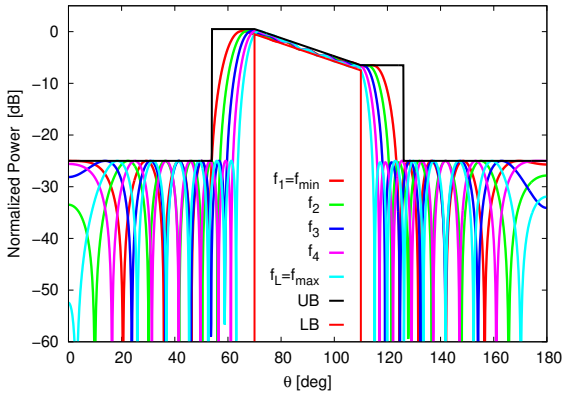

Figure 5.9: The power pattern at multi-frequency $f_i, i = 1, 2, 3, 4, 5$.

Roots:

In the following step, because $\{D_p\}, p = 0, \pm 1, ..., \pm N - 1$ are not our final goal. The only complex-valued I_n, $n = 1, 2, .., N$ comprised of amplitudes and phases excitations are our main goal. Then, to move from $\{D_p\}, p = 0, \pm 1, ..., \pm N - 1$ into $I_n n = 1, 2, .., N$, the Roots z_i, $i = 1, 2, ..., 2N - 2$ of polynomial $|F(u)|^2$ in eq. (5.10) is found as in fig. 5.10:

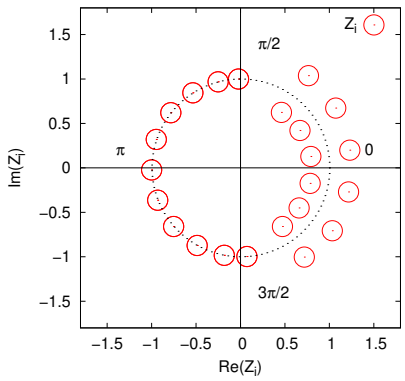

Figure 5.10: Roots z_i, $i = 1, 2, ..., 2N - 2$

One important point here, the array only need $N - 1$ roots to recover the I_n. However in the fig. 5.10 there are more than $N - 1$ roots due to the polynomial $|F(u)|^2$ in eq. (5.10) is the polynomial of $2N - 2$ order.

The number of roots inside (outside) the unitary circle is equal to $N_0 = 6$. Therefore, there are $K = 2^{N_0} = 64$ different set of excitations $\{I_n\}^k = \{I_n^k, n = 0, 1, ..., N - 1\}$,$k = 1, 2, ..., K$, generating the power pattern defined operating over multiple frequencies by the solution of the CP problem.

Patterns:

Obtained by means of the combinations of all roots outside of the unitary circle for $Q = 5$ frequencies. The fig. 5.11 shows the all possible $K = 64$ patterns for the 64 set of achieved $\{I_n\}^k = \{I_n^k, n = 0, 1, ..., N-1\}, k = 1, 2, ..., K$ for each frequency $q = 1, 2, 3, 4,$ and $Q = 5$ in fig. 5.11(a),(b),(c),(d), and (e), respectively.

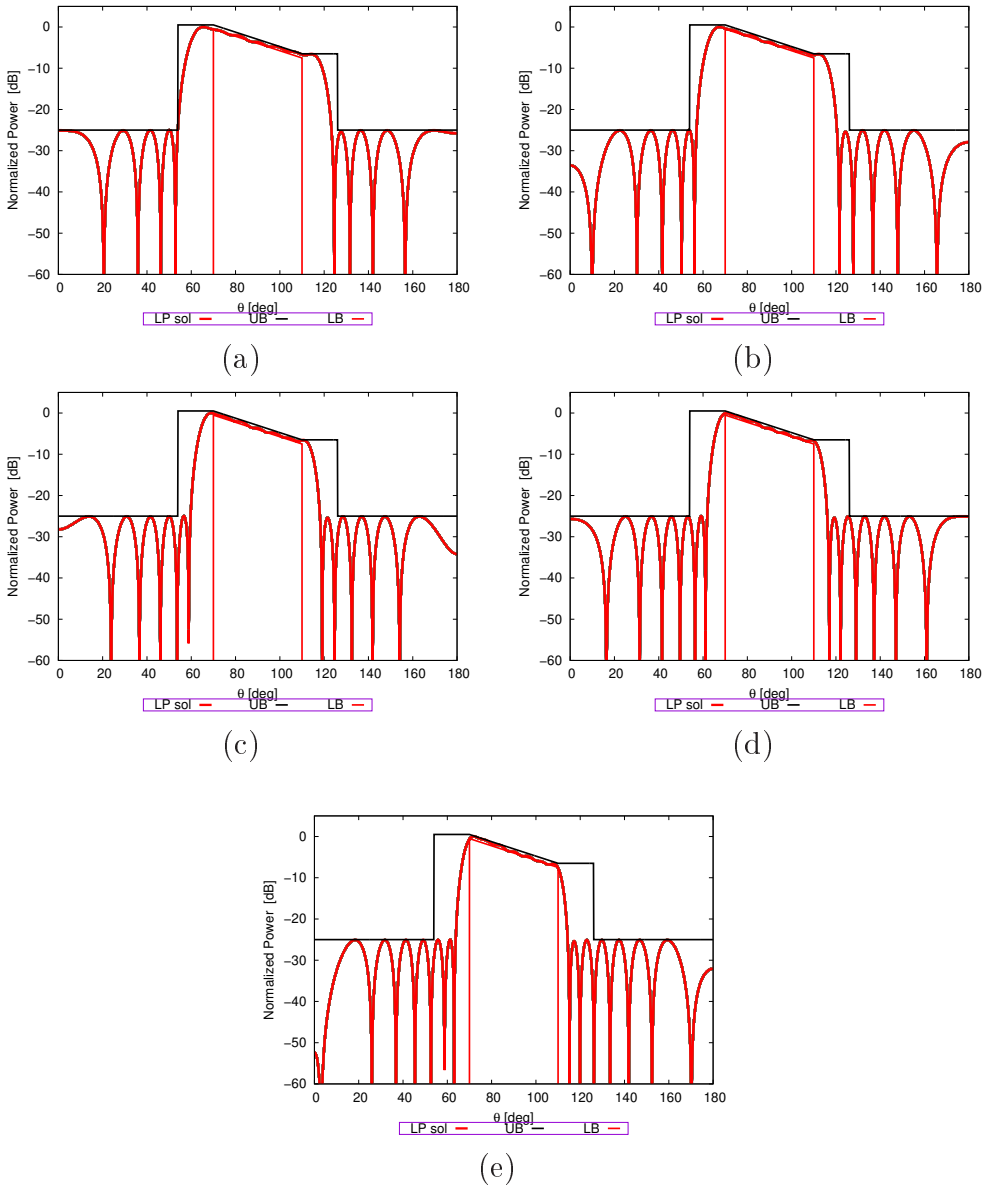

Figure 5.11: Pattern reconstruction from Power to Array at different frequencies - (a) $f_1 = f_{min}$, (b) f_2, (c) f_3, (d) f_4, and (e) $f_L = f_{max}$. All $K = 64$ patterns are completely the same at each frequency, therefore only red pattern displays at each frequency due to overlap among all $K = 64$ patterns.

Excitation Amplitudes: $\{|I_n|; n = 0, 1, .., N-1\}$

Conversion from optimized $\{D_p\}, p = 0, \pm 1, ..., \pm N-1$ to the excitations in the eq. (5.3), indeed results in a set of $K = 64$ of $\{I_n^k\}, n = 0, 1, .., N-1, k = 1, 2, ..., K$. That means that conversion from one optimized solution using CP in new domain to the original domain gives 64 complex-valued solutions as in fig. 5.12 and fig. 5.13. And each solution produces shaped-beam pattern operating at multiple frequencies.

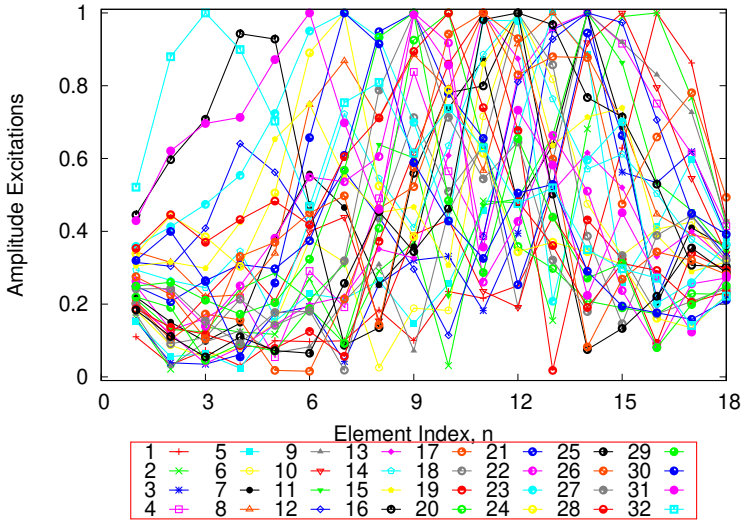

(a)

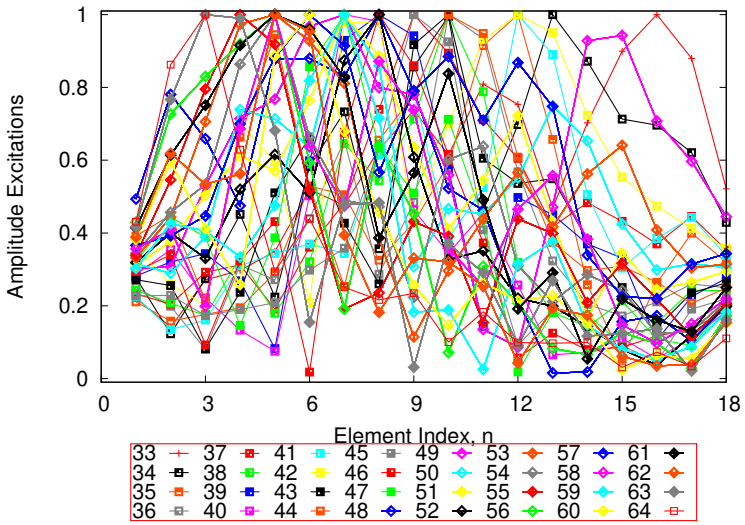

(b)

Figure 5.12: Excitation Amplitudes: $|I_n|; n = 1, 2, .., N$

Excitation Phases: $\{\phi_n^q, n = 0, 1, ..., N-1\}$, $q = 1, 2, ..., Q$

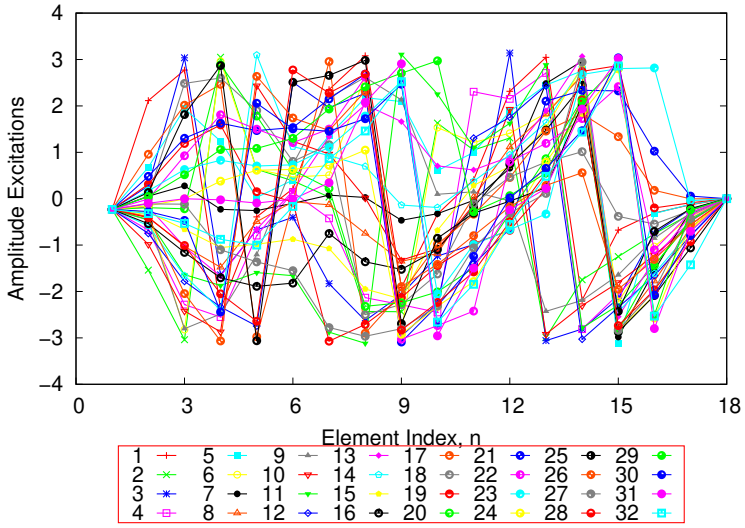

(a)

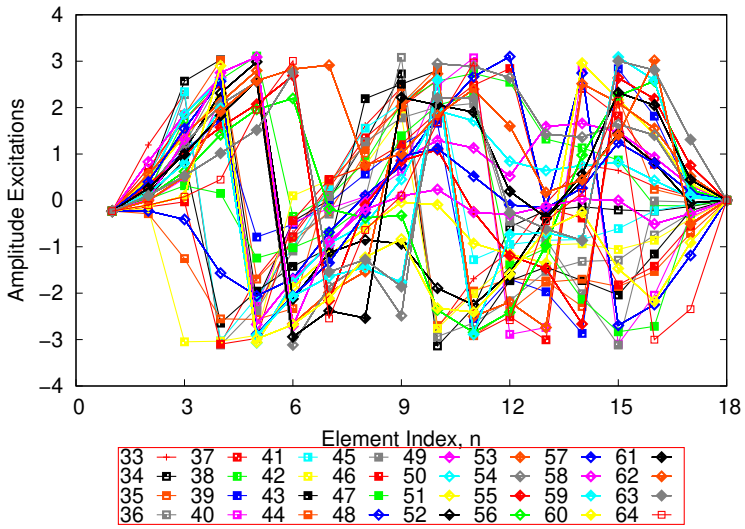

(b)

Figure 5.13: Excitation Phases: $\{\phi_n^q, n = 1, 2, ..., N\}$, $q = 1, 2, ..., Q$

Dynamic range ratio (DRR)

The DRR is important value for fabrication, this is the ratio of the maximum absolute and minimum absolute value of excitations. The smaller DRR is, the easier to fabricate the array. In the previous discussion, the achieved flattop synthesis have 32 solutions, and the DRR for each solution is computed and reported in Tab. 5.2. The solutions 15 and 50 have good DRR, and can be used to fabricate.

q	DRR_Q	$min\{DDR_q\}$	q	DRR_Q	$min\{DDR_q\}$	q	DRR_Q	$min\{DDR_q\}$	q	DRR_Q	$min\{DDR_q\}$
1	32.49		17	64.98		33	7.08		49	11.51	
2	47.21		18	54.35		34	8.13		50	3.45	X
3	28.64		19	55.69		35	18.25		51	6.09	
4	18.48		20	21.96		36	12.47		52	27.48	
5	41.98		21	4.84		37	5.23		53	8.73	
6	39.32		22	12.24		38	10.91		54	8.11	
7	10.27		23	4.95		39	12.13		55	8.66	
8	4.55		24	7.41		40	18.22		56	34.90	
9	39.91		25	18.22		41	7.43		57	4.55	
10	8.67		26	12.13		42	4.95		58	10.27	
11	8.11		27	10.91		43	12.24		59	39.32	
12	8.74		28	5.23		44	4.84		60	41.97	
13	27.48		29	12.47		45	21.95		61	18.48	
14	6.09		30	18.25		46	55.90		62	28.63	
15	3.45	X	31	8.13		47	54.35		63	47.21	
16	11.52		32	7.04		48	64.97		64	32.50	

Table 5.2: Dynamic range of all solutions obtained

Fractional Bandwidth (FBW)

The array operates in the bandwidth $BW = [4.80 : 6.72]$ [GHz], which is equivalent to $FBW = 0.32$. The array operates in WB.

5.4 Conclusion

In this chapter, $CP-$based strategy is proposed based on two steps. In the first step, the power pattern formulation with old weights in non-convex formulation has been converted into the convex form that is simply the linear combination of new weights and sine, cosine functions. In the second step, the optimized old weights are obtained by converting new weights through some manipulations. Toward this end, the two-step $CP-$based procedure successfully synthesized the shaped-beam pattern by using only one common set of excitation, guaranteeing an equal inter-element spacing linear array operating over multiple frequencies . A set of examples on shaped-beam (e.g., flattop and cosec^2) are carried out to prove the effectiveness of the proposed $CP-$based strategy.

Chapter 6

Timed Array Synthesis

In the synthesis methods used in previous chapters, Chapter 3, 4, and 5 refer to phased array synthesis because the domain carried out the synthesis is in the frequency domain, in which the array factor depending on the phased delay that is narrow bandwidth. In order to make the phased array antenna operate over wideband, the iterative $CP-$based approach introduced in [54] was applied to the constraints over multiple frequencies. However, there is still a misalignment of the beam in the target direction when beam-steering is involved in section 3.3.3. To overcome this drawback, the phase compensation for each frequency can be used, therefore it is not flexible and efficient. In this chapter, the time array synthesis is done because timed array in the case of beam-steering is dependent on the time delay that are independent-frequency.

6.1 Introduction

When the antenna arrays is considered, usually it refers to phased arrays that are steady-state systems, in which each radiator element is weighted by an amplitude, delayed by a phase shifter using narrowband signals, such as continuous sinusoidal signals operating at a particular frequency of interest.

The term "phased" is related to the capability of using phase shifters to electronically scan the main beam pattern to the direction where the target is located, instead of mechanically moving the antenna. The idea of phase is useful only if the phased arrays is considered in the frequency domain. Although the phased array is efficient when tackling with narrowband signals, its behavior is very poor when dealing with wideband or time-variant signals because distinctive frequency components show different phase. Indeed, the relation between time and phase is $\phi = 2\pi ft$, then time can be converted to phase easily. However, the reciprocal is not valid due to phase period of 2π while time is linear property [112][25]. Therefore, to deal with wideband signals, time delay units are required to avoid problems, such as beam squint, and pulse dispersion.

Timed arrays are becoming popular because the increasing number of ap-

plications require the wideband and ultra-wideband signals, [105][106][107]. By inspiring the spirit of the phased array, in timed arrays, similarly, the each radiating element are excited by each input pulse instead of a narrowband signal [103]. In addition, each input waveform is scaled/weighted by a real-valued weight and delayed in order to produce a frequency-independent beam steering [108]. Furthermore, unlike the narrowband signals, performing the time array analysis in the temporal-spacing dimension enables to add a new degree of freedom DoF to the array excitation design: the signals' waveform [104].

By weighting the input pulses in order to shape the transmitted or received pulses, the unconventional performance of the UWB arrays can be obtained. However, over last decades, there are very few optimization techniques applied to the timed array synthesis. For example, in [104], the author proposed a strategy based on the iterative projection method to synthesize timed array for arbitrary time-angle mask constraints on the TD radiated field. However, the results shown in the test paper cases are not optimum solution, which is evident from the synthesized field is not completely lying between upper bound and lower bound imposing on the TD radiated field.

In this chapter, a $CP-$based synthesis are introduced for the timed array synthesis to overcome the drawback of technique mentioned in [104]. That means the solution of an arbitrary time-angular mask imposing on the TD radiated field is optimum.

6.2 Mathematical Formulation

6.2.1 Electric Field Definition

TD Radiated Field obtained from frequency domain

In order to obtain electric field expression in time domain, an efficient and simple way starts from field expression in frequency domain (the most familiar and popular) and then using inverse Fourier transform to convert the frequency-dependent field expression into the time-dependent field expression. Below is the brief conversion summary:

In the frequency, let us assume that the electric field in free space of any single antenna can be easily obtain in [103]

$$\underline{E}(f;\theta,\phi) = j\eta\frac{I\underline{L}}{2\lambda r}exp^{-jkr} = \eta_0\frac{i2\pi f I\underline{L}}{4\pi rc}exp^{-j\frac{2\pi fr}{c}}, \tag{6.1}$$

wherein, $\underline{E}(f;\theta,\phi)$ is the radiated electric field in the spherical coordinated system (r,θ,ϕ), $I = I(f)$ is the antenna input current, $\underline{L} = \underline{L}(f;\theta,\phi)$ is the effective length of the antenna, $\lambda = c/f$ is the wavelength, $k = \omega/c = 2\pi/\lambda$ is the wave number, η_0 the intrinsic impedance of free space and c is the speed of light in vacuum.

The transition from frequency domain to time domain is carried out by implementing inverse Fourier transform of the eq. (6.1). The lower case symbols corresponding to the inverse Fourier transform are referred to the same time-dependent quantities

$$\underline{e}(t;\theta,\phi) = \frac{\eta_0}{4\pi rc} i(t-\frac{r}{c}) \otimes \frac{\partial \underline{\ell}(t-\frac{r}{c};\theta,\phi)}{\partial t}, \tag{6.2}$$

wherein, $\underline{\ell}$ is the Fourier transform of the antenna effective length $\underline{L}$ and the symbol $\otimes$ denotes the convolution operator.

If we deal with broadband, non-dispersive antenna system, its frequency domain effective length can be assumed frequency independent: $\underline{L}(f;\theta,\phi) = \underline{L}(\theta,\phi)$ and its time-domain counterpart is $\underline{\ell}(t;\theta,\phi) = \underline{\ell}(\theta,\phi)\delta t$ where δt is the Dirac function. Then, performing the convolution in eq. (6.2), we obtain simplified form of single element field in the time domain

$$\underline{e}(t;r;\theta,\phi) = -\eta_0 \frac{\underline{L}(\theta,\phi)}{4\pi rc} \frac{\partial i(t-\frac{r}{c})}{\partial t}. \tag{6.3}$$

Assuming that if array antenna comprised of N elements located at coordination $r_n = (x_n, y_n, z_n)$, $n = 1, 2, ..., N$, then the total field will be summation of each field from eq. (6.3):

$$\underline{E}_{tot}(t;r;\theta,\phi) = \sum_{n=1}^{N} \underline{e}_n(t-\frac{r}{c}-t_n(\theta,\phi)) = -\eta_0 \frac{\underline{L}(\theta,\phi)}{4\pi rc} \sum_{n=1}^{N} \frac{\partial i_n(t-\frac{r}{c}-t_n(\theta,\phi))}{\partial t} \tag{6.4}$$

wherein $t_n(\theta,\phi) = \frac{\hat{\underline{r}} \bullet r_n}{c}$ is the time delay due to array position in the array, $\hat{\underline{r}} = (sin\theta cos\phi, sin\theta sin\phi, cos\theta)$ unit angle and array element positions $r_n = (x_n, y_n, z_n)$, $n = 1, 2, ..., N$. In addition, $i_n(t)$, $n = 1, 2, ..., N$ are input pulse currents for elements in the array. The eq. (6.4) will become

$$\underline{E}_{tot}(t;r;\theta,\phi) = \sum_{n=1}^{N} \underline{e}_n(t-\frac{r}{c}-t_n(\theta,\phi)) = -\eta_0 \frac{\underline{L}(\theta,\phi)}{4\pi rc} \sum_{n=1}^{N} \frac{\partial i_n(t-\frac{r}{c}-t_n(\theta,\phi))}{\partial t} \tag{6.5}$$

To simplified the Eq. (6.5), we assign:

$$\underline{A} = -\eta_0 \frac{\underline{L}(\theta,\phi)}{4\pi rc}$$
$$f_n(t-\frac{r}{c}-t_n(\theta,\phi)) = \frac{\partial i_n(t-\frac{r}{c}-t_n(\theta,\phi))}{\partial t}$$

Then Eq. (6.5) will become:

$$\underline{E}_{tot}(t;r;\theta,\phi) = \underline{A} \sum_{n=1}^{N} f_n(t-\frac{r}{c}-t_n(\theta,\phi)), \tag{6.6}$$

wherein, $f_n(t-\frac{r}{c}-t_n(\theta,\phi))$, $n=1,2,...,N$ are the derivative of the input pulse currents for each antenna in the array, $t_n(\theta,\phi)=\frac{\hat{r}\bullet r_n}{c}+t_n$ is the relative time delay due to either the physical displacement of element in the array $\frac{\hat{r}\bullet r_n}{c}$ or to wanted scanning angle (t_n).

TD Radiated Field obtained in time domain

In [104] an given linear array of N elements placed along $z-axis$ fed by a set of input currents $\{i_n, n=1,...,N\}$, the time-domain array factor is defined as

$$AF(\theta,t)=\sum_{n=1}^{N} i_n\left(t-t_n(\theta)\right), \tag{6.7}$$

where N is the number of elements, i_n is the input current into the n^{th} element and $t_n(\theta)$ is the time delay along direction θ of the n^{th} element, which also depends on d that is the inter-element spacing.

Let us assume that all the array elements radiates the same radiation pattern, the total radiated field of the array is obtained as (see in [104])

$$\underline{E}(\theta,t)=-\frac{\eta_0}{4\pi rc}\underline{h}^T\left(\theta,t-\frac{r}{c}\right)\otimes AF\left(\theta,t-\frac{r}{c}\right), \tag{6.8}$$

wherein, $\underline{h}^T\left(\theta,t-\frac{r}{c}\right)$ is the transmitting effective length of common isotropic radiating antenna, η_0 the intrinsic impedance of free space and c is the speed of light in vacuum, and $\otimes$ is the convolution operation.

In[104] the effective height (or another name is the effective length) is defined for isotropic array element as follows:

$$\underline{h}^T(\theta,t)=\delta^{(q)}(\tau)\,cos^p(\theta), \tag{6.9}$$

where $\delta^{(q)}$ stands for the q^{th}derivative of the input signals, and p modulates the antenna's angular beamwidth.

Finally, by bringing those equations, eq. (6.7), eq. (6.8), and eq. (6.9) together, the total radiated field can be simplified and re-written as follows:

$$\underline{E}(\theta,t)=-\frac{\eta_0}{4\pi rc}\sum_{n=1}^{N}\frac{\partial i_n^{(q)}\left(t-\frac{r}{c}-t_n(\theta)\right)}{\partial t}cos^p(\theta) \tag{6.10}$$

To simplified the eq. (6.10), we assign:

$$\underline{A'}=-\frac{\eta_0}{4\pi rc}$$
$$f_n^{(q)}(t-\tfrac{r}{c}-t_n(\theta))=\frac{\partial^{(q)}i_n(t-\frac{r}{c}-t_n(\theta))}{\partial^{(q)}t}$$

Then, the eq. (6.10) can be written in simplified form as follows:

$$\underline{E}(\theta,t) = \underline{A'}\sum_{n=1}^{N} f^{(q)}\left(t - \frac{r}{c} - t_n(\theta)\right) cos^p(\theta) \tag{6.11}$$

As it can be seen that, if neglect the term ϕ (e.g., considered the linear array) in the eq. (6.6) and if we set $q = 1$, and neglect the term $cos^p\theta$ in eq. (6.11), those two equation are very similar. In general, the total field is the summation of the derivative of the input pulse applied to each element array. Although going in two different approaches to obtain the total electric field of the array in time domain, they are quite similar.

6.2.2 TD Radiated Field with Weights

Let us assume that, an array of N isotropic elements is considered. Therefore, in the eq. (6.11), the TD radiated field is simplified the summation of the q-th derivative of the input pulse for each array element. There are no any degree of freedom (DoF) to focus or shape the radiation pattern along the desired direction. Then, taking the spirit in the phased array, when each phased shifter having amplitudes and phases to control the far-field radiation pattern. In this chapter, assuming that each input pulse is weighted different values $\alpha = [\alpha_1, \alpha_2, ..., \alpha_N]$ that need to be optimized to have the desired field in far-field radiation. Therefore the eq. (6.11) then can be recast as:

$$\underline{E}(\theta,t) = \underline{A'}\sum_{n=1}^{N} \alpha_n f^{(q)}\left(t - \frac{r}{c} - t_n(\theta)\right) cos^p(\theta), \tag{6.12}$$

wherein α_n,$n = 1, 2, ..., N$ is associated weights that is the DoF.

In our synthesis the term $\frac{r}{c}$ is neglected by setting the distance r ($r/c = 0$) since it is constant for all the radiating elements and does not influence the results. If the steering direction θ_s of the main beam is concerned, $t_n(\theta)$ is defined as following

$$t_n(\theta) = \left(n - \frac{N+1}{2}\right)\frac{d}{c}\left(sin(\theta) - sin(\theta_s)\right), \tag{6.13}$$

the total radiated field can be re-written as

$$\underline{E}(\theta,t) = \underline{A'}\sum_{n=1}^{N} \alpha_n f^{(q)}\left(t - \left(n - \frac{N+1}{2}\right)\frac{d}{c}\left(sin(\theta) - sin(\theta_s)\right)\right) cos^p(\theta), \tag{6.14}$$

6.2.3 TD Beam Forming Network

As can be seen from eq. (6.10), in the array design, the TD pulsed radiation is dependent on the new $DoFs$ that are the input signal's waveform $i_n(t), n =$

$1, ..., N$ and the waveform scaling factor $\alpha_n, n = 1, ..., N$ for each waveform. By exploiting the spacing-time beamforming technique in [104],[109], in which each antenna or source is fed by a linear combination of real-valued weights and ultra-wideband pulses. The ultra-wideband pulses can be deployed such as Hermite waveforms in [110][111]. It can be more clearly to visualize the space-time beamforming in fig. 6.1.

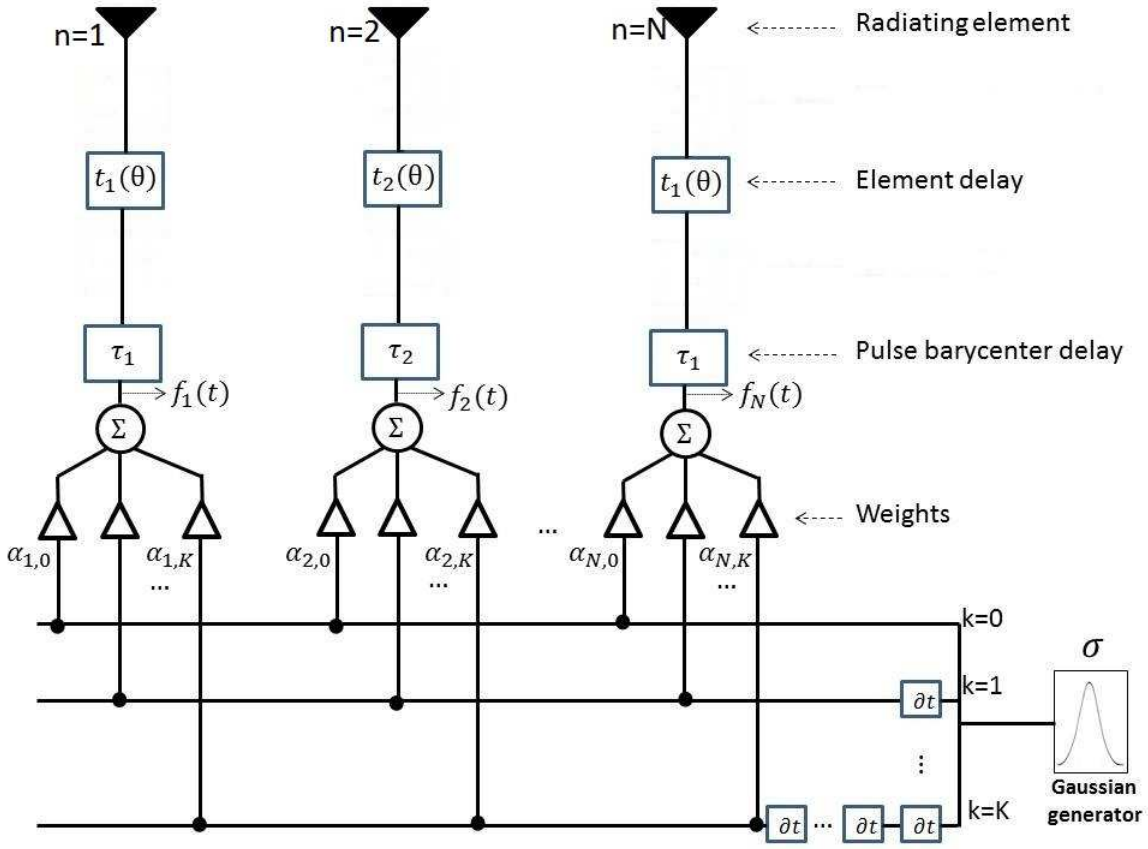

Figure 6.1: Spacing-time beamforming network using Hermite waveforms

The space-time beamforming depicted in the fig. 6.1 can be mathematically represented according to the Hermite functions in [104] as

$$\psi_k(t) = \frac{1}{\sqrt{2^k k!}} H_k\left(\frac{t}{\sigma}\right) \frac{1}{\sqrt{\pi}\sigma} e^{-t^2/\sigma^2}, \tag{6.15}$$

where σ is a scale parameter proportional to the pulse duration T, and $H_k(t)$ is the Hermite polynomial of order k expressed as

$$H_k(t) = (-1)^k e^{t^2} \frac{d^k}{dt^k} e^{-t^2}. \tag{6.16}$$

In eq. (6.15), $\psi_k(t)$ are the successive derivative of a Gaussian pulse. Therefore, the eq. (6.14) can be re-written as

$$\underline{E}\left(\theta,t\right)=\underline{A'}\sum_{n=1}^{N}\sum_{k=0}^{K}\alpha_{n,k}\psi_k^{(q)}\left(t-\left(n-\frac{N+1}{2}\right)\frac{d}{c}\left(sin\left(\theta\right)-sin\left(\theta_s\right)\right)\right)cos^p\left(\theta\right), \tag{6.17}$$

The weights α_n in eq. (6.14) to $\alpha_{n,k}$ in eq. (6.17) due to beamforming network added.

6.2.4 $CP-$based Synthesis Procedure

In the frequency domain, the synthesis optimization can applied on the array factor because the array factor and the radiated field is linear relation if neglecting the mutual coupling. However, in the time domain, the array factor can not be used to synthesis, instead the radiated field should be used because the radiated field is obtained by an angular-temporal filtering of the array factor due to antenna effective' height, and the array factor's time dependence is much different from the radiated field.

In eq. (6.17), let us assume that q that is $q-th$ derivative of the input pulse is known, p the antenna's angular beamwidth modulation is fixed, the order K of the beamforming network is given. Then, the TD radiated field is the linear combination of the weights $\alpha_{n,k}$, $n=1,..,N$, $k=0,1,...,K$ and the known ultra-wideband input pulses $\psi_k(t)$. Hence, the radiated field is convex, if the lower bound or upper bound are applied on the radiated field to shape the desired radiated field, the inequities become convex over convex set. The CP optimization can be used to solve.

$$\begin{cases}\underline{E}\left(\theta,t\right)\leq UB(\theta,t)\\ \underline{E}\left(\theta,t\right)\geq LB(\theta,t)\end{cases} \tag{6.18}$$

The $UB(\theta,t)$ and $LB(\theta,t)$ introduced in eq. (6.18) are called mask constraints and are defined in fig. 6.2.

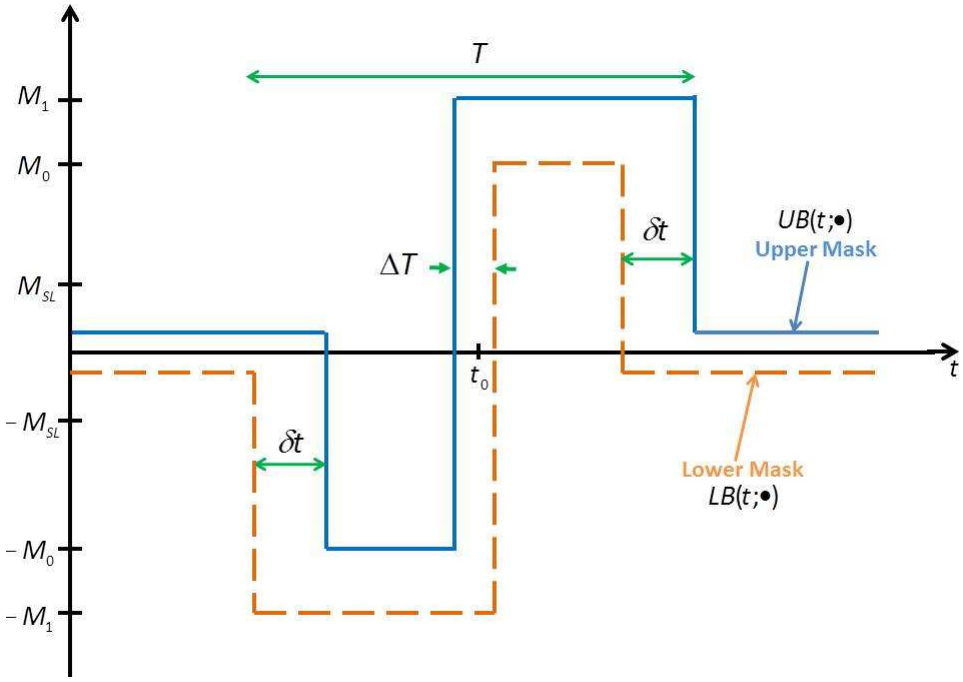

(a)

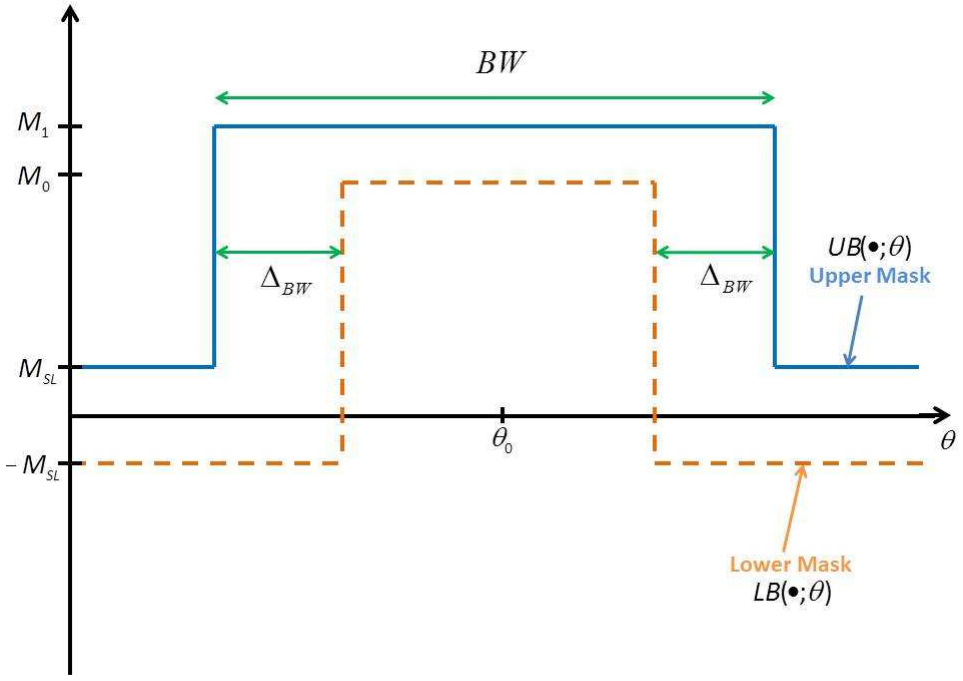

(b)

Figure 6.2: Upper Bound (a), and Lower Bound (b) mask constraints on the time domain that imposing on the TD radiated fields

In the fig. 6.2(a) represented for the mask along the time (t) domain of the radiated field , in which T is the pulse duration of input pulse from Hermite functions eq. (6.15), ΔT and δt are the time transition. In the fig. 6.2(b) depicted the mask along the angular direction θ, in which Δ_{BW} is the angular transition, and BW is the main beamwidth.

The formal expression of the array beamwidth in [104], and [103] the array geometry

$$Nd = \frac{2cT}{BW} \tag{6.19}$$

It is also suggested to have $d < cT$ to avoid grating lobes and also to choose $d < cT/2$ to reduce the strength of the side lobes.

6.3 Numerical Results

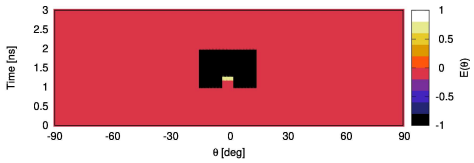

(a)

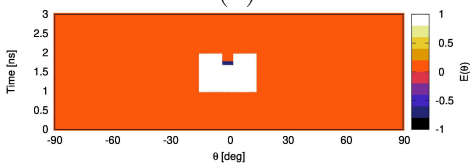

(b)

Figure 6.3: The time-angular mask constraints in two dimensions θ and t, (a) lower mask, (b) upper mask. Where $\theta \in [-90 : 90]$ [deg] and $t \in [0 : 3]$ [ns] generated from the time mask in fig. 6.2(a) and the angular mask in fig. 6.2(b) given $\theta_0 = 0$ [deg]

In all the test cases, the linear array comprised of N elements with equal inter-element spacing d is deployed. Towards this end, the timed array synthesis is carried out by optimizing the $CP-$based procedure on eq. (6.18) in order to determine the weights $\alpha_{n.k}$ $n = 1, ..., N$ $k = 0, ..., K$ for each Hermite waveforms $\psi_k(t)$ in eq. (6.15), the number of Hermite waves is decided by K that is chosen to form the beamforming network at the beginning of the optimization. Finally, the TD radiated field defined in eq. (6.17) must fulfill the time-angular arbitrary mask defined in 6.3.

6.3.1 Broadside radiation

In the first example, the broadside radiation is carried out where the main radiated field concentrated on the $\theta_s = 0$ [deg]. The linear array of $N = 10$ elements with equal inter-element spacing $d = 10$ [cm] are used in the synthesis proposed in the eq. (6.18). The value d is picked such that meet the requirements in the eq. (6.19) to avoid grating lobes that can arise.

The time and angular mask cut introduced in fig. 6.2, for building the fig. 6.3 with fixed parameters. For the direction along time dimension, the optimized TD radiated field has duration time $T = 1$ [ns] where almost the energy lying inside while the visible range of time is 3 [ns], the maximum level of the time-angular mask is normalized to $M_0 = 1$, and the lower upper bound of the time-angular mask is $M_1 = 0.7$ while the sidelobe level is set to be less than $M_{sl} = 0.1$. The value t_0 along the time direction is set to 1.5 [ns]. Regarding to the angular mask, the beamwidth of the mask $BW = 30$ [deg] from $\theta \in [-15, 15]$ [deg], the optimized TD radiated field is expected less than $M_{sl} = 0.1$ in sidelobe regions.

Regards to the Hermite waveforms in the beamforming networks, the value of $K = 4$ is chosen with five input Hermite waveforms indexed $k = 0, 1, 2, 3, 4$ for each antenna array. In fig. 6.1 Before reaching to antenna array, five input Hermite waveforms are weighted at $n-th$ antenna with weights α_{nk}, $k = 0, 1, 2, 3, 4$. The width scaling factor of the Hermite function σ is set to fixed value $\sigma = 0.4T$ for this example. In the eq. (6.9), the assumption on the effective height $\underline{h}^T(\theta, t)$ of single radiator is the $q - th$ differentiation $\underline{h}^T(\theta, t) = \delta^{(q)}(\tau)\, cos^p(\theta)$, $q = 1$, and $p = 1$ are set in this example.

The fig. 6.4(a) shows the optimized excitations $\alpha_{n,k}$, $n = 1, .., 10$, and $k = 0, ..., 4$, and the fig. 6.4(b) is the optimized TD radiated field generated from the excitations $\alpha_{n.k}$ in fig. 6.4(a).

Although claiming that the optimized results is perfectly fit the time-angular mask pattern constraints proposed in fig. 6.3, $2D$ pattern in fig. 6.4(b) is hard to view. Therefore, fig. 6.4(d) is the cut at $\theta = 0$ [deg] where the white stripe represented in fig. 6.4(c). Indeed, as it can be seen, the solid red line represented for the radiated field at $\theta = 0$ is perfectly fit the upper and lower mask specified in this example.

Furthermore, in fig. 6.4(f) and fig. 6.4(g) show the TD radiated cuts at $t = 1.25$ [ns] and $t = 1.75$ [ns] where two stripes illustrated in the fig. 6.4(e). As it is clearly that the radiated fields along two cuts completely match the angular masks at $t = 1.25$ [ns] and $t = 1.75$ [ns]. Therefore, the $CP-$based approach is successfully synthesizing the radiated field lying between the upper angular-time mask and the lower angular-time mask.

In the last fig. 6.4(h), the energy radiation computed and shown by average sum square of the optimized TD radiated field along time dimension. The results show that, all the energy focus at the broadside $\theta = 0$, the highest sidelobes are around 0.2. Although it is higher than the value $M_{sl} = 0.1$, it is not our interest here because the angular-time mask applied on the TD radiated field, not on the

energy radiation and the DoF number of elements here is just $N = 10$ elements is quite small. For example, in fig. 6.10, when $N = 65$ the energy is totally fit the angular mask while we are not intended to optimized to fit only angular mask.

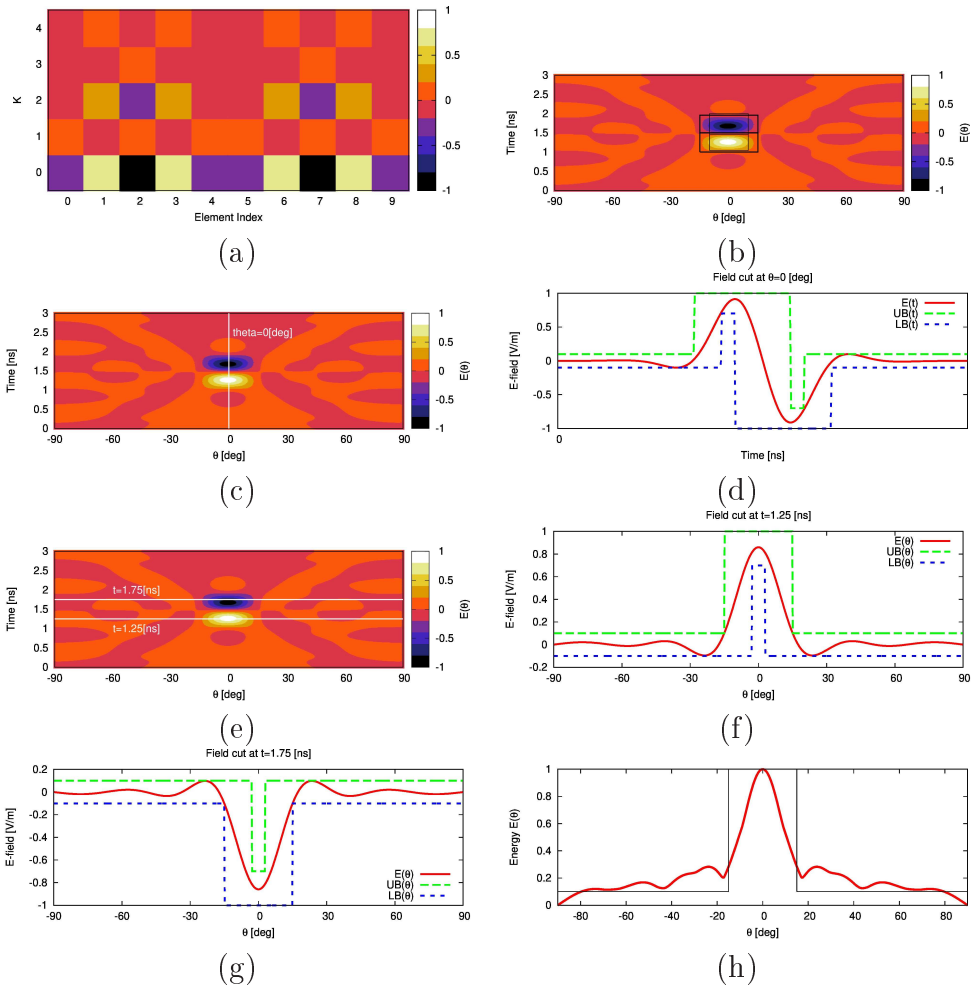

Figure 6.4: Broadside monocycle (BW, t)=(30 [deg], 1 [ns]) - Synthesis setup: $d = 10$ [cm], $N = 10$, $K = 4$, $q = 1$, $p = 1$,$\theta_s = 0$ - (a) Weights applied on each input pulse, (b) TD radiated field, (c) TD radiated field with white stripe along $\theta = 0$ [deg], (d) A cut at $\theta = 0$ [deg] from 6.4(c), TD radiated field with two white stripes along $t = 1.25$ [ns], and $t = 1.75$ [ns], (f) A cut at $t = 1.25$ [ns] from 6.4(e), (g) A cut at $t = 1.25$ [ns] from 6.4(e), and (h) Total energy obtained from 6.4(b)

6.3.2 Steering Radiation

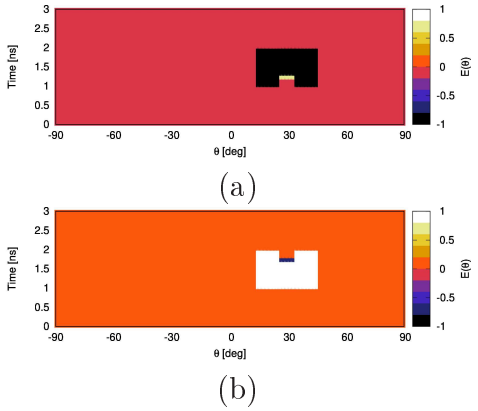

Figure 6.5: The time-angular mask constraints in two dimensions θ and t, (a) lower mask, (b) upper mask. Where $\theta \in [-90 : 90]$ [deg] and $t \in [0 : 3]$ [ns] generated from the time mask in fig. 6.2(a) and the angular mask in fig. 6.2(b) given $\theta_0 = 30$ [deg]

In the second example, to prove the effectiveness of $CP-$based synthesis in the eq. (6.18), the steering radiation is carried out where the main radiated field concentrated on the $\theta_s = 30$ [deg]. The linear array of $N = 10$ elements is kept the same in previous example with equal inter-element spacing $d = 10$ [cm]. The value d is chosen such that meet the requirements in the eq. (6.19) to avoid grating lobes that can appear.

The radiated field fit in the angular-time mask presented in fig. 6.5 with specifications. For the direction along time dimension, the optimized TD radiated field has duration time $T = 1$ [ns] where almost the energy lying inside while the visible range of time is 3 [ns], the highest level of the time-angular mask is normalized to $M_0 = 1$, and the lower upper bound of the time-angular mask is $M_1 = 0.7$ while the sidelobe level is set to be less than $M_{sl} = 0.1$. The value t_0 along the time direction is set to 1.5 [ns]. Regarding to the angular mask, the beamwidth of the mask $BW = 30$ [deg] from $\theta \in [15, 45]$ [deg], the optimized TD radiated field is expected less than $M_{sl} = 0.1$ in sidelobe regions.

For the Hermite waveforms in the beamforming networks, the value of $K = 8$ is chosen with nine input Hermite waveforms indexed $k = 0, ..., 8$ for each antenna array. In fig. 6.1 Before reaching to antenna array, nine input Hermite waveforms are weighted at $n - th$ antenna with weights α_{nk}, $k = 0, ..., 8$. The width scaling factor of the Hermite function σ is set to fixed value $\sigma = 0.4T$ for this example. In the eq. (6.9), the assumption on the effective height $\underline{h}^T(\theta, t)$ of single radiator is the $q - th$ differentiation $\underline{h}^T(\theta, t) = \delta^{(q)}(\tau)\, cos^p(\theta)$, $q = 1$, and $p = 1$ are set in this example.

The fig. 6.4(a) shows the optimized excitations $\alpha_{n,k}$, $n = 1, .., 10$, and

$k = 0, ..., 8$, and the fig. 6.4(b) is the optimized TD radiated field generated from the excitations $\alpha_{n.k}$ in fig. 6.4(a).

The optimized results is perfectly fulfilled the time-angular mask pattern constraints proposed in fig. 6.5, $2D$ pattern in fig. 6.6(b) is hard to view. Therefore, fig. 6.6(d) is the cut at $\theta = 30$ [deg] where the white stripe represented in fig. 6.6(c). Indeed, as it can be seen, the solid red line represented for the radiated field at $\theta = 30$ is perfectly fit the upper and lower mask specified in this example.

Furthermore, in fig. 6.6(f) and fig. 6.6(g) show the TD radiated cuts at $t = 1.25$ [ns] and $t = 1.75$ [ns] where two stripes illustrated in the fig. 6.6(e). As it is clearly that the radiated fields along two cuts completely match the angular masks at $t = 1.25$ [ns] and $t = 1.75$ [ns]. Therefore, the $CP-$based approach is successfully synthesizing the radiated field lying between the upper angular-time mask and the lower angular-time mask.

In the last fig. 6.6(h), the energy radiation computed and shown by average sum square of the optimized TD radiated field along time dimension. The results show that, all the energy focus at the broadside $\theta = 0$, the highest sidelobes are around 0.2. Although it is higher than the value $M_{sl} = 0.1$, it is not our interest here because the angular-time mask applied on the TD radiated field, not on the energy radiation and the DoF number of elements here is just $N = 10$ elements is quite small. For example, in fig. 6.10, when $N = 65$ the energy is totally fit the angular mask while we are not intended to optimized to fit only angular mask.

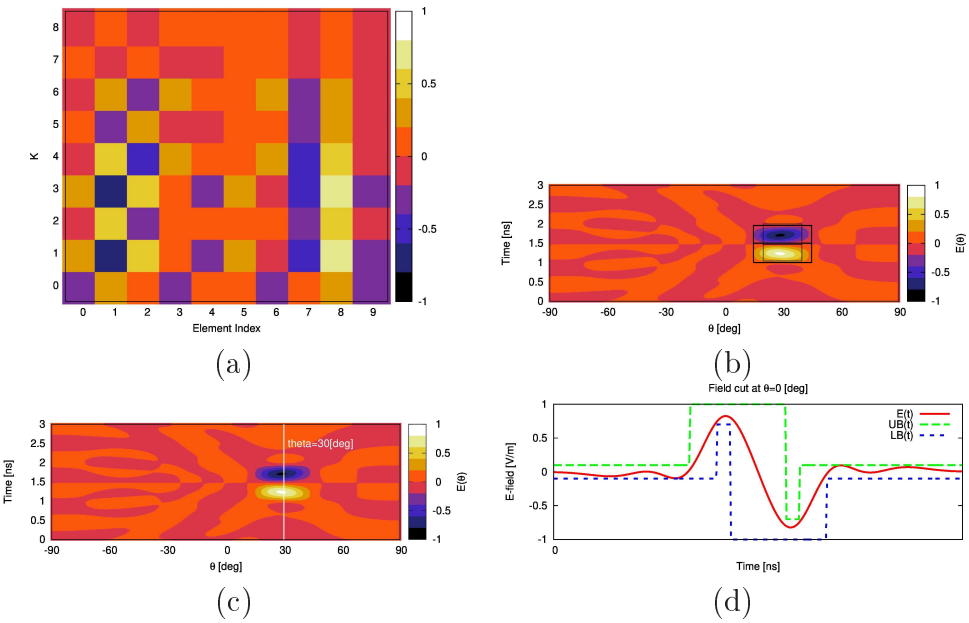

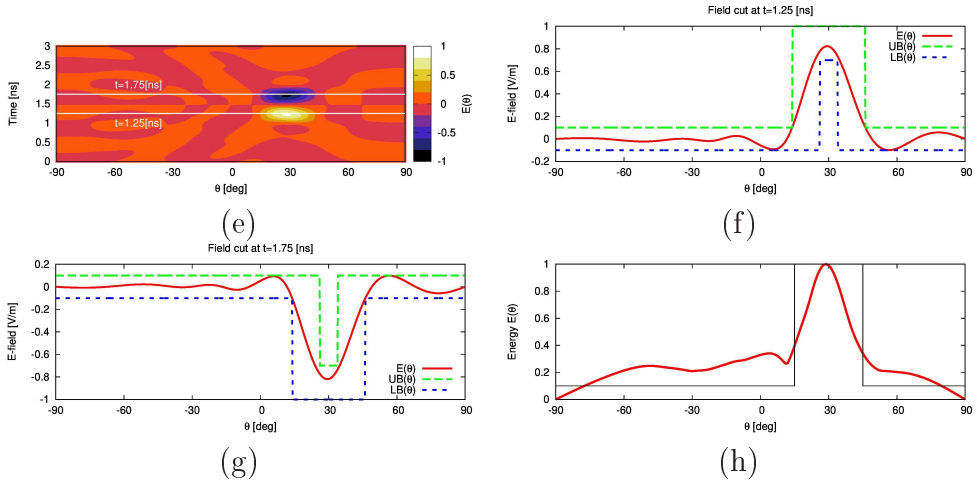

Figure 6.6: Broadside monocycle (BW, t)=(30 [deg], 1 [ns]) - Synthesis setup: $d = 10$ [cm], $N = 10$, $K = 4$, $q = 1$, $p = 1$,$\theta_s = 30$ - (a) Weights applied on each input pulse, (b) TD radiated field, (c) TD radiated field with white stripe along $\theta = 0$ [deg], (d) A cut at $\theta = 30$ [deg] from 6.6(c), TD radiated field with two white stripes along $t = 1.25$ [ns], and $t = 1.75$ [ns], (f) A cut at $t = 1.25$ [ns] from 6.6(e), (g) A cut at $t = 1.25$ [ns] from 6.6(e), and (h) Total energy obtained from 6.6(b)

6.3.3 Comparison PSO with CP

In this section, the two synthesis experiments is carried out on the PSO particle swarm optimization that is the "global" optimization to compare the effectiveness and the efficiency between CP and PSO optimization when applied to the timed array synthesis.

6.3.3.1 Broadside Single Monopulse

The fig. 6.7 show the results for the timed array synthesis using PSO optimization with the array geometry, the time-angular mask constraints, and the input Hermite waveforms exactly the same with configurations in the section 6.3.1. The fig. 6.7(b) shows that the synthesized TD radiated field is fit the time-angular mask imposing, however, the radiated field cut at $\theta = 0$ shows the solid red line is cut the blue dash-line a little bit, not perfectly match the mask. In addition, 6.7(f) and (g) illustrate the radiated field in the solid red not really fulfill the mask. Therefore, the $CP-$based synthesis is more effective when applied to the timed array compared to the PSO.

Indeed, the execution of synthesis is done on the personal computer with 10 GB RAM, and 2.5 GHz CPU, the $CP-$based procedure takes only less than 5 minutes to produce the optimal weights. However, the PSO optimization takes more than 24 hours to finish 500 iterations and returns the results for the linear

array of $N = 10$ elements. Then, of courses we can confirmed that the $CP-$based is more not only efficient but also reliable than PSO.

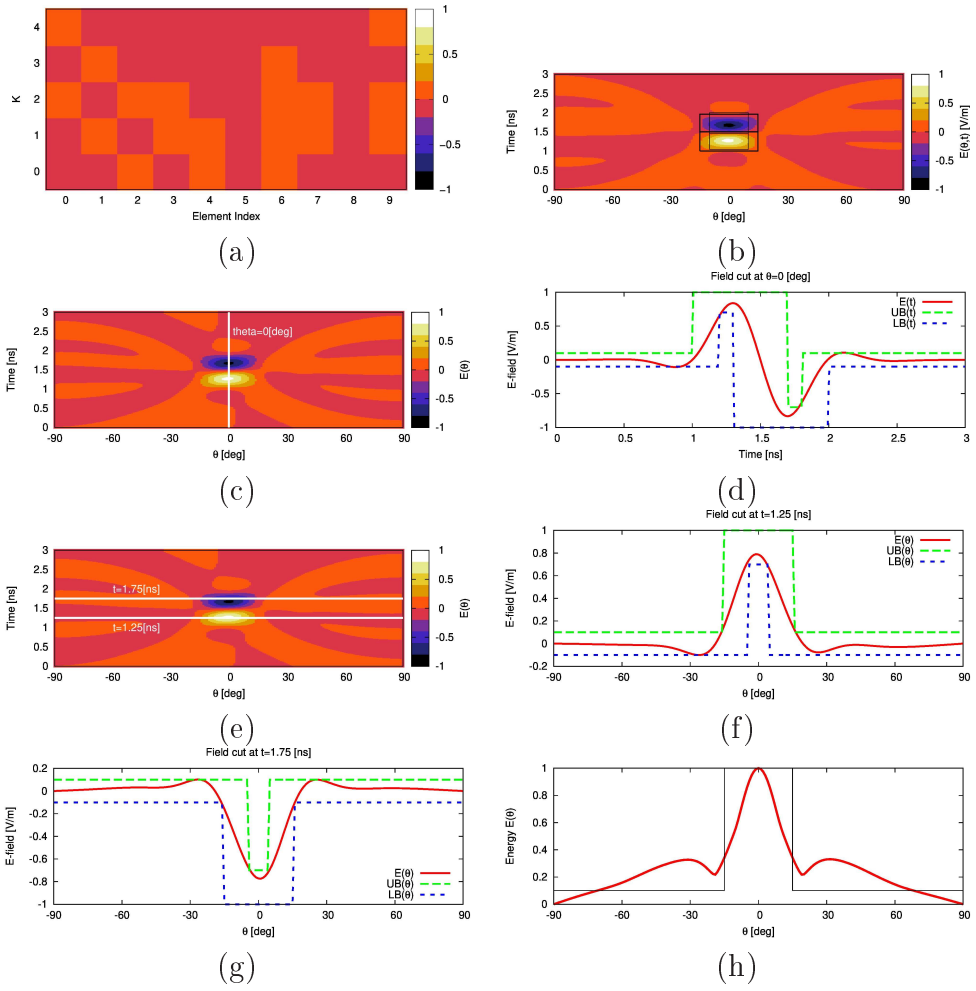

Figure 6.7: Broadside monocycle (BW, t)=(30 [deg], 1 [ns]) - Synthesis setup: $d = 10$ [cm], $N = 10$, $K = 4$, $q = 1$, $p = 1$,$\theta_s = 0$ - (a) Weights applied on each input pulse, (b) TD radiated field, (c) TD radiated field with white stripe along $\theta = 0$ [deg], (d) A cut at $\theta = 0$ [deg] from 6.7(c), TD radiated field with two white stripes along $t = 1.25$ [ns], and $t = 1.75$ [ns], (f) A cut at $t = 1.25$ [ns] from 6.7(e), (g) A cut at $t = 1.25$ [ns] from 6.7(e), and (h) Total energy obtained from 6.7(b)

6.3.3.2 Steering Monopulse

The fig. 6.8 show the results, including weights for each input Hermite waveforms, TD radiated field, and those cut at $\theta = 30$ [deg], $t = 1.25$ [ns], $t = 1.75$ [ns] for the timed array synthesis using PSO optimization with the array geometry, the time-angular mask constraints, and the input Hermite waveforms exactly the

same with configurations in the section 6.3.2. The fig. 6.8(b) depicts that the synthesized TD radiated field is fit the imposing time-angular mask, however, the radiated field cut at $\theta = 30$ shows the solid red line cut the blue solid-line a large portion, very bad matching for the mask. In addition, 6.8(f) and (g) illustrate the radiated field in the solid red poorly fulfill the imposing angular-time mask. Therefore, the $CP-$based synthesis in the section 6.3.2 produces the results that is more effective when applied to the timed array compared to the PSO.

In terms of efficiency, the execution of synthesis is done on the personal computer with 10 GB RAM, and 2.5 GHz CPU, the $CP-$based procedure finishes the experiment with no more than 5 minutes to produce the optimal weights for the imposing shaped TD radiated field. However, the PSO optimization spends more than 30 hours to finish 1000 iterations and produces the results for the linear array of $N = 10$ elements, beam-forming network order $K = 9$, which are still not really perfectly fit the constraints angular-time mask. Then, of courses we can confirmed that the $CP-$based is more not only efficient but also reliable than PSO.

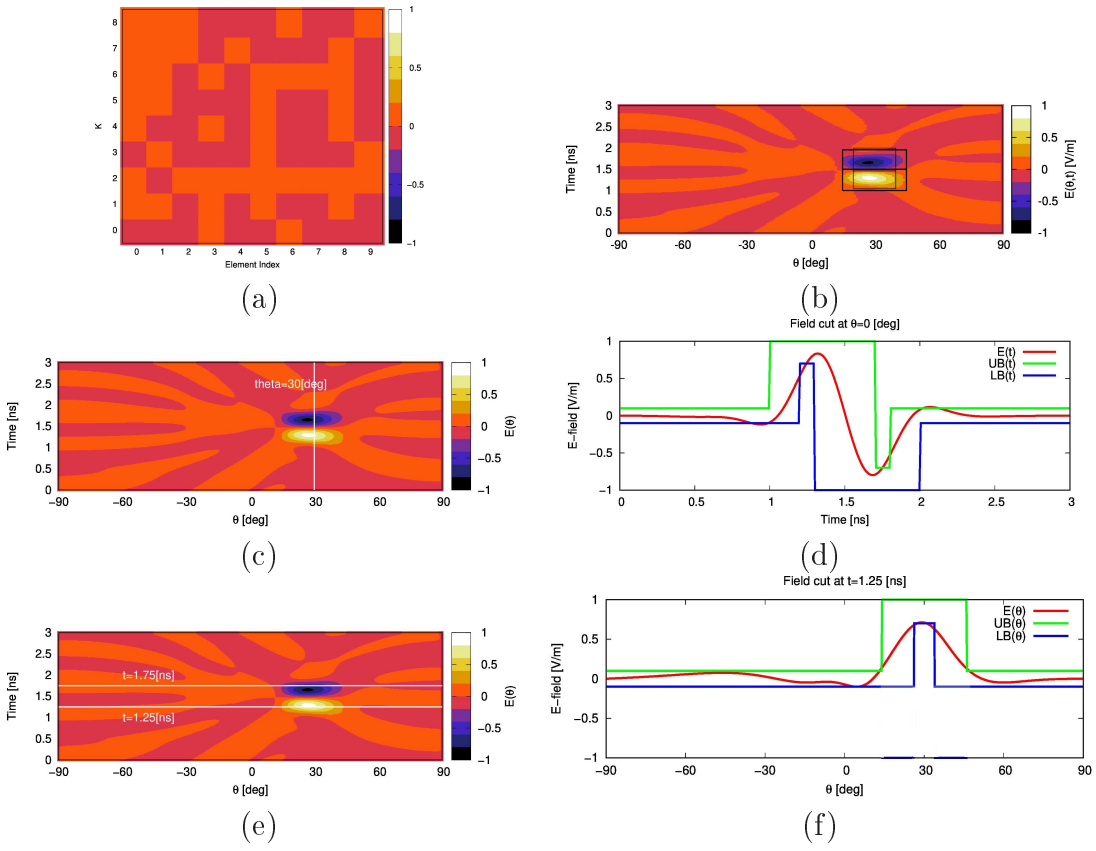

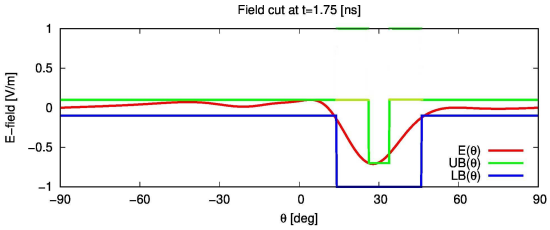

(g)

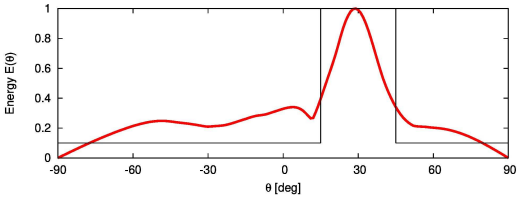

(h)

Figure 6.8: Broadside monocycle (BW, t)=(30 [deg], 1 [ns]) - Synthesis setup: $d = 10$ [cm], $N = 10$, $K = 4$, $q = 1$, $p = 1$,$\theta_s = 30$ - (a) Weights applied on each input pulse, (b) TD radiated field, (c) TD radiated field with white stripe along $\theta = 0$ [deg], (d) A cut at $\theta = 30$ [deg] from 6.6(c), TD radiated field with two white stripes along $t = 1.25$ [ns], and $t = 1.75$ [ns], (f) A cut at $t = 1.25$ [ns] from 6.6(e), (g) A cut at $t = 1.25$ [ns] from 6.6(e), and (h) Total energy obtained from 6.6(b)

6.3.4 Highly collimated Monopulse

In this last example, to prove the effectiveness and the efficiency of the $CP-$based synthesis applied to the TD radiated field. The larger of linear array comprised of $N = 65$ elements are used. The steering radiation is carried out where the main radiated field concentrated on the $\theta_s = 10$ [deg]. The inter-element spacing $d = 5$ [cm]. The value d is chosen such that meet the requirements in the eq. (6.19).

The angular-time mask pattern constraints are defined as, for the direction along time dimension, the optimized TD radiated field has duration time $T = 1$ [ns] out of the visible range of time is 3 [ns], the highest level of the time-angular mask is normalized to $M_0 = 1$, and the lower upper bound of the time-angular mask is $M_1 = 0.7$ while the sidelobe level is set to be less than $M_{sl} = 0.1$. The value t_0 along the time direction is fixed to 1.5 [ns]. Regarding to the angular mask, the beamwidth of the mask $BW = 5$ [deg] from $\theta \in [7.5, 12.5]$ [deg], the optimized TD radiated field is expected less than $M_{sl} = 0.1$ in sidelobe regions.

For the Hermite waveforms in the beamforming networks, the value of $K = 4$ is chosen with five input Hermite waveforms indexed $k = 0, ..., 4$ for each antenna array. In fig. 6.1 before reaching to antenna array, five input Hermite waveforms are weighted at $n - th$ antenna with weights α_{nk}, $k = 0, ..., 4$. The Hermite parameter σ is set to fixed value $\sigma = 0.7T$ for this example. In the eq. (6.9), the assumption on the effective height $\underline{h}^T(\theta, t)$ of single radiator is the $q - th$ differentiation $\underline{h}^T(\theta, t) = \delta^{(q)}(\tau)\, cos^p(\theta)$, $q = 1$, and $p = 1$ are set in this example.

The fig. 6.9(a) shows the optimized excitations $\alpha_{n,k}$, $n = 1, .., 65$, and $k = 0, ..., 4$, and the fig. 6.9(b) is the optimized TD radiated field generated from the excitations $\alpha_{n.k}$ in fig. 6.9(a).

The optimized results is perfectly fulfilled the time-angular mask pattern constraints proposed the specifications. Indeed, fig. 6.9(d) is the cut at $\theta = 10$ [deg] where the white stripe represented in fig. 6.9(c). Indeed, as it can be seen, the solid red line represented for the radiated field at $\theta = 10$ is perfectly fit the upper and lower mask specified in this example.

Moreover, in fig. 6.9(f) and fig. 6.9(g) show the TD radiated cuts at $t = 1.25$ [ns] and $t = 1.75$ [ns] where two stripes illustrated in the fig. 6.9(e). It is evident from the radiated fields along two cuts that they completely match the angular masks at $t = 1.25$ [ns] and $t = 1.75$ [ns]. Therefore, the $CP-$based approach succeeded in synthesizing the radiated field lying between the upper angular-time mask and the lower angular-time mask.

In the last fig. 6.10(h), the energy radiation calculated and shown by average sum square of the optimized TD radiated field along time dimension. The results show that, all the energy focus at the steered angle $\theta_s = 10$, the highest sidelobes are around 0.0 which is much below from the constraints $M_{sl} = 0.1$.

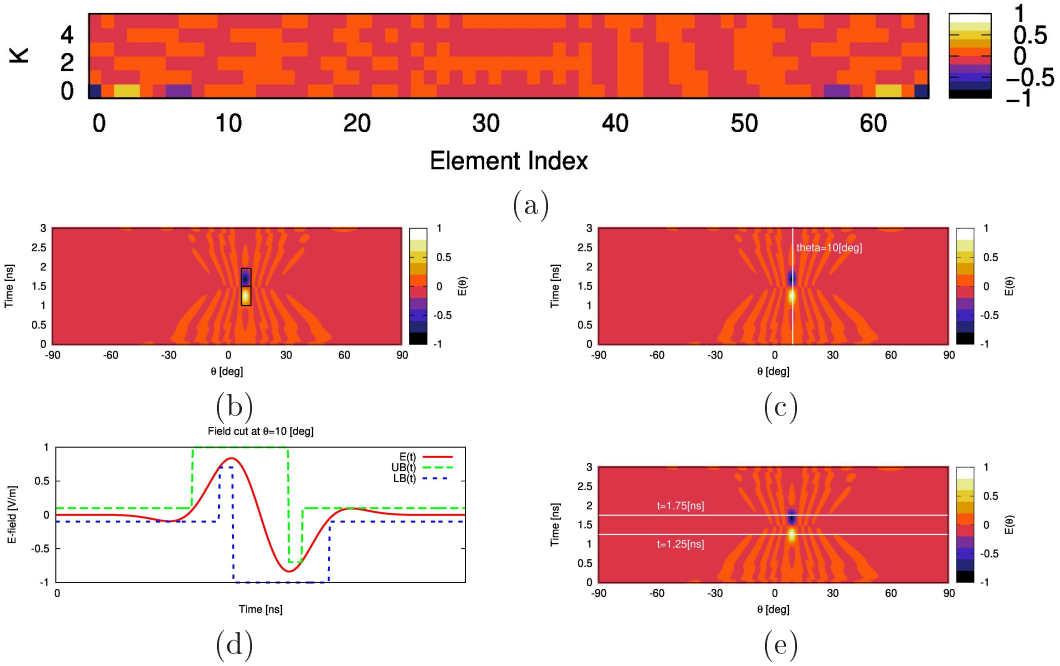

(a) (b) (c) (d) (e)

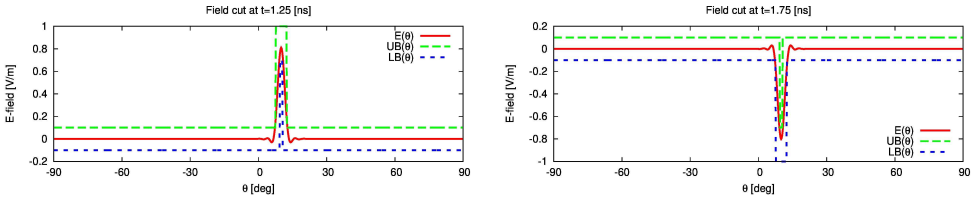

(f) (g)

Figure 6.9: Broadside monocycle (BW, t)=(30 [deg], 1 [ns]) - Synthesis setup: $d = 10$ [cm], $N = 65$, $K = 4$, $q = 1$, $p = 1$,$\theta_s = 10$ - (a) Weights applied on each input pulse, (b) TD radiated field, (c) TD radiated field with white stripe along $\theta = 0$ [deg], (d) A cut at $\theta = 10$ [deg] from 6.9(c), TD radiated field with two white stripes along $t = 1.25$ [ns], and $t = 1.75$ [ns], (f) A cut at $t = 1.25$ [ns] from 6.9(e), (g) A cut at $t = 1.25$ [ns] from 6.9(e).

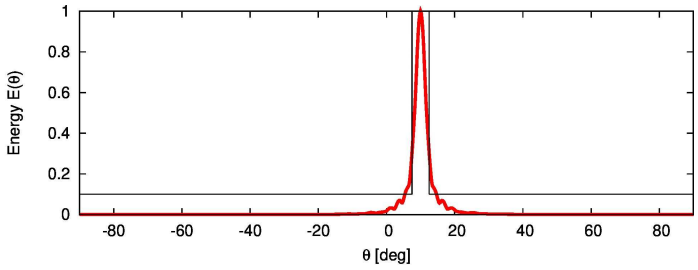

Figure 6.10: The total energy obtained from 6.9(b)

6.4 Conclusion

In this chapter, the non-convex form of TD radiated field has been converted into the convex form by simplifying the properties of the effective length of the antenna as isotropic source. In addition, Hermite waveforms are chosen as input waveforms due to its compact and ultra-wideband properties for higher order derivative. A set of examples are carried out to prove the effectiveness and efficiency of the proposed method on synthesis of TD radiated field. In addition, a stochastic optimization namely PSO has been deployed to prove that the convex programming is more efficient and effective than PSO in terms of the computational time execution.

Chapter 7

Conclusions and Final Remarks

In this chapter, the important observations about the proposed methods and their performances for various applications have been concluded. In addition of concluding remarks, a scope of future research has been listed.

In this thesis, the outcomes of this thesis are concluded as follows:

- *Chapter 2* - the state-of-the-art $CP-$based synthesis procedures are reviewed;
- *Chapter 3* - An innovative and effective strategy for the optimal synthesis of linear arrays is proposed, ensuring the maximum possible bandwidth operation for a imposing fixed SLL power mask. The extremely low SLL values and high directivity are obtained thanks to the design of ultra-wideband arrays. In addition, many numerical experiments are shown. Taking advantages of the super fast execution times and the optimal achieved solution, the ultra-wideband array synthesis can be cast as sequential convex optimization. The optimal results obtained can be used for many applications, such radar and remote sensing as well as next-generation small satellites and 5G communications.
- *Chapter 4* - An innovative CP method for synthesis of the sum and difference pattern used in monopulse radar systems operating at multiple frequencies with sharing a number of elements at the tail of the array has been presented and analyzed. The CP-based strategy provided the optimal excitations including imposing common parts for monopulse patterns. The strategy allows the monopulse radar systems to operate over a wide bandwidth and control user-defined bounds on sum and difference patterns. The examples provided has shown the optimal solutions and the reliability of the convex programming.
- *Chapter 5* - The $CP-$based procedure provided in the chapter are successfully synthesizing the shaped-beam pattern for an linear array with equal inter-element spacing operating over multiple frequencies by using only one common set of excitations. Two shaped-beam that are flattop and cosec^2 are provided to confirmed the effectiveness and efficiency of the proposed $CP-$based strategy.
- *Chapter 6* - In this chapter the proposed method have provided a flexible and fully-controlled way of shaping the TD radiated field. The synthesis scheme allows to build a beamforming networks that are depending on a set of signals and related parameters for different imposing masks. The TD radiated field can be constructed by using different input waveforms other than Hermite waveforms, then increasing the DoF for synthesis problems. The examples in the chapter also show that $CP-$based synthesis approach is outperformed the $PSO-$based and the one mentioned in [104] by producing an optimal weights for each different input waveform. The $CP-$based is really efficient and reliable for each example with less than few minutes to finish the execution of the synthesis compared to the PSO that took more than 24 hours.

The future research can be listed as follows:

- Chapter 3 - The work in this chapter can be extended to planar array for future work where an array should have elements located on a plane instead of linear array.
- Chapter 4 - In the future work, the analysis and the synthesis can extend to the planar array for the monopulse system where the both azimuth and elevation plane are considered. Therefore the detection and tracking are more general and practical. For the linear array, only azimuth plane is considered.
- Chapter 5 - Future work can be done in planar array where more challenging when the number of elements are increasing, the number of discretizing samples for the visible domain also increasing dramatically. However, thanks to the CP, this future work is able to carry out. Also, the example should considered the iso-flux shaped-beam pattern for the synthesis.
- Chapter 6 - Further work is able to extend the geometry of the array to $2D$ array instead of the linear array considered in this thesis. In this chapter, the only weights are the parameters need to be optimized under CP methodology, however, due to the convex programming's efficiency, effectiveness and reliability properties, one can extend the synthesis of weights of the known input waveforms to synthesis of the unknowns of input waveforms, and that input waveforms are arbitrary and the problem now is try to synthesize the input waveform as unknowns.

Bibliography

[1] R. J. Mailloux, *Phased Array Antenna Handbook*, 2nd ed. Norwood, MA: Artech House, 2004.

[2] C. A. Balanis, *Antenna Theory, Analysis, and Design*, 3rd ed. NY: John Willey & Sons, 2005.

[3] R. S. Elliott, *Antenna Theory and Design*, Englewood Cliffs, NJ, USA: Prentice-Hall, 1981.

[4] P. Rocca, G. Oliveri, R. J. Mailloux, A. Massa, "Unconventional Phased Array Architectures and Design Methodologies - A Review," *Proc. IEEE*, vol. 104, no. 3, pp. 544 - 560, Mar. 2016.

[5] G. Oliveri, G. Gottardi, F. Robol, A. Polo, L. Poli, M. Salucci, M. Chuan, C. Massagrande, P. Vinetti, M. Mattivi, R. Lombardi, and A. Massa, "Co-design of unconventional array architectures and antenna elements for 5G base stations," *IEEE Trans. Antennas Propag.*, vol. 65, no. 12, pp. 6752-6767, Dec. 2017.

[6] N. Anselmi, P. Rocca, M. Salucci, and A. Massa, "Contiguous phase-clustering in multibeam-on-receive scanning arrays," *IEEE Trans. Antennas Propag.*, vol. 66, no. 11, pp. 5879-5891, Nov. 2018.

[7] G. Oliveri and A. Massa, "Bayesian compressive sampling for pattern synthesis with maximally sparse non-uniform linear arrays," *IEEE Trans. Antennas Propag.*, vol. 59, no. 2, pp. 467-481, Feb. 2011.

[8] F. Viani, G. Oliveri, and A. Massa, "Compressive sensing pattern matching techniques for synthesizing planar sparse arrays," *IEEE Trans. Antennas Propag.*, vol. 61, no. 9, pp. 4577-4587, Sep. 2013.

[9] L. Poli, P.Rocca, L. Manica, and A. Massa, "Pattern synthesis in time-modulated linear arrays through pulse shifting," *IET Microw. Antennas Propag.*, vol. 4, no. 9, p. 1157-1164, Sep. 2010.

[10] J. I. E. Guzman, "New methods for the synthesis of radiation pat- terns of coupled antenna arrays," Ph.D. dissertation, Universidad Politecnica de Madrid, 2016.

[11] C. Bencivenni, “Aperiodic Array Synthesis for Telecommunications,” Ph.D. dissertation, Chalmers University of Technology, 2017.

[12] P. Rocca, L. Poli, A. Polo, and A. Massa, “Optimal Excitation Matching Strategy for Sub-Arrayed Phased Linear Arrays Generating Arbitrary-Shaped Beams,” *IEEE Trans. Antennas Propag.*, vol. 68, no. 6, pp. 4638-4647, Jun. 2020.

[13] M. H. Novak, F. A. Miranda and J. L. Volakis, "Ultra-wideband phased array for small satellite communications", *IET Microw. Antennas Propag.*, vol. 11, no. 9, pp. 1234-1240, Jul. 2017.

[14] N. Anselmi, P. Rocca, M. Salucci and A. Massa, "Contiguous phase-clustering in multibeam-on-receive scanning arrays", *IEEE Trans. Antennas Propag.*, vol. 66, no. 11, pp. 5879-5891, Nov. 2018.

[15] P. Rocca, M. A. Hannan, L. Poli, N. Anselmi and A. Massa, "Optimal phase-matching strategy for beam scanning of sub-arrayed phased arrays", *IEEE Trans. Antennas Propag.*, vol. 67, no. 2, pp. 951-959, Feb. 2019.

[16] J. S. Herd and M. D. Conway, "The evolution to modern phased array architectures", Proc. IEEE, vol. 104, no. 3, pp. 519-529, Mar. 2016.

[17] H. Steyskal, R. A. Shore, and R. L. Haupt, “Methods for Effects on Null Control and Their the Radiation Pattern,” *IEEE Trans. Antennas Propag.*, vol. AP-34, no. 3, pp. 404-409, Mar. 1986.

[18] G. Oliveri, L. Poli, and A. Massa, “Maximum Efficiency Beam Synthesis of Radiating Planar Arrays for Wireless Power Transmission,” *IEEE Trans. Antennas Propag.*, vol. 61, no. 5, pp. 2490-2499, May. 2013.

[19] Y.-J. Ren and K. Chang, "New 5.8 GHz circularly polarized retrodirective rectenna arrays for wireless power transmission", *IEEE Trans. Microwave Theory Tech.*, vol. 54, no. 7, pp. 2970-2976, Jul. 2006.

[20] A. Massa, G. Oliveri, F. Viani, and P. Rocca, "Array Designs for Long-Distance Wireless Power Transmission: State-of-the-Art and Innovative Solutions", *Proc. IEEE*, vol. 101, no. 6, pp. 1464-1481, 2013.

[21] W. P. M. N. Keizer, “Synthesis of Monopulse Antenna Patterns for Elliptical Phased Array Antennas With Different Peak Sidelobes Along the Principal Planes,” *IEEE Trans. Antennas Propag.*, vol. 67, no. 9, pp. 5943-5950, Sep. 2019.

[22] G. Oliveri, L. Poli and A. Massa, “Maximum effiency beam synthesis of radiating planar arrays for wireless power transmission,” *IEEE Trans. Antennas Propag.*, vol. 61, no. 5, pp.2490-2499, May 2013.

[23] A. K. M. Baki, N. Shinohara, H. Matsumoto, K. Hashimoto, and T. Mitani, "Study of isosceles trapezoidal edge tapered phased array antenna for solar power station/satellite," *IEICE Trans. Commun.*, vol. E90-B, no. 4, pp. 968-977, Apr. 2007.

[24] S. Rangan, T. S. Rappaport, and E. Erkip, "Millimeter-wave cellular wireless networks: potentials and challenges." *Proc. IEEE*, vol. 102, no. 3, pp. 366-385, Mar. 2014.

[25] R. L. Haupt, "Antenna Arrays in the Time Domain: An introduction to timed arrays," *IEEE Antennas Propag. Magazine*, Jun. 2017.

[26] C. L. Dolph, "A current distribution for broadside arrays which optimizes the relationship between beam width and side-lobe level", *Proc. IRE*, vol. 34, pp. 335-348, June 1946.

[27] T. K. Sarkar, and O. Pereira, "Using the matrix pencil method to estimate the parameters of a sum of complex exponentials," *IEEE Antennas Propag. Magazine*, vol. 37, no. 1, pp. 48-55, 1995.

[28] T. T. Taylor, "Design of Line-Source Antennas for Narrow Beamwidth and Low Side Lobes," *Proc. IRE*, vol. 3, no. 1, pp. 16-28, June 1955.

[29] E. T. Bayliss, "Design of Monopulse Antenna Difference Patterns with Low Sidelobes," *Bell System Tech. Journal*, vol. 47, no. 5, pp. 623-650, Jun. 1968

[30] H. G. Booker and P. C. Clemmow, "The concept of an angular spectrum of plane waves, and its relation to that of polar diagram and aperture distribution," *Pro. IEE* (London), paper No. 922, Radio Section, vol. 97, pt. III, pp. 11-17, Jan. 1950.

[31] P. M. Woodward, "A method for calculating the field over a plane aperture required to produce a given polar diagram," *Journal IEE*, vol. 93, pt. IIIA, pp. 1554-1558, 1946.

[32] P. M. Woodward and J. D. Lawson, "The theoretical precision with which an arbitrary radiation-pattern may be obtained from a source of a finite size," *Journal IEE*, vol. 95, pt. III, no. 37, pp. 363-370, Sep. 1948.

[33] S. A. Schelkunoff, "A mathematical theory of linear arrays," *Bell System Tech. Journal,* vol. 22, no. 1, pp. 80-107, Jan. 1943.

[34] O. M. Bucci, D. D. Elia, G. Mazzarella, and G. Panatiello, "Antenna pattern synthesis: A new general approach," *Proc. IEEE*, vol. 82, pp. 358-371, Mar. 1994.

[35] B. Widrow and S. D. Stearns, *Adaptive Signal Processing.* EnglewoodCliffs, NJ: Prentice-Hall, 1985.

[36] V. Murino, A. Trucco, and C. S. Regazzoni, "Synthesis of unequally spaced arrays by simulated annealing," *IEEE Trans. Signal Process.*, vol. 44, no. 1, pp. 119-123, Jan. 1996.

[37] D. G. Kurup, M. Himdi, and A. Rydberg, "Synthesis of uniform amplitude unequally spaced antenna arrays using the differential evolution algorithm", *IEEE Trans. Antennas Propag.*, vol. 51, no. 9, pp. 2210-2217, 2003.

[38] K. K. Yan and Y. Lu, "Sidelobe reduction in array-pattern synthesis using genetic algorithm," *IEEE Trans. Antennas Propag.*, vol. 45, no. 7, pp. 1117-1122, Jul. 1997.

[39] M. M. Khodier and C. G. Christodoulou, "Sidelobe level and null control using particle swarm optimization," *IEEE Trans. Antennas Propag.*, vol. 53, no. 8, pp. 2674-2679, Aug. 2005.

[40] S. Boyd, L. El Ghaoui, E. Feron, and V. Balakrishnan, *Linear Matrix Inequalities in System and Control Theory*, vol. 15 of Studies in Applied Mathematics. Philadelphia, PA: SIAM, June 1994.

[41] U. Kirsch, *Structural Optimization*. Berlin: Springer-Verlag, 1993.

[42] A. W. Potchinkov and R. M. Reemtsen, "FIR filter design in the complex domain by a semi-infinite programming technique. II. Examples," *AEU, Archiv Elektronik Uebertragungstechnik: Electron. Commun.*, vol. 48, no. 4, pp. 200-209, July 1994.

[43] C. Byrne, "Iterative image reconstruction algorithms based on crossentropy minimization," *IEEE Trans. Image Process.*, vol. 2, pp. 96-103, Jan. 1993.

[44] P. Sancheti and S. Sapatnekar, "Interconnect design using convex optimization," in *Proc. IEEE Custom Integrated Circuits Conf.*, pp. 549-552,1994.

[45] S. P. Wu, S. P. Boyd, and L. Vandenberghe, B. Datta, Ed., "FIR filter design via spectral factorization and convex optimization," *Appl. Comput. Contr. Signals Circuits*, vol. 1, no. 5, pp. 215-245, 1998.

[46] S. S. Sapatnekar, "A convex programming approach to problems in VLSI design," Ph.D. dissertation, Coordinated Sci. Lab., Univ. of Illinois, Urbana-Campaign, Aug. 1992.

[47] H. Lebret and S. Boyd, "Antenna array pattern synthesis via convex optimization," *IEEE Trans. Signal Process.*, vol. 45, no. 3, pp. 526-532, Mar. 1997.

[48] P. J. Bevelacqua and C. A. Balanis, "Geometry and weight optimization for minimizing sidelobes in wideband planar arrays," *IEEE Trans. Antennas Propag.*, vol. 57, n. 4, pp. 1285-1289, 2009.

[49] P. J. Bevelacqua and C. A. Balanis, "Minimum sidelobe levels for linear array," *IEEE Trans. Antennas Propag.*, vol. 55, n. 12, pp. 3442-3449, Dec. 2007.

[50] A. F. Morabito, "Synthesis of maximum-efficiency beam arrays via convex programming and compressive sensing," *IEEE Antennas Wire. Propag. Lett.*, vol. 16, pp. 2404-2407, 2017.

[51] O. M. Bucci, L. Caccavale, and T. Isernia, "Optimal far-field focusing of uniformly spaced arrays subject to arbitrary upper bounds in nontarget directions," *IEEE Trans. Antennas Propag.*, vol. 50, n. 11, pp. 1539-1554, 2002.

[52] G. Gottardi, L. Poli, M. A. Hannan, and P. Rocca, "wideband phased arrays optimal design though convex programming," *Proceedings of the 2016 IEEE AP-S International Symposium and USNC-URSI Radio Science*, Fajardo, Puerto Rico, USA, 26-June - 1-July, 2016.

[53] L. T. P. Bui, N. Anselmi, G. Gottardi, L. Poli, and P. Rocca, "Wideband phased arrays synthesis with maximum bandwidth through iterative convex optimization," *Proceedings of the 2017 IEEE AP-S International Symposium and USNC-URSI Radio Science*, San Diego, California, USA, pp. 479-480, July 9-15, 2017.

[54] L. T. P. Bui, N. Anselmi, T. Isernia, P. Rocca & A. F. Morabito, "On bandwidth maximization of fixed-geometry arrays through convex programming," *Journal of Electromagnetic Waves and Applications*, 34:5,581-600,DOI:10.1080/09205071.2020.1724832

[55] P. Rocca and A. F. Morabito, "Optimal synthesis of reconfigurable planar arrays with simplified architectures for monopulse radar applications," *IEEE Trans. Antennas Propag.*, vol. 63, n. 3, pp. 1048-1058, 2015.

[56] A. F. Morabito and P. Rocca, "Optimal synthesis of sum and difference patterns with arbitrary sidelobes subject to common excitations constraints," *IEEE Antennas Wire. propag. Lett.*, vol. 9, 2010.

[57] G. Gottardi, L. Poli, P. Rocca, A. Montanari, A. Aprile and A. Massa, "Optimal monopulse beamforming for side-looking airbone radar," *IEEE Antennas Wire. propag. Lett.*, vol. 16, 2017.

[58] B. Fuchs and J. J. Fuchs, "Optimal polarization synthesis of arbitrary array with focused power pattern," *IEEE Trans. Antennas Propag.*, vol. 59, n. 12, pp. 4512-4519, Dec. 2011.

[59] B. Fuchs, A. Skrivervik, and J. R. Mosig, "Shaped beam synthesis of arrays via sequential convex optimizations," *IEEE Antennas Wire. propag. Lett.*, vol. 12, 2013.

[60] S. E. Nai, W. Ser, Z. L. Yu, and H. Chen, "Beampattern synthesis for linear and planar arrays with antenna selection by convex optimization," *IEEE Trans. Antennas Propag.*, vol. 58, no. 12, pp. 3923-3930, Dec. 2010.

[61] B. Fuchs, "Application of convex relaxation to array synthesis problems," *IEEE Trans. Antennas Propag.*, vol. 64, no. 2, pp. 634-640, Feb. 2014.

[62] B. Fuchs, "Antenna selection for array synthesis problems," *IEEE Antennas Wire. propag. Lett.*, vol. 16, 2017.

[63] S. Boyd, and L. Vandenberghe, *Convex Optimization,* Cambridge, U.K., Cambridge Univ. Press, 2004.

[64] L. T. P. Bui, L. Poli, P. Rocca, and A. Massa, "Maximum-Bandwidth Synthesis of Monopulse Array Antennas with Fixed Geometry Through Convex Optimization," *Proc. 2018 IEEE AP-S International Symposium on Antennas and Propagation & USNC/URSI National Radio Science Meeting*, Boston, Massachusetts, 8-13 July 2018.

[65] L. T. P. Bui, L. Poli, and P. Rocca, "Optimal synthesis of wideband beamforming weights for monopulse tracking radar: the linear array case," *Proc. 2018 IEEE AP-S International Symposium on Antennas and Propagation & USNC/URSI National Radio Science Meeting*, Atlanta, Georgia, 7-12 July 2019.

[66] M. Capek, L. Jelinek, and P. Hazdra, "On the functional relation between quality factor and fractional bandwidth," *IEEE Trans. Antennas Propag.*, vol. 63, n. 6, pp. 2787-2790, 2015.

[67] B. Allen, T. Brown, K. Schwieger, E. Zimmermann, W. Q. Malik, D. J. Edwards, L. Ouvry, and I. Oppermann, "Ultrawideband: applications, technology and future perspectives," *Proceedings of the International Workshop on convergent technologies (IWCT)*, 6-10 June 2005, Oulu, Finland.

[68] M. Ettorre, W. A. Alomar, and A. Grbic, "Radiative wireless power-transfer system using wideband, wide-angle slot arrays," *IEEE Trans. Antennas Propag.*, vol. 65, n. 6, pp. 2975-2982, 2017.

[69] P. Rocca, R. J. Mailloux, and G.Toso, "GA-based optimization of irregular subarray layouts for wideband phased arrays design," *IEEE Antennas Wire. Propag. Lett.*, vol. 14, pp. 131-134, 2015.

[70] S. G. Zhou, Z. H. Peng, G. L. Huang, J. Y. Li, and C. Y. D. Sim, "Design of wideband and dual polarized cavity antenna planar array," *IEEE Trans. Antennas Propag.*, vol. 64, n. 10, pp. 4565-4569, 2016.

[71] J. Wu, Y. J. Cheng, and Y. Fan, "Millimeter-wave wideband high-efficiency circularly polarized planar array antenna," *IEEE Trans. Antennas Propag.*, vol. 64, n. 2, pp. 535-542, 2016.

[72] Q. Liu, Z. N. Chen, Y. Liu, and C. Li, "Compact ultrawideband circularly polarized weakly coupled patch array antenna," *IEEE Trans. Antennas Propag.*, vol. 65, n. 4, pp. 2129-2134, 2017.

[73] O. M. Bucci, T. Isernia, and A. F. Morabito, "Optimal synthesis of circularly symmetric shaped beams," *IEEE Trans. Antennas Propag.*, vol. 62, n. 4, pp. 1954-1964, 2014.

[74] O. M. Bucci, T. Isernia, and A. F. Morabito, "Optimal synthesis of directivity constrained pencil beams by means of circularly symmetric aperture fields," *IEEE Antennas Wire. Propag. Lett.*, vol. 8, pp. 1386-1389, 2009.

[75] A. F. Morabito, "Synthesis of maximum-efficiency beam arrays via convex programming and compressive sensing," *IEEE Antennas Wire. Propag. Lett.*, vol. 16, pp. 2404-2407, 2017.

[76] D. A. M. Iero, T. Isernia, A. F. Morabito, I. Catapano, and L. Crocco, "Optimal constrained field focusing for hyperthermia cancer therapy: a feasibility assessment on realistic phantoms," *Progress Electro. Research*, vol. 102, pp. 125-141, 2010.

[77] O. M. Bucci, L. Caccavale, and T. Isernia, "Optimal far-field focusing of uniformly spaced arrays subject to arbitrary upper bounds in nontarget directions," *IEEE Trans. Antennas Propag.*, vol. 50, n. 11, pp. 1539-1554, 2002.

[78] A. A. Salas-Sanchez, J. Fondevila-Gomez, J. A. Rodriguez-Gonzalez, and F. J. Ares-Pena, "Parametric synthesis of well-scanning isophoric pencil beams," *IEEE Trans. Antennas Propag.*, vol. 65, n. 3, pp. 1422-1427, 2017.

[79] T. Isernia and G. Panariello, "Optimal focusing of scalar fields subject to arbitrary upper bounds," *Electronics Lett.*, vol. 34, n. 2, pp. 162-164, 1998.

[80] R. Vescovo, "Reconfigurability and beam scanning with phase-only control for antenna arrays," *IEEE Trans. Antennas Propag.*, vol. 56, n. 6, pp. 1555-1565, 2008.

[81] A. F. Morabito and P. Rocca, "Reducing the number of elements in phase-only reconfigurable arrays generating sum and difference patterns," *IEEE Antennas Wire. Propag. Lett.*, vol. 14, pp. 1338-1341, 2015.

[82] M. Alvarez Folgueiras, J. A. Rodriguez Gonzalez, and F. Ares Pena, "Optimal compromise among sum and difference patterns in monopulse antennas: use of subarrays and distributions with common aperture tail," *Journal Electro. Waves Applications*, vol. 23, n. 17-18, pp. 2301-2311, 2009.

[83] J. A. Rodriguez, A. Trastoy, J. C. Bregains, F. Ares, and G. Franceschetti, "Beam reconfiguration of linear arrays using parasitic elements," Electronics Letters, vol. 42, no. 3, pp. 131-133, 2006.

[84] A. F. Morabito, A. Massa, P. Rocca, and T. Isernia, "An effective approach to the synthesis of phase-only reconfigurable linear arrays," *IEEE Trans. Antennas Propag.*, vol. 60, n. 8, pp. 3622-3631, 2012.

[85] D. K. Cheng, "Optimization techniques for antenna arrays," *IEEE Trans. Antennas Propag.*, vol. 59, no. 12, pp. 1664-1674, 1971.

[86] O. M. Bucci, C. Gennarelli, and C. Savarese, "Representation of electromagnetic fields over arbitrary surfaces by a finite and nonredundant number of samples," *IEEE Trans. Antennas Propag.*, vol. 46, n. 3, pp. 351-359, 1998.

[87] M. C. Tang, T. Shi, and R. W. Ziolkowski, "Planar ultrawideband antennas with improved realized gain performance," *IEEE Trans. Antennas Propag.*, vol. 64, n. 1, pp. 61-69, 2016.

[88] L. Manica, P. Rocca, A. Martini, and A. Massa, "An innovative approach based on a tree-searching algorithm for optimal matching of independently optimum sum and difference excitations," *IEEE Trans Antennas Propag.*, vol. 56, no. 1, pp. 58-66, Jan. 2008.

[89] S. M. Sherman and D. K. Barton, *Monopulse Principles and Techniques*, 2nd ed. Norwood, MA, USA: Artech House, 2011.

[90] P. Lopez, J. A. Rodriguez, F. Ares, and E. Moreno, "subarray weighting for difference patterns of monopulse antennas: Joint optimization of subarray configurations and weights," *IEEE Trans Antennas Propag.*, vol. 49, no. 11, pp. 1606-1608, Nov. 2001.

[91] S. Caorsi, A. Massa, M. Pastorino, and A. Randazzo, "Optimization of the difference patterns for monopulse antennas by a hybrid real/integer-coded differential evolution method," *IEEE Trans Antennas Propag.*, vol. 53, no. 1, pp. 372-376, Jan. 2005.

[92] M. Alvarez-Folgueiras, J. Rodriguez-Gonzales, and F. Ares-Pena, "Optimal compromise among sum and difference patterns in monopulse antennas: Use of subarrays and distributions with common aperture tail," *J. Electromagn. Waves Appl.* , vol. 23, pp. 2301-2311, 2009.

[93] CVX Research, Inc. CVX: Matlab software for discipline convex programming, version 2.0 beta. http://cvxr.com/cvx, September 2012.

[94] F. J. Ares-Pena, J. A. Rodriguez-Gonzales, E. Villaneava-Lopez, and S. R. Rengarajan, "Genetic algorithms in the design and optimization of antenna array patterns," IEEE Trans. Antennas Propag., vol. 47, no. 3, pp. 506-510, Mar. 1999.

[95] O. M. Bucci, G. Franceschetti, G. Mazzarella, and G. Panariello, "Intersection approach to array pattern synthesis," *Inst. Elect. Eng. Proc. H, Microw., Antennas Propag.*, vol. 137, no. 6, pp. 349-358, Dec. 1990.

[96] L. I. Vaskelainen, "Iterative least-squares synthesis methods for conformal array antennas with optimized polarization and frequency properties," *IEEE Trans. Antennas Propag.*, vol. 45, no. 7, pp. 1179-1185, Jul. 1997.

[97] A. F. Morabito, A. R. Lagana, and T. Isernia, "On the optimal synthesis of ring symmetric shaped patterns by means of uniformly spaced planar arrays," Prog. Electromagn. Res. B, vol. 20, pp. 33-48, 2010.

[98] S. E. Nai, W. Ser, Z. L. Yu, and S. Rahardja, "Beampattern synthesis with linear matrix inequalitues using minimum array sensors," Progr. Electromagn. Res. M, vol. 9, pp. 165-176, 2009.

[99] H. G. Hoang, H. D. Tuan, and B. N. Vo, "Low-dimensional SDP formulation for large antenna array synthesis," *IEEE Trans Antennas Propag.*, vol. 55, pp. 1716-1725, Jun. 2007.

[100] T. Isernia , O.M. Bucci ,and N. Fiorentino, "Shaped Beam Antenna Synthesis Problems: Feasibility Criteria and New Strategies," *Journal of Electromagnetic Waves and Applications*, vol. 12, no. 1, pp. 103-138, 1998.

[101] B. Fuchs, A. Skrivervik, and J. R. Mosig, "Shaped beam synthesis of arrays via sequential convex optimization," *IEEE Antennas Wire. Propag. Lett.*, vol. 12, pp. 1049-1052, 2013.

[102] S. P. Boyd, and L. Vandenberghe, *Convex Optimization.* Cambridge, U.K.: Cambridge Univ. Press, 2004.

[103] G. Franceschetti, J. Tatoian, and G. Gibbs, "Timed array in a Nutshell," *IEEE Trans. Antennas Propag.*, vol. 53, no. 12, pp. 4073-4082, Dec. 2005.

[104] M. Ciattaglia, and G. Marrocco, "Timed domain synthesis of pulsed arrays," *IEEE Trans. Antennas Propag.*, vol. 56, no. 7, pp. 1928-1938, Jul. 2008.

[105] K. Siwiak, and D. McKeown, *Ultra-wideband radio technology.* New York: Wiley 2004.

[106] M. G. M. Hussain, "Principles of spacing-time array processing for ultrawide-band impulse radar and radio communications," *IEEE Trans. Veh. Technol.*, vol. 51, no. 3, pp. 393-403, 2002.

[107] J. McCorkle, V. Sabio, R. Kapoor, and N. Nandhakumar, "Transient synthetic aperture radar and the extraction of anisotropic and natural frequency information," *in Dectection and Identification of Visually Obscured Targets*, C. E. Baum, Ed. London, U.K.: Taylor and Francis, 1998, pp. 377-430.

[108] W. Sogel, C. Sturn, and W. Wiesbeck, "Impulse response of linear UWB antenna arrays and the application to beam steering," *in IEEE Int. Conf. Ultra-Wideband*, pp. 275-280, 2005.

[109] E. J. Bond, X. Li, S. C. Hagness, and B. D. V. veen, "Microwave imaging via space-time beamforming for early detection for breast cancer," *IEEE Trans. Antennas Propag.*, vol. 51, no. 8, pp. 1690-1705, Jul. 2003.

[110] L. R. L. Conte, R. Merletti, and G. V. Sandri, "Hermite expansions of compact support waveforms: Application to myolectrics signals ," *IEEE Trans. Biomed. Eng.*, vol. 41, no. 2, pp. 1147-1159, 1994.

[111] L. E. Miller, "Autocorrelation functions for Hermite-polynimial ultrawide-band pulses," *Electron. Lett.*, vol. 39, no. 11, pp. 870-871, 2003.

[112] R. L. Haupt, *Timed Arrays Wideband and Time Varying Antenna Arrays*, Hoboken, NJ: Wiley, 2015.